

國立交通大學

機械工程研究所

碩士論文

機載合成孔徑雷達訊號之運動補償

Motion Compensation in Airborne Synthetic Aperture  
Radar Signal



研究生： 楊嘉豐

指導教授： 成維華 教授

中華民國九十三年六月

機載合成孔徑雷達訊號之運動補償

Motion Compensation in Airborne Synthetic Aperture Radar Signal

研究生：楊嘉豐

Student : Chia-Feng Yang

指導教授：成維華

Advisor : Wei-Hua Chieng

國立交通大學

機械工程學系



Submitted to Institute of Mechanical Engineering  
College of Engineering  
National Chiao Tung University  
in partial Fulfillment of the Requirements  
for the Degree of  
Master  
in

Mechanical Engineering

June 2004

Hsinchu, Taiwan, Republic of China

中華民國九十三年六月

# 機載合成孔徑雷達訊號之運動補償

研究生：楊嘉豐

指導教授：成維華 教授

國立交通大學機械工程研究所

## 摘要

合成孔徑雷達系統為一不受晝夜及天候影響之主動式微波影像偵測系統，已廣泛應用在軍事或民事上來遙測地表資訊。由於機載合成孔徑雷達在天空中合成陣列天線時，受到飛機載具不預期的偏航或大氣亂流的干擾以及飛機本身結構的振動等，造成雷達掃瞄軌跡的偏移，使得高解析度的影像被模糊化。為解決此問題，雷達系統必須適時補償飛機之運動變化，穩定雷達天線，並改變參考訊號，消除相位誤差，使回波之雷達訊號能被正確的量得。本論文之主旨將闡述合成孔徑雷達系統成像原理、軟硬體架構及運動補償功能。在成像處理流程中，將以感測器為基礎，整合飛機之慣性導航系統，產生參考相位來修正微波訊號，並提出追蹤控制法則來穩定雷達天線。另一方面，利用相位梯度自動聚焦演算法來估測相位誤差，以接收訊號為基礎做訊號之運動補償。藉此，機載之孔徑雷達解決了影像的失焦，並確定掃瞄目標位置的準確性，防止解析度的降低以確保微波影像的品質。

# Motion Compensation in Airborne Synthetic Aperture Radar Signal

Student : Chia-Feng Yang

Advisor : Dr. Wei-Hua Chieng

Institute of Mechanical Engineering  
National Chiao Tung University

## Abstract

Synthetic Aperture Radar (SAR) is the active microwave remote sensing image system immune to the night and adverse weather and applied on the military and civil affairs to obtain terrain information widely. The antenna mounted on the aircraft deviates from its predicted trajectory by pilot-induced maneuvers, atmospheric gusts disturbance and structural vibrations, and will smear the high-resolution images. To gain correct echo pulses from array antenna synthesized on air, the system must be compensated the motion uncertainty of aircraft by correcting the motion deviation of radar properly, stabilizing the antenna, updating the phase of reference signal and eliminating phase error. This study proposes to describe architecture and signal processing of a SAR system and generalized approach to motion compensation. In the image formatting procedure, radar will integrate into the airplane's inertial navigation system to generate the sensor-based reference function and use the tracking control to stabilize the antenna gimbals. On the other way, the signal-based motion compensation uses the phase gradient autofocus algorithm to estimate the phase error of receiving microwave signal. Then, both of the positioning accuracy and the image quality will be guaranteed.

## Acknowledgement

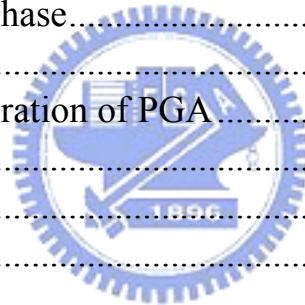
Thanks sincerely for all contributed to this thesis especially for my advisor  
Dr. Wei-Hua Chieng.



## Contents

摘要 .....	i
Abstract .....	ii
Acknowledgement .....	iii
Contents .....	iv
List of Figures .....	vi
List of Tables .....	viii
<b>Chapter 1 Introduction</b> .....	1
1.1 Motives and Objectives .....	1
1.2 Research Orientation .....	2
<b>Chapter 2 Synthetic Aperture Radar System</b> .....	4
2.1 Architecture of Synthetic Aperture Radar System .....	5
2.2 Concept of Synthetic Aperture Radar .....	6
2.2.1 The Doppler Frequency .....	8
2.3 Resolution Analysis .....	9
2.3.1 Range Resolution .....	9
2.3.2 Angular Resolution .....	10
2.4 SAR Operating Modes .....	11
<b>Chapter 3 Signal Processing</b> .....	14
3.1 Signal of Array .....	14
3.2 Signal Processor Structure .....	15
3.2.1 RFG0 .....	16
3.2.2 RFG1 .....	16
3.2.3 RFG2 .....	17
3.2.4 RFG3 .....	17
3.2.5 RFG4 .....	18
3.3 Processing in Range .....	18
3.3.1 LFM for Pulse Compression .....	19
3.3.2 Reconstruction .....	20
3.4 Processing in Azimuth .....	21
3.4.1 Abscissa Analysis .....	22
3.4.2 Resolution of Azimuth .....	25
3.4.3 Focusing .....	25
3.5 Simulations .....	27
<b>Chapter 4 Sensor-based Motion Compensation</b> .....	29
4.1 Motion Measurement Sensor .....	29

4.2 Motion Compensation for Phase Adjustment .....	31
4.2.1 Translational Displacement Path .....	31
4.2.2 Lever Arm Path.....	34
4.2.3 Antenna Stabilization.....	35
4.2.4 Motion Compensation in SAR Operation Mode.....	37
4.3 Radar Control Mechatronical System .....	38
4.3.1 Radar Mechanism.....	39
4.3.2 Motion Control Card .....	39
4.3.3 Radar Control Using Tracking Algorithm.....	40
<b>Chapter 5 Signal-based Motion Compensation.....</b>	<b>44</b>
5.1 Autofocus.....	44
5.2 Phase Gradient Autofocus Algorithm.....	45
5.2.1 Center Shifting.....	46
5.2.2 Windowing .....	47
5.2.3 Phase Estimation .....	48
5.2.4 Linear Phase Removal.....	50
5.2.5 Correcting Phase.....	51
5.2.6 Iterating.....	52
5.3 Low SNR Consideration of PGA.....	54
<b>Chapter 6 Conclusion.....</b>	<b>55</b>
<b>References .....</b>	<b>56</b>
<b>Figures .....</b>	<b>59</b>
<b>Tables.....</b>	<b>94</b>



## List of Figures

Figure 2-1	A Radar System Architecture .....	59
Figure 2-2	Electromagnetic Spectrum and Microwave Frequency Bands Useful for Imaging.....	60
Figure 2-3	Geometry of SAR .....	61
Figure 2-4	Spotlight Mapping .....	62
Figure 2-5	Strip Mapping .....	62
Figure 2-6	Doppler Beam Sharpening (DBS) Mapping .....	63
Figure 3-1	Synthetic Array and Real Array.....	63
Figure 3-2	Beam Pattern in Synthetic and Real Array.....	64
Figure 3-3	Beam Pattern of Removing Grating Lobe.....	64
Figure 3-4	Signal Processing Function Block.....	65
Figure 3-5	SAR Array Sampling Diagram.....	65
Figure 3-6	Point Target Spread Function in Azimuth Direction .....	66
Figure 3-7	Focusing Diagram.....	67
Figure 3-8	Resolution of Focused and Unfocused SAR .....	67
Figure 3-9	(a)Raw data Image after Range Compression.....	68
Figure 3-9	(b) Azimuth Compression without Focusing .....	68
Figure 3-9	(c)Azimuth Compression with Focusing .....	69
Figure 3-10	Ground Data Processing Unit Interface.....	69
Figure 3-11	Targets on Ground and Slant Plane .....	70
Figure 3-12	Video Data Image .....	70
Figure 3-13	Image after DDC (RFG1).....	71
Figure 3-14	Image after Range Compression .....	71
Figure 3-15	Processing Final Image.....	72
Figure 4-1	Motion Measurement System.....	72
Figure 4-2	Actual Pictures of Motion Measurement System.....	73
Figure 4-3	Mapping Geometry in Geographic Coordinates .....	74
Figure 4-4	Lever Arm Phase Correction .....	74
Figure 4-5	Hardware Implementation Diagram of Motion Compensation .....	75
Figure 4-6	SAR Azimuth Mechanism Prototype .....	75
Figure 4-7	SAR Antenna Gimbals 1 <sup>st</sup> G Overview .....	76
Figure 4-8	SAR Antenna Gimbals 4 <sup>th</sup> G Overview.....	76
Figure 4-9	NI 7334 Motion Control Card and Extending Board.....	77
Figure 4-10	Power and Signal Flows of Antenna Gimbals.....	77



Figure 4-11	Console Program and User Interface of Antenna Gimbals .....	78
Figure 4-12	Polynomial Curve Fitting .....	79
Figure 4-13	InterSense Gyroscope .....	79
Figure 4-14	InterSense Gyroscope Data with Sampling Frequency 100Hz .....	79
Figure 4-15	3 <sup>rd</sup> Tracking in InterSense Gyroscope .....	80
Figure 4-16	Tracking Errors of InterSense Gyroscope .....	80
Figure 4-17	Spectrum of InterSense Gyroscope .....	81
Figure 4-18	Bode Diagram of (1-3 <sup>rd</sup> Order Highpass) Butterworth Filter .....	81
Figure 4-19	IMU Sampling Data with 100Hz Sampling Frequency .....	82
Figure 4-20	Spectrum of IMU .....	82
Figure 4-21	3 <sup>rd</sup> Tracking in IMU .....	83
Figure 4-22	Tracking Errors of IMU .....	83
Figure 5-1	Algorithmic Steps in PGA .....	84
Figure 5-2	Input Image of PGA .....	84
Figure 5-3	Center-shifted Image .....	85
Figure 5-4	(a)Non-coherent Average .....	85
Figure 5-4	(b)Windowed Image by 20dB .....	86
Figure 5-5	Image without Linear Phase Removal .....	86
Figure 5-6	Corrected Image with Estimating Phase by PGA .....	87
Figure 5-7	(a)Center-shifting after PGA .....	87
Figure 5-7	(b)Non-coherent Average after PGA .....	88
Figure 5-7	(c)Windowed Image by 20dB after PGA .....	88
Figure 5-8	Corrected Image by Second Iteration of PGA .....	89
Figure 5-9	Original Image .....	89
Figure 5-10	Estimated Phase Error Functions .....	90
Figure 5-11	Low SNR Image for PGA Simulation .....	90
Figure 5-12	PGA Steps .....	91
Figure 5-13	Low SNR Image after 2 Iterations PGA .....	92
Figure 5-14	Estimated Phase Error Functions of Low SNR Imagery .....	92
Figure 6-1	Actual Antenna and Gimbals .....	93

## List of Tables

Table 2-1	Radio Frequency Bands .....	94
Table 4-1	Motion Cutoff Frequency of a UAV .....	94
Table 4-2	Tracking RMS Errors of Intersense Gyroscope and IMU .....	95



## Chapter 1 Introduction

### 1.1 Motives and Objectives

The word RADAR is derived from radio detection and ranging, thus conveying these two purposes of detection and location range. By transmitting radio waves and listening for their echoes, a radar can detect objects day or night and in all kinds of weather. Image radar is one kind of advanced radar systems. The importance of imaging sensors for Earth's surface observation is well established and planetary missions have also largely benefited from use of such system. Imaging sensor systems can be generally classified as passive and active. The synthetic aperture radar (SAR) system is the classical active imaging sensor system as know to all for high resolution images. In the last few years, high quality images of the Earth produced by SAR systems carried on a variety of airborne and space platforms have become increasingly available like in the Persian Gulf War. SAR is a coherent imaging sensor base on the advantages of all-weather, day and night imaging capabilities coupled with the achievable high resolutions. By the improvement of technique today, resolutions of a SAR system on the order of a few meters or tens of meters can almost be achieved with optical sensing system like visible and infrared sensors etc. The sensing system can be operated at hundreds of kilometers of altitude.

A critical problem in most of airborne SAR sensors is the compensation of motion errors induced by atmospheric turbulence, i.e. the compensation of changes of platform forward velocity vector in orientation and magnitude. The necessity to take into account these perturbations is well-known and exhaustive

discussions on aberrations caused by uncompensation motion errors. In particular, the main effects introduced by motion errors in the SAR images are degradation of the geometric and radiometric resolutions, azimuth ambiguities, and geometric and phase distortions. Motion perturbations can be measured by using systems like the inertial measuring unit (IMU) or the inertial navigation system (INS). Appropriate processing of the data acquired by accelerometers and gyroscopes of the IMU or INS allows reconstruction of the three translation components (along track, cross track, vertical) of the airplane motion as well as the three angular ones - roll, pitch, yaw (or calling heading) at the IMU location.

SAR mapping involves the ground reflectivity as measured in range and Doppler filters. The Doppler filters are the synthetic antennas, which provide the high resolution. If the range gates and Doppler filters move on the ground during the integration time, the resultant image will be smeared by motion errors. So variation in the location of the synthetic array elements can cause degradation and resolution loss of the processed synthetic antenna pattern if the motion error is uncompensated.

All we do is to decrease even eliminate the motion effects on the radar images. In another word is to figure out the motion errors from the inertial sensing system and make the relative data from aircraft body to signal processing procedure.

## **1.2 Research Orientation**

Motion compensation refers to corrections for any change in the velocity vector. The preliminary work of this research is to build up the actual airborne antenna gimbals and use many kinds of sensors to generate various flying parameters of an aircraft. All kinds of sensors can be classified the following

three systems: global position system (GPS), inertial measurement unit (IMU) and inertial navigation system (INS).

Under the PC-based environments, steer the antenna gimbals to the right orientation exactly through the NI motion control card and use the Microsoft Visual C++ 6.0 to program appropriate application software. In addition, there is a tracking control algorithm written in this software to predict aircraft's attitudes. For simulation, we will exercise by using MATLAB for signal process in high-speed computer and stabilize the aircraft vehicle of antenna gimbals using six-axis Stewart platform with two-axis gimbals mounted on it and estimate for real-time requirements of aircraft on air. For experience, van test runs on highlands or cross-bridges of freeway may an ideal action before flight runs.

In signal processing procedure, we must analyze the synthetic array signals. Integrate the motion sensors on the aerial vehicle and antenna gimbals for echo signals. Another approach for dynamic compensation considers the autofocus of synthetic signal. Technology of autofocus adopts the phase gradient autofocus (PGA) algorithm to avoid smeared images. Finally the main purpose is to compensate the aircraft motion effecting on the airborne radar through reading the data back form the navigation system, and make the radar image have normal display.

## Chapter 2 Synthetic Aperture Radar System

As the meanings of the words RADAR, by concentrating the waves into a narrow beam, it can determine direction. And by measuring the transit time of waves, it can measure range. To find a target, the radar beam is repeatedly swept through a search scan. Once detected, the target may be automatically tracked and its relative velocity computed on the basis of either periodic samples of its range and direction obtained during the scan or continuous data obtained by training the antenna on the target. Usually, the radio frequency bands useful for radar are listed by [Table 2-1](#)<sup>[1]</sup> and RF designers will keep bands away from the GSM and other wireless system to avoid interference in military applications.

Because of the Doppler Effect, the radio frequencies of the radar echoes are shifted in proportion to the reflecting object's range rates. By sensing these shifts, which is possible if the radar's pulses are coherent, the radar can measure target closing rates, reject clutter, and radar can measure ground return and differentiate between ground return and moving vehicles on the ground. It can even measure its own velocity. Since radio waves are scattered in different amounts by different features of terrain, a radar can map the ground. Basically, SAR system is the same with a common radar but different from that Doppler frequency shift equals in phase varying. It can be regarded as the strategy of time replacing space to form an array antenna on the sky. Terminology of array signal processing is Fourier Beamforming. On the other words, SAR does an uniform linear array (ULA) antenna as a spatial filter. With SAR, detailed maps can be made<sup>[2][3][4]</sup>. [Figure 2-1](#) shows the architecture of a SAR system.

## 2.1 Architecture of Synthetic Aperture Radar System

As Figure 2-1, there are many function elements in a SAR system. Most airborne radars employ only one antenna, which is time-shared for transmission and reception, to conserve space and minimize cost. The transmitter generates the radio signal which is used to illuminate the target and from which the echo is derived. Transmitter can be either amplifying type where the waveform is generated at low levels and amplified, or they can be power oscillators, where the illumination signal is generated at the required energy level. The receiver amplifies the echo signals to a level sufficient for later system components, such as the signal processor. It filters incoming signals to remove out-of-band interference and to optimize the response in a specific type of interference. The antenna concentrates the illumination signal into a narrow beam radiated in a signal preferred direction, intercepts the target echo signals from this same preferred direction, and matches the system impedance to those of the propagation medium. The antenna can be steered, so that the radar can search or track in many directions. The synchronizer times the transmission of the radar pulses. The modulator provides pulses of input power to the transmitter. High level modulators supply the main direct current (DC) operating power for the transmitter. The duplexer switches the shared antenna between transmitter and receiver. Since the switching action must take place within nanoseconds, the switch is electronic. The antenna servo positions the antenna beam to the desired azimuth and elevation angles and reports these angles to the system. The signal processor may a high-speed microprocessor like TMS320C6x or Intel series with RAID storages to do image formatting. The procedure will expound on next chapter later. To be provided with the above elements, SAR can operate

specifically.

As explained above, SAR takes advantages of the forward motion of the radar to produce the equivalent of a long antenna. Each time a pulse is transmitted, the radar occupies a position a little farther along on the flight path. By pointing a reasonably small antenna out to one side and summing the returns from successive pulses, it is possible to synthesize a very long sidelooking linear array.

## 2.2 Concept of Synthetic Aperture Radar

However, for the altitudes at which satellite or airborne imaging sensors operate in the 1-10GHz of frequency region, engineering difficulties make it is impossible to achieve value of good resolution. For example, the new Canadian satellite RADARSAT, launched in 1995, orbits at 792km and operated at C-band (5.3GHz frequency). The real aperture limit to the azimuth resolution would be about 3km. But through the use of synthetic aperture technology, however, RADARSAT can achieve a very fine resolution as low as 9m, several hundred times of the real aperture.

The SAR concept is usually attributed to Carl Wiley of Goodyear Aircraft Corporation in 1951. However, its first experimental validation was carried out in 1953 by a group of scientists at the University of Illinois. This was the beginning of a series of activities that contributed to the development of SAR techniques<sup>[5]</sup>. Before understanding it, there is something to know. Following lists introduce the nouns interested in radar territory.

Pulse repetition frequency: This is the rate at which a radar's pulses are transmitted - the number of pulses per second. It is referred to as the Pulse Repetition Frequency (PRF) and is commonly represented by  $f_r$ . The PRFs of



airborne radars range anywhere from a few hundred hertz to several hundred kilohertz. For reasons, PRF should consider of the radio frequency, the portion of electromagnetic spectrum for any radar is shown in [Figure 2-2](#). During the course of radar's operation, its PRF may be changed from time to time. Another measure of pulse rate is the period between the start of one pulse and the start of the next pulse. This is called the interpulse period or the pulse repetition interval (PRI). It is generally represented by the upper case letter  $T$  and  $T = \frac{1}{f_r}$ .

**Coherence:** The first wave front of each pulse must be separated from the last wave front of the same polarity in the preceding pulse by a whole number of wavelengths – a quality called coherence.

**Beamwidth:** A radar antenna concentrates all of the transmitted energy into a narrow beam within which the power is uniformly distributed. The width of the mainlobe is called the beamwidth. It is the angle between opposite edges of the beam. Beamwidth is determined primarily by dimensions of antenna aperture. For a uniformly illuminated circular aperture of diameter  $d$ , the 3dB beamwidth is about

$$\theta_{3dB} \cong \frac{\lambda}{d} \quad (2-1)$$

where  $\lambda$  is wavelength of radiated energy and  $d$  is diameter of circular aperture.

**Azimuth and elevation angle:** In most airborne radars, direction is measured in terms of the angle between the line of sight to the target and a horizontal reference direction such as north, or the longitudinal reference axis of the aircraft's fuselage. This angle is usually resolved into its horizontal and vertical components. The horizontal component is called azimuth and the vertical component is elevation, shown as the geometry of airborne radar of [Figure 2-3](#).

The along track axis is the velocity direction making aircraft's forward and another, cross track axis is perpendicular to along track coordinate axis. The slow time means the aircraft velocity much slower than the radio wave velocity of propagation, so fast time means the direction of microwave transmitted.

### 2.2.1 The Doppler Frequency

The Doppler frequency of the return from a patch of ground is also proportional to the range rate divided by the wavelength. The only difference is that the range rate of a patch of ground is due entirely to the radar's own velocity. Therefore, the projection of the radar's velocity on the line of sight to the patch can substitute for  $-\dot{R}$ . For a ground patch dead ahead, this projection equals the radar's full velocity,  $V_R$ . For a ground patch directly to the side or directly below, the projection is zero. In between, it equals  $V_R$  times the sine of the angle,  $\theta_L$ , between  $V_R$  and the line of sight to the patch, as [Figure 2-3](#). Since the return echo will be shifted by the same amount, the Doppler frequency shift for the ground target is

$$f_d = 2 \frac{V_R \sin \theta_L}{\lambda} \approx \frac{2V_R x}{\lambda R} \quad (2-2)$$

where  $f_d$  is Doppler frequency of ground patch,  $V_R$  is velocity of radar,  $\theta_L$  is angle between ground target and line of sight to patch,  $\lambda$  is transmitted wavelength,  $x$  is the target position on the ground in azimuth coordinate, and  $R$  is the slant range. This value provides a means of determining exactly where the echo signal came from. For a return signal detected by the antenna at a time corresponding to the slant range  $R$  and with a Doppler frequency shift of  $f_d$ , the ground target of the azimuth coordinate must be the following.

$$x = \frac{f_d \lambda R}{2V_R} \quad (2-3)$$

Even if another target is at range  $R$  and within the beam at the same time, measurement of its Doppler frequency shift  $f_d$  still allows us to associate it with an azimuth coordinate.

## 2.3 Resolution Analysis

The performance of a SAR system is depended on the images quality. The quality of the ground maps produced by radar is gauged primarily by the ability of the radar to resolve closely spaced features of the terrain. This ability is generally defined in terms of resolution distance and cell size<sup>[6]</sup>. Resolution distance is the minimum distance on the ground by which two points on the ground may be separated and still be discerned individually by the radar. The separation is usually expressed in terms of a range component and an azimuth or cross-range component. Overall, the resolution of a radar antenna can be described by two parts, range resolution and cross-range (azimuth or angular) resolution. Resolution required for various mapping applications should be different for features to be resolved. Usually, coast lines, large cities, and the outlines of mountains are required about 100m or above per cell size. Major highways, variations in field are 20m to 30m per cell about. Road map details are 10m, and vehicles, house, small buildings are 1m to 3m per cell size, respectively.

### 2.3.1 Range Resolution

Range resolution is the ability to separate multiple targets at the same angular position, but at different ranges. Range resolution is a function of the

radar's RF (radio frequency) signal bandwidth, with wide bandwidths allowing targets closely spaced in range being resolved. To be resolved in range, the basic criterion is that targets must be separated by at least the range equivalent of the width of the processed echo pulse. The waveforms represent the echoes as a function of time (ranges). The pulses are shown after reception and signal processing. Targets, if they are to be resolved, must be separated by a larger range width the long pulse than with the short. A handy way of estimating range and range resolution is that one microsecond propagation time corresponds to a two-way range of 150 meters. That can be expressed by following equations.

$$\Delta R = \frac{c\tau}{2} \quad (2-4)$$

where  $\Delta R$  is the range resolution,  $c$  is the velocity of propagation and  $\tau$  is the processed target pulse width. The effective bandwidth of any pulsed wave is approximately the reciprocal of the pulse processed width. Thus range resolution can also be described in bandwidth terms as following

$$B \approx \frac{1}{\tau} \quad \text{and} \quad \Delta R \approx \frac{c}{2B} \quad (2-5)$$

where  $B$  is the transmitted signal matched bandwidth.

### 2.3.2 Angular Resolution

Angular resolution is the azimuth resolution or cross-range resolution in SAR. Cross-range is the linear dimension perpendicular to the axis of the antenna, specified as azimuth (horizontal) or elevation (vertical) cross-range. Cross-range resolution gives the radar the ability to separate multiple targets at the same range. Resolution in cross-range is determined by the antenna's

effective beamwidth, with narrow antenna beams resolving more closely spaced targets. The criterion for cross-range resolution is that targets at the same range separated by more than the antenna beamwidth are resolved. Those separated by less than a beamwidth are not. The principle of cross-range resolving width antenna beams with a scanning search radar can be described by

$$\Delta X_{az} \approx R\theta_{3dB} \quad (2-6)$$

where  $\Delta X_{az}$  is the cross-range resolution,  $R$  is target range and  $\theta_{3dB}$  is the antenna beamwidth.

By using the equation (2-1), the beamwidth of an antenna is related to its length and the wavelength of the electromagnetic wave, which is the length of one cycle of the sinusoidal wave as it propagates through the propagation medium (usually in the atmosphere). The cross-range relationship becomes



$$\Delta X_{az} \approx R \frac{\lambda}{L_{eff}} \quad (2-7)$$

where  $\lambda$  is the signal's wavelength,  $L_{eff}$  is the effective length of the antenna in the direction and then the 3dB beamwidth is being calculated.

## 2.4 SAR Operating Modes

Operationally, SAR has several striking advantages. First, with a small physical antenna operating at wavelengths suitable for long-range mapping, SAR can provide azimuth resolutions as fine as a foot or so. Second, by increasing the length of the array in proportion to the range of the area to be mapped and the resolution can be made independent of range. Third, since the array is formed in the signal processor, the basic SAR technique can conveniently be adapted to a wide variety of operational requirements.

Added to these advantages are those of all radar mapping. Maps can be made equally well day or night, through smoke, haze, fog, or clouds. The maps are plan views and can be made even at shallow grazing angles. So far it has been improved upon and adapted to special requirements in a variety of modes. Some of the more important of these are squinted array, multilook mapping, spotlighting, Doppler beam sharpening (DBS), strip mapping, moving-target display, and inverse SAR (ISAR) imaging. Now, we just briefly described spotlighting, Doppler beam sharpening, and strip mapping in the followings.

Spotlight mapping, by gradually changing the look angle of the real antenna as the radar advances and making appropriate phase corrections, the radar can repeatedly map a given region of interest. This mode, called spotlight, see [Figure 2-4](#), not only enables the operator to maintain surveillance over an area for an appreciable period of time but can produce maps of superior quality.

Strip mapping, in real-time SAR mapping, if the radar's azimuth look angle is  $90^\circ$ , this is called the strip mapping. For a strip map, the central point must travel along the ground in a straight line at the speed of the aircraft. For a fully stabilized map, the central point moves along a straight line in inertial space regardless of the motion of the aircraft, see [Figure 2-5](#). A tube of some reasonable diameter is established to allow reasonable maneuvering and yet not unduly complicate the motion compensation problem.

Doppler beam sharpening (DBS), this mode differs from other SAR modes in that the length of the array is not increased in proportion to the area to be mapped but is the same for all ranges. The maps, therefore, are the same as those produced by a real array having an extremely narrow beam—hence the name Doppler beam sharpening. Typically, the antenna continuously scans the region of interest on one side of the flight path or the other, or both, see [Figure](#)

## 2-6.

Operationally, SAR has many compelling advantages. They are followings.

- (a) Affords excellent resolution with a small antenna even at very long ranges.
- (b) Where desired, provides resolution as fine as a foot or so.
- (c) Enable resolution to be made independent of range.
- (d) Produces recognizable images of ships and aircraft on the basis of their rotational motions.
- (e) Long standoff for threat avoidance.
- (f) Flexible flight profile.
- (g) Immune to adverse weather and battle induced atmosphere condition.
- (h) Steerage beam, shadow avoidance, and optimum data acquisition, and
- (i) It is exceptionally versatile.



## Chapter 3 Signal Processing

The kernel of synthetic aperture radar system is its signal process. This chapter will describe the primary flow of procedure of the received echo signal. As each pulse had been transmitted, a receiver gate has to open for input information of the signal to front end of RF. A SAR processor will work real time on this moment. Following, we will discuss the signal processing of a SAR.

### 3.1 Signal of Array

A SAR processor is the technical realization of the signal compression in the range and azimuth. For further speaking, it can be regarded as space-time process. Image pixels on down-range axis are processed by pulse compression in time domain and image pixels on cross-range axis are formed by spatial matched filter (Fourier beamformer) in space domain<sup>[7]</sup>. In SAR, the signal is synthetic array little different from a real array. In synthetic array, the incremental elements are sequentially and their outputs must be stored until the full array has been summed and formed. But in real array, the incremental elements are formed simultaneously, and the beam is formed by summing the outputs of each element. These can be interpreted the drift by [Figure 3-1](#). Now, considering a uniform linear array, the one-way radiation pattern for a real array is

$$E_{\text{Real}}(\sin \theta) = 1 + e^{jkd \sin \theta} + \dots + e^{jk(M-1)\sin \theta} = \sum_{i=1}^M e^{jk(i-1)d \sin \theta}, \quad k = \frac{2\pi}{\lambda} \quad (3-1)$$

and the real two-way radiation pattern in magnitude is



$$P_{real}(\sin \theta) = |E_{real}(\sin \theta)|^2 = \left| \frac{\sin(\frac{kMd}{2} \sin \theta)}{\sin(\frac{kd}{2} \sin \theta)} \right|^2 \quad (3-2)$$

where  $\theta$  is the incident angle of source from far field and  $M$  is the antenna array number, and  $d$  is inter-pulse distance (IPD) of each antenna. For a synthetic array, as a result of one antenna transmitting and receiving itself, two-way radiation pattern is

$$E_{syn}(\sin \theta) = 1 + e^{j2kd \sin \theta} + \dots + e^{j2k(M-1) \sin \theta} = \sum_{i=1}^M e^{jk2(i-1)d \sin \theta}, \quad k = \frac{2\pi}{\lambda} \quad (3-3)$$

and the synthetic two-way radiation pattern in magnitude is

$$P_{syn}(\sin \theta) = |E_{syn}(\sin \theta)| = \left| \frac{\sin(kMd \sin \theta)}{\sin(kd \sin \theta)} \right| \quad (3-4)$$

Figure 3-2 shows the simulation of beam pattern in synthetic and real array using MATLAB<sup>[8]</sup>. As the figure exhibiting, the synthetic array will increase the resolution but induce the grating lobe with same elements in real array. To avoid grating lobe, choose  $d = \frac{\lambda}{4}$  and increase synthetic array numbers, i.e. increase

coherent integration time (CIT) showed in Figure 3-3. By this method, we can both obtain the good resolution and avoid the ambiguity.

### 3.2 Signal Processor Structure

Generally, SAR image is a 2-D image formation, one is down-range and another is cross-range. The purpose of signal processor is to derive from the SAR raw data. Starting from optical techniques, over analog electronics up to modern digital SAR processors, several possibilities are existent to realize the

necessary computational steps. Nowadays, in the time of very powerful digital hardware, mostly digital methods are used, either realized in software or by using hardware signal processing. The principal sequence of processing SAR raw data is shown in [Figure 3-4](#). In the processing, the signal is complex in flow. It can be separated into five parts of reference function generator (RFG). The reference function means signals which had been formulated to compare or calculate in flow. These reference functions are important for signal processing when a good image is producing. We will discuss by following now.

### **3.2.1 RFG0**

The zeroth reference function generator (RFG0) includes the direct digital synthesis (DDS) hardware and the general motion compensation function. In the past, the circuit to generate and control a carrier for RF end was analogy. For now, mixed integrated circuits replace traditions in modern technology. DDS is consisted of auto gain controller (AGC), pulse generator, oscillator and mixer, and other digital control circuits etc. Motion compensation I is the key in this function block. It compensates the deviation of the receiving signal by inertial navigation sensor (INS). It affects linear phase adjustment for path translation primarily. The detail of motion compensation will be discussed in next chapter. The number zero stands for a most front of processing and the importance of RFG0 is indispensable and essential.

### **3.2.2 RFG1**

After RFG0, the data are converted by analog-to-digital converter (ADC). It is down digital conversion (DDC). In this time, signal will be filtered out the intermediate frequency (IF) and sometimes take both components for IQ

sampling and detection. When removing IF, signals locate in base band and also in complex form, and stored in a register or the memory.

### 3.2.3 RFG2

Because of the data transmitted by a linear frequency modulation (LFM), that must be demodulate in range domain. It is the so-called range compression including a FFT and an inverse FFT operation like the block of RFG2 of the [Figure 3-4](#). After an one-dimensional Fourier transformation, multiplying demodulation reference function, and an inverse Fourier transformation, images will produce range bin which compressed signal to have good resolutions. There will be some description of pulse compression theory later.

### 3.2.4 RFG3

After range compression, each range gate fits the range resolution but may disperse energy because of airplane deviation and variance of pulse repeated frequency (PRF). There are two kinds of PRF designed for motion. One is fixed PRF and the other is variable PRF with respect to airplane's velocity. Either fixed or variable PRF might do range gate phase adjustment to gather point energy. To do RFG3 is depend on motion models. Targets contained at or near the ground plane and located in the upper half of the image, actually are located below the slant plane and have a greater grazing angle. The shadows are a little shorter. On the contrary, targets contained at or near the ground plane and located in the lower half of the image, actually are located above the slant plane and have a lesser grazing angle. The shadows are a little longer. Fixed PRF cause each antenna position wrong and need to resample. Furthermore, precision time is a key point in RFG3 which is only just supported on INS. The

data are interpolated to obtain correct new data. Then, the position error is sensed by the motion measurement subsystem (MMS) and is used to compensate for the range to the image central reference line (CRL).

Autofocus is another point in RFG3. In general, to do autofocus in first step need to transform the image to the range compression domain. In real time consideration, the computer reduces one times the Fourier transformation in this data flow of RFG3. Therefore, next Fourier transformation of RFG4 will be as an inverse Fourier transformation for autofocus to back to image domain. By this design, autofocus will occupy only less than one percent of CPU running time for real time imaging. About autofocus, we will discuss in later chapter.

### **3.2.5 RFG4**

Finally, the step of data flow is azimuth compression. In this function block also has two FFT computations. But before doing this, memory stored the range compression data after RFG3 need to transpose. Such memory as this is called corner turn memory. Read in row direction and write in column vector. Azimuth compression as a Fourier beamformer forms array antenna to obtain good angle resolution and also described later. The focusing problem is caused near field of ground target. Like human's eyes, SAR image also has a focus section in large map. Luckily, that can be refocused by signal processing compensating to achieve each pixel (range bin) on focal distance.

## **3.3 Processing in Range**

In range direction of a SAR can work just like a conventional radar. To achieve a high resolution in the direction perpendicular to the flight direction, only a short pulse duration is necessary. In practice, it can be problematic to

generate a very short and high power pulse, as the resulting energy densities are hard to handle. Another possibility to generate a high signal bandwidth is to use a long but frequency modulated pulse. It is common to use for this a linear frequency modulation (LFM), also be called “chirp”.

### 3.3.1 LFM for Pulse Compression

A pulsed chirp or LFM radar signal is defined as

$$p(t) = a(t) \exp(j\beta t + j\alpha t^2) \quad (3-5)$$

where  $a(t) = 1, 0 \leq t \leq T_p$  and is zero otherwise.  $T_p$  is chirp pulse duration and  $\alpha$  is chirp rate. A chirp pulse is a phase modulation (PM) signal. So the instantaneous frequency of the chirp pulse in pulse duration is the derivative of its phase function with respect to time, as following

$$\omega_{ip} = \frac{d}{dt}(\beta t + \alpha t^2) = \beta + 2\alpha t \quad (3-6)$$

If the chirp rate is larger than zero, the instantaneous frequency is an increasing function of time, and such a chirp is said to be upsweep. Thus the carrier (central frequency) of a chirp pulse is

$$\omega_c = \beta + \alpha T_p \quad (3-7)$$

and its baseband bandwidth is

$$B = 2\alpha T_p \quad (3-8)$$

Clearly the baseband bandwidth of a chirp pulse increases with its duration. In the case of a pulsed chirp radar signal, the echoed signal from the target scene can be rewritten as follows

$$\begin{aligned}
s(t) &= \sum_n \sigma_n a\left(t - \frac{2x_n}{c}\right) \exp\left[j\beta\left(t - \frac{2x_n}{c}\right) + j\alpha\left(t - \frac{2x_n}{c}\right)^2\right] \\
&= \sum_n \sigma_n a\left(t - \frac{2x_n}{c}\right) \exp\left[j\beta\left(t - \frac{2x_n}{c}\right)\right] \exp\left[j\left(\alpha t^2 - \frac{4\alpha x_n}{c}t + \frac{4\alpha x_n^2}{c^2}\right)\right] \quad (3-8)
\end{aligned}$$

where  $\sigma_n$  is the reflective intensity from the  $n$ th target. Then we replace the equation (3-8) by  $t_n = \frac{2x_n}{c}$ , and we obtain the equation as

$$s(t) = \sum_n \sigma_n a(t - t_n) \exp[j\beta(t - t_n)] \exp[j(\alpha t^2 - 2\alpha t_n t + \alpha t_n^2)] \quad (3-9)$$

In equation (3-9),  $t_n$  is the round-trip delay for the echoed signal from the  $n$ th target<sup>[9]</sup>.

### 3.3.2 Reconstruction

If we mix the complex conjugate of signal with the phase of the transmitted chirp signal, we obtain

$$\begin{aligned}
s_c(t) &= s^*(t) \exp(j\beta t + j\alpha t^2) \\
&= \sum_n \sigma_n a^*(t - t_n) \exp(j\beta t_n + j\alpha t_n^2) \exp(2\alpha t_n t) \quad (3-10)
\end{aligned}$$

which is called the time domain compressed or dechirped or deramped signal. Similar to the mixing of the echoed signal with the carrier for baseband conversion, the pulse compression is also performed by hardware or software. The resultant signal is then lowpass filtered and sampled. The presence  $\exp(j2\alpha t_n t)$  of the equation (3-10) is the sinusoidal in the deramped signal. The frequency of this sinusoidal carrier is  $2\alpha t_n$  which carries information on the round-trip delay  $t_n$  or the target range  $x_n$ . Thus, by examining the Fourier

spectrum of the compressed signal, one should see some kind of energy distribution at the frequency  $2\alpha t_n$  which can be used to identify the target range.

In fact the Fourier transform of the compressed signal is

$$\begin{aligned} S_c(\omega) &= \sum_n \sigma_n \exp(j\beta t_n + j\alpha t_n^2 - j\omega t_n) \text{psf}(\omega - 2\alpha t_n) \\ &= \sum_n \sigma_n \exp(j\beta t_n + j\alpha t_n^2 - j\omega t_n) \text{psf}\left(\omega - \frac{4\alpha x_n}{c}\right) \end{aligned} \quad (3-11)$$

where the point spread function in frequency domain for pulse compression is defined as

$$\text{psf}(\omega) = \mathcal{F}[a^*(t)] \quad (3-12)$$

and the  $a(t)$  is a rectangular pulse, such that the point spread function is a *sinc* function. This indicates that the signature of the  $n$ th target appears at the frequency as following

$$x_n = \frac{c}{4\alpha} \omega \quad (3-13)$$

which carries information on the range coordinates of the target. By this, the range resolution is

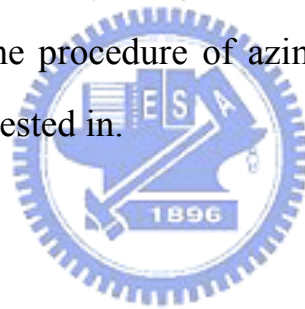
$$\Delta x = \frac{\pi c}{2\alpha T_p} \quad (3-14)$$

The above indicates that the mixing of the complex conjugate of  $s_n(t)$  with the phase  $p(t)$  results in a single-tone sinusoid. Thus a spectral analysis of the resultant signal  $s_c(t)$  yields information on the location of the targets<sup>[9]</sup>.

### 3.4 Processing in Azimuth

The echo of a single point target is contained in many received radar pulses and appears therefore defocused. The aim of SAR processing is to focus all received energy of a target, distributed over the illumination time, on one point at the reference position. In order to achieve this, the typical phase history coming from the data acquisition process is used. That is the same as processing in range.

Regardless of range of targets, different azimuth positions of targets have different Doppler frequency effect. If the velocity of the aircraft is constant and maintain only one direction, all targets will be properly located at the different portion of Doppler frequency domain. Because the Doppler filter can be used to distinguish any target individually, targets can be determined on the right position. Now we abridge the procedure of azimuth compression but analysis some we concerned and interested in.



### 3.4.1 Abscissa Analysis

The abscissa where we discuss here means cross-range coordinates. From Giorgio Franceschetti's<sup>[5]</sup> point of view, the sampling distance in synthetic arrays is different from the real phase array radar. It is not half of the wavelength  $\lambda$ . Let us consider a platform carrying the radar system and moving along a linear trajectory in azimuth direction. Consider  $(2N+1)$  equally spaced positions of the real antenna and  $n = -N, \dots, N$   $n = -N, \dots, N$ , as depicted in Figure 3-5. Assume that the antenna to radiate isotropically within its beam width and according equation (2-1), thus it provides the illuminated patch that

$$X \approx \frac{\lambda r}{L} \quad (3-15)$$



over the ground, and where the  $L$  is the real antenna physical effect size. The signal backscattered by the target and received by the antenna after the heterodyne process is given by

$$f(nd) \approx \exp\left[-j\omega \frac{2r}{c} - j \frac{2\pi}{\lambda r} (nd)^2\right] \quad (3-16)$$

So the azimuth-dependent part of the return is given by

$$f(nd) \approx \exp\left[-j \frac{2\pi}{\lambda r} (nd)^2\right], \quad n = -N \dots N \quad (3-17)$$

where  $nd$  is the discrete abscissa of SAR system along its path. This processing operation corresponds to synthesizing an array of length  $X=2Nd$ . We introduce the azimuth reference function as

$$g(nd) \approx \exp\left[j \frac{2\pi}{\lambda r} (nd)^2\right], \quad n = -N \dots N \quad (3-18)$$

where the term  $2\pi / \lambda r$  is as chirp rate  $\alpha$  of equation (3-1). As for range case, processing is usually performed in the transformed domain by multiplying the discrete Fourier transformation (DFT) of equation (3-17) and equation (3-18) by each other, and then coming back to the spatial domain. Then we obtain the following

$$y(nd) = \frac{\sin\left[\frac{2\pi d^2}{\lambda r} n(2N+1-n)\right]}{\sin\left(\frac{2\pi d^2}{\lambda r} n\right)} \cong 2N \frac{\sin\left(\frac{2\pi Xd}{\lambda r} n\right)}{2N \sin\left(\frac{2\pi d^2}{\lambda r} n\right)} \quad (3-19)$$

Moreover, normalization is convenient and this is accomplished by dividing all lengths by  $X$ . Accordingly, equation (3-19) becomes

$$y(nd) = \frac{\sin(\frac{2\pi X^2}{\lambda r} x)}{\frac{X}{d} \sin(\frac{2\pi X d^2}{\lambda r} x)} = \frac{\sin(\frac{2\pi X}{L} x)}{\frac{X}{d} \sin(\frac{2\pi d}{L} x)} \quad (3-20)$$

by replacing the normalized discrete azimuth abscissa  $x = \frac{nd}{X}$  of the platform.

To ignore the amplitude factor  $\frac{X}{d}$  of equation (3-20), the target in the neighbors of the position  $x$  is zero, we have

$$y(x) \cong \text{sinc}(\frac{2\pi X}{L} x) = \text{sinc}(\frac{\pi}{\Delta x} x) \quad (3-21)$$

with

$$\Delta x = \frac{L}{2X} \quad (3-22)$$

that represents the normalized azimuth resolution. This apparently surprising result is that the smaller the antenna is, the better the resolution. The other word is easily explained by noting that a decrease of  $L$  implies an increase of  $X$  and a larger number of elements of the synthetic array. The former of equation (3-21) is periodic and its absolute value exhibits successive identical maxima at

$$2\pi \frac{d}{L} x = q\pi, \quad q = 0, \pm 1, \dots \quad (3-23)$$

If we require the envelope of  $y(t)$  in equation (3-20) to be a decreasing function of  $x$  within the azimuth signal extension  $|x| \leq 1/2$  to avoid azimuth ambiguity, then

$$2\pi \frac{d}{L} \frac{1}{2} \leq \frac{\pi}{2} \quad (3-24)$$

That is

$$d \leq \frac{L}{2} \quad (3-25)$$

which sets a limitation on the synthetic array spacing. In the case of real arrays the constraint set by equation (3-25) corresponds to the avoidance of grating lobes, as showing in Figure 3-6.

### 3.4.2 Resolution of Azimuth

Therefore, the spatial sampling rate of strip map SAR is  $d \leq \frac{L}{2}$  but not  $d \leq \frac{\lambda}{4}$ . Actually, the focusing of side-looking SAR has resolution by

$$\Delta x_{az} = r \theta_{syn \ 3dB} = \frac{\lambda r}{2L_{eff}} \quad (3-26)$$

and is instead of equation (3-15), the azimuth resolution will be obtained as

$$\Delta x_{az} = \frac{L}{2} \quad (3-27)$$

### 3.4.3 Focusing

The relationships are realizable only if the data are corrected to simulate a circular flight path around each scatterer. This process is called focusing. In Physics, the interval between the constructive interference and the destroyed interference is half of wavelength. To obtain a resulted image, we define the target distance between the farthest and the nearest must be less than  $\frac{\lambda}{8}$  (sometimes  $\frac{\lambda}{8}$ ). Therefore, for a round-trip, the distance of the longest and

nearest is  $(r + \frac{\lambda}{16})$  and  $r$ , respectively. By the Pythagorean Theorem, it derives that

$$(r + \frac{\lambda}{16})^2 = (\frac{L_{eff}}{2})^2 + r^2 \quad (3-28)$$

As Figure 3-7, if the processing is unfocused, the scatterers must always be in the far field of the synthetic antenna, limiting its length to the following value

$$L_{eff}^2 < \frac{\lambda r}{2} \quad (3-29)$$

Substituting this maximum value for effective synthetic array length into SAR resolution of equation (3-26) gives the best resolution for an unfocused SAR system by

$$\Delta x_{unfocused} = \sqrt{\frac{\lambda r}{2}} \quad (3-30)$$

Figure 3-8 shows the resolutions of real circular antenna, unfocused sidelooking SAR, and focused sidelooking SAR with respect to the range distance. For a focused SAR, the phase correction for the  $n$ th array element of the image each cell if the complete focusing is to be done. As following form giving by Pythagorean Theorem

$$(\Delta r + r)^2 = r^2 + (nd)^2 \quad (3-31)$$

where  $\Delta r$  is the range difference between the broadside SAR element and the  $n$ th element. Solving the above equation  $\Delta r$  gives

$$\Delta r_n = \frac{(nd)^2}{2r} \quad (3-32)$$

and the phase error associated with the range error is

$$\Delta\phi_n = \frac{2\pi(2\Delta r_n)}{\lambda} = \frac{2\pi(nd)^2}{\lambda r} \quad (3-33)$$

In addition, the phase correction required for focused operation is dependent on the range  $r$  which is called depth of focus. It is combined with equation (3-33) and given by

$$|\Delta\phi_n| = \frac{2\pi(nd)^2}{\lambda} \left| \frac{1}{r} - \frac{1}{r + \Delta r_n} \right| \quad (3-34)$$

Focusing of the synthetic array involves some process which corrects the elemental signal phases such that all elements of the resulting array are at the same distance from the target. It also can be said to another phase correction of static motion compensation.

### 3.5 Simulations

First, we simulate the RFG4 with a picture in raw data downed by the web <http://epsilon.nought.de/>. The parameters of processing are 0.056m by wavelength, 100m/s by sensor velocity, 3000m by sensor height, range distance by 4000m, 500Hz by PRF, and 100MHz by range sampling. From above, the azimuth resolution can be determined to 0.5m. Figure 3-9(a) shows the simulation of RFG4 of raw data after range compression. Figure 3-9(b) shows the azimuth compression without focusing processing. Figure 3-9(c) does the range adaptation with focusing azimuth.

Second, we simulate the overall signal processing from received raw data to the final image. Figure 3-10 is the interface of SAR ground data processing unit. The video signal model expressed for the IF signal due to a single point garget is derived form Franceschetti<sup>[5]</sup> in references . That is

$$f(t) = \exp\left[-j\omega\frac{2r}{c} + j\frac{\alpha}{2}\left(t - \frac{2r}{c}\right)^2\right] \text{rect}\left[\frac{t - 2r/c}{\tau}\right] \quad (3-35)$$

Figure 3-11 shows the corner reflectors on the ground plane corresponding to slant plane. In the Figure 3-11, the apparent target location is modified by both the true position (via the true grazing angle) and its real height above the assumed ground plane. Figure 3-12 shows the simulation of video data image. Figure 3-13 is the image after DDC (RFG1). Figure 3-14 shows the image after range processing and Figure 3-15 displays the final image.



## Chapter 4 Sensor-based Motion Compensation

SAR was assumed that the aircraft was flying at constant speed in a perfectly straight line. But this is virtually never the case. Since the whole SAR concept revolves around the effect of very slight differences in the phases of signals received over a comparatively long period of time, typically 1 to 10 seconds, it is essential that any acceleration of the aircraft during that period be compensated. The acceleration may be measured either by accelerometers mounted on the antenna or by a separate inertial navigation system (INS), the outputs of which are referenced to the phase center of the antenna.

On the basis of the measured acceleration, phase corrections are computed, that is called sensor-based motion compensation. These may be applied to the received signals at virtually any point in the radar system, from local oscillator to final integration. Where presuming is employed, the corrections may, for example, be applied on a sample-by-sample basis after the presuming. The formation of the synthetic aperture requires a coherent phase history be maintained during the time it takes to fly the synthetic aperture. Variation in the location of the synthetic array elements, if uncompensated, can cause degradation of the processed synthetic antenna pattern. Without motion compensation the aircraft is required to fly at a constant velocity (magnitude and direction). Motion compensation involves the electronic phase adjusting of the synthetic array element to achieve the coherent phase history.

### 4.1 Motion Measurement Sensor

Speaking simply, Motion Measurement system consists of the three parts:

global position system (GPS)<sup>[10]</sup>, inertial navigation system (INS) and inertial measurement unit (IMU). GPS is that a network of 24 satellites continuously transmits high-frequency radio signals, containing time and distance data that can be picked up by any GPS receiver, allowing the user to pinpoint their position anywhere on Earth. It has 1 hertz update rate to correct the drifted error caused by Earth's itself rotation. From GPS, we adopt the Earth-centered Earth-fixed (ECEF) coordinates. IMU consists of three gyroscopes and three accelerometers. Even modern IMU system, however, determining platform position to the required tolerances over the entire synthetic aperture can prove to be a difficult task. This is especially true for SAR system designed to produce high-resolution imagery. The required least precision of IMU in SAR is defined as following



$$T = \frac{K_s \lambda r}{2V \Delta x_{az}} \quad (4-1)$$

and

$$2\left(\frac{1}{2} \Delta a \times T^2\right) = \lambda \quad (4-2)$$

and

$$\Delta x_{az} = \Delta V \times T \quad (4-3)$$

where  $\Delta x_{az}$  is cross-range resolution,  $\lambda$  is the wavelength of radio frequency (RF),  $V$  is aperture velocity,  $R$  is Range, and  $K_s$  is synthetic array weighting constant. By this, we got coherent integration time  $T$  is about 3 seconds, and line-of-sight acceleration accuracy  $\Delta a$  is about 0.35 mg, and perpendicular velocity accuracy  $\Delta V$  is 1 m/s.

Overall, what we got from the MMS is the only four parameters: position,



velocity, attitude, and time to do motion compensation. [Figure 4-1](#) is the brief MMS block diagram. [Figure 4-2](#) shows the picture of actual MMS system which includes IMU in [Figure 4-2\(a\)](#) and navigation computer in [Figure 4-2\(b\)](#).

## 4.2 Motion Compensation for Phase Adjustment

Aircraft motion is caused by both weather disturbances and intentional maneuver. High frequency motion causes a loss in dynamic range, i.e. degraded sidelobes, and resolution loss. The effect of very low frequency motion is to cause geometric distortion and poor map accuracy. Motion compensation refers to corrections for any change in the velocity vector caused by either atmosphere disturbances or intentional maneuvering.

To provide motion compensation the location of the aircraft with respect to the ground being imaged must be accurately known and differential motion changes must be measured very accurately. Motion compensation is applied to the received signal by way of the reference function. This is the central motion compensation path. Other functions, such as integration time, range gating, and the display must also be compensated<sup>[11][12]</sup>.

Before the following, the mapping geometry must to be understood. The unit vector is defined by two angles, one is azimuth and the other is elevation. The azimuth angle is called the map heading angle  $H_M$ , and is the angle from the inertial reference north to the ground point being imaged, measured in a plane parallel to the Earth's surface. The elevation angle  $E_S$ , is measured form the horizontal plane of the aircraft to the ground point in a vertical plane. These angles are illustrated in [Figure 4-3](#).

### 4.2.1 Translational Displacement Path

In SAR processing the reference function must accurately track the input signal so that there is no time-varying phase is to displace energy from the main beam of the filter (synthetic antenna) into the sidelobes causing a loss in amplitude, resolution, and higher sidelobes. An offset error in prediction the location of a point on the ground or a small constant  $\Delta V$  error will cause an azimuth shift in the location of the target.

The phase return of the ground point which is to be imaged is given by

$$\phi(t) = \frac{4\pi}{\lambda} R(t) \quad (4-4)$$

and

$$R(t) = R_0 - \int V_L dt \quad (4-5)$$

where  $R_0$  is the initial range and  $V_L$  is the line-of-sight velocity between the antenna and the ground point. The line-of-sight velocity is found from

$$V_L = \vec{u} \cdot \vec{V} \quad (4-6)$$

where  $\vec{u}$  is the unit vector to the ground point and  $\vec{V}$  is the aircraft velocity vector. Thus, both velocity vector and pointing vector must be known. Notice that the range is computed to find the phase reference and, thus, the range gate position is adjusted by slaving the range gates to  $R(t)$ . The velocity vector is generally provided by an inertial reference and is usually in the geographic coordinates of north, east, and vertical. The unit vector is determined by tracking the ground point, as shown in Figure 4-3. That is, the position vector between antenna and ground point is dynamically computed and the unit vector is thus defined. The position vector is given by

$$\vec{P} = \vec{P}_0 - \int \vec{V} dt \quad (4-7)$$

and the unit vector is given by

$$\vec{u} = \frac{\vec{P}}{|\vec{P}|} \quad (4-8)$$

where  $\vec{P}_0$  is the initial position.

The reasoning so far has been to develop the phase reference for a single ground point. But a ground map is made up of many such points or cells and, in general, each cell must be motion-compensated differentially. If the velocity vector is rotated through  $H_M$  and  $E_S$ , rather than using the dot product, the velocity vector  $\vec{V}$  in map coordinate is obtained.

$$\vec{V} = \begin{bmatrix} V_L \\ V_A \\ V_K \end{bmatrix} \quad (4-9)$$

$V_L$  is the line-of-sight velocity to a map point,  $V_A$  is the velocity at which the projected synthetic aperture is flown (normal to  $V_L$ ), and  $V_K$  is the velocity normal to the slant range plane determined by  $V_L$  and  $V_A$ . For another next point n, located at an azimuth angle  $\Delta a$  and elevation angle  $\Delta e$  with respect to the main point O, the line-of-sight velocity is

$$V_{L_N} = \begin{bmatrix} \cos(\Delta a) \cos(\Delta e) \\ \sin(\Delta a) \cos(\Delta e) \\ -\sin \Delta e \end{bmatrix}^T \begin{bmatrix} V_{L_o} \\ V_{A_o} \\ V_{K_o} \end{bmatrix} \quad (4-10)$$

For small angular displacement, equation 3-7 becomes

$$V_{L_N} = V_{L_o} + \Delta a V_{A_o} - \Delta e V_{K_o} \quad (4-11)$$

Thus, all the motion compensation points are easily and linearly related, and only one point need be tracked for typical mapping situations.

The unit vector, besides determining the velocity vector rotation, also stabilizes the real antenna and determines the lever arm correction for the displacement between antenna phase center and inertial navigation system (INS) axis. Next subjects will discuss the motion compensation for the antenna stabilization and lever arm path.

#### 4.2.2 Lever Arm Path

The antenna and inertial sensor are physically displaced with respect to each other. The inertial platform measures displacement between its axis and the image point. It is necessary that the motion compensation be applied with respect to the antenna phase center, since this how the signal phase shift occurs. Therefore, the motion as measured at the center of the inertial sensor must be translated to the center of the antenna. Let the physical displacement between the inertial sensor and antenna as measured in the aircraft body axis be  $\vec{l}_B$ . Then the lever arm phase correction is

$$\phi_L = \frac{4\pi}{\lambda} \vec{u}_B \cdot \vec{l}_B = \frac{4\pi}{\lambda} l \cos \alpha \quad (4-12)$$

where  $\vec{l}_B$  is the vector of the lever arm with respect to aircraft body and the phase reference as measured at the antenna is

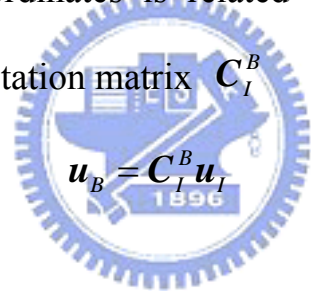
$$\phi_L = \phi_{ANT} = \phi_I - \phi_L \quad (4-13)$$

where  $\phi_I$  is the phase reference computed from the inertial measured velocity vector. This is illustrated in [Figure 4-4](#), for a mechanically scanned antenna. The effect of the displacement between antenna gimbals axis and antenna phase center can be neglected, since this vector is parallel to the unit vector. The lever

arm is constant in aircraft body coordinates and easily measured. Figure 4-5 shows the design of implementation of the hardware function blocks. By summary, to compensate the spare phase of the translation path and lever arm path on-board is the primary stage in real time processing.

### 4.2.3 Antenna Stabilization

The radar antenna is servo to the unit vector by the antenna driving system. Its stabilization involves a series of coordinate rotations. The inertial reference is related to the aircraft axis through the heading (yaw), pitch, and roll gimbal angles,  $\psi$ ,  $\theta$ ,  $\varphi$  respectively, called aircraft Euler angle. Thus, the unit vector in aircraft body coordinates is related to the unit vector in inertial geographic coordinates by rotation matrix  $C_I^B$



$$\mathbf{u}_B = C_I^B \mathbf{u}_I \quad (4-14)$$

where

$$\mathbf{u}_I = \begin{bmatrix} \cos(H_M) \cos(E_S) \\ \sin(H_M) \cos(E_S) \\ -\sin E_S \end{bmatrix} \quad (4-15)$$

and

$$C_I^B = [\varphi][\theta][\psi] \quad (4-16)$$

and where  $[\varphi],[\theta],[\psi]$  are the 3x3 coordinate rotation matrixes:

$$\text{Roll angle} \quad [\varphi] = \begin{bmatrix} 1 & 0 & 0 \\ 0 & \cos \varphi & \sin \varphi \\ 0 & -\sin \varphi & \cos \varphi \end{bmatrix} \quad (4-17)$$

$$\text{Pitch angle} \quad [\theta] = \begin{bmatrix} \cos \theta & 0 & -\sin \theta \\ 0 & 1 & 0 \\ \sin \theta & 0 & \cos \theta \end{bmatrix} \quad (4-18)$$

$$\text{Heading angle} \quad [\psi] = \begin{bmatrix} \cos \psi & \sin \psi & 0 \\ -\sin \psi & \cos \psi & 0 \\ 0 & 0 & 1 \end{bmatrix} \quad (4-19)$$

In the above, the suffix letter I means inertial coordinate, letter B means aircraft body, and letter A means antenna gimbals coordinate.

For an electronically scanned antenna,  $\mathbf{u}_B$  can be used to calculate the beam-steering phase shifts which electronically point the antenna beam. For a mechanically scanned antenna,  $\mathbf{u}_B$  must further be rotated into antenna coordinates by another rotation matrix  $\mathbf{C}_B^A$



$$\mathbf{u}_A = \mathbf{C}_B^A \mathbf{u}_B \quad (4-20)$$

and

$$\mathbf{C}_B^A = [\sigma_E][\sigma_A] \quad (4-21)$$

where  $\sigma_A$  and  $\sigma_E$  are the antenna gimbals angles with the coordinate transform matrixes being

$$[\sigma_A] = \begin{bmatrix} \cos \sigma_A & \sin \sigma_A & 0 \\ -\sin \sigma_A & \cos \sigma_A & 0 \\ 0 & 0 & 1 \end{bmatrix} \quad (4-22)$$

$$[\sigma_E] = \begin{bmatrix} \cos \sigma_E & 0 & -\sin \sigma_E \\ 0 & 1 & 0 \\ \sin \sigma_E & 0 & \cos \sigma_E \end{bmatrix} \quad (4-23)$$

Combine (3-9) and (3-15), we got

$$\mathbf{u}_A = \mathbf{C}_B^A \mathbf{C}_I^B \mathbf{u}_I = \mathbf{C}_I^A \mathbf{u}_I \quad (4-24)$$

Note that all using the  $u$  this letter is the unit vector. Since the Euler angles are in Cartesian coordinate space, but in our radar gimbals mechanism is defined in sphere coordinates, we will transform from the Cartesian space to the sphere space or from the sphere space to the Cartesian space. And we assumed that the unit vector in radar antenna coordinates by following

$$\mathbf{u}_A = \begin{bmatrix} \Delta x \\ \Delta y \\ \Delta z \end{bmatrix} \quad (4-25)$$

where  $\mathbf{u}_A$  is the servo command for three dimensions in Cartesian space. The servo errors should be zero when the antenna is aligned to the unit vector. In our radar gimbals mechanism, there are only two axes to stabilize the aircraft body rotation which has three rotation degrees of freedom. Therefore, the final commands order to antenna gimbals can be written in arctangent form by

$$AZ = \tan^{-1}\left(\frac{\Delta y}{\Delta x}\right) \quad (4-26)$$

$$EL = \tan^{-1}\left(\frac{\Delta z}{\sqrt{\Delta x^2 + \Delta y^2}}\right) \quad (4-27)$$

Another way, our radar gimbals mechanism is elevation axis mounted on the azimuth axis, shown by [Figure 4-7](#) and [Figure 4-8](#). So that the order of  $[\sigma_E][\sigma_A]$  can not be exchanged absolutely.

#### 4.2.4 Motion Compensation in SAR Operation Mode

For a spotlight map, the above equations apply directly, since the spotlight map involves a small area about some central point. If the map is built up by stepping the processor azimuth filters across the ground area in azimuth, then

this stepping is accomplished by stepping the incremental angle  $\Delta a$  about the central point defined by  $H_M$  and  $E_S$ .

For a strip map, the central point must travel along the ground in a straight line at the speed of the aircraft. For a fully stabilized map, the central point moves along a straight line in inertial space regardless of the motion of the aircraft. A tube of some reasonable diameter is established to allow reasonable maneuvering and yet not unduly complicate the motion compensation problem. The motion compensation for the strip map case is accomplished by freezing the map heading angle  $H_M$ .

For a Doppler beam sharpening (DBS) mapping, as long as the map is inertial registered, full motion compensation can be applied. In general, DBS mapping is registered with respect to the velocity vector and, thus, only limited motion compensation can be applied as a rotating  $\vec{V}$  will smear the map. If a large angular sector with respect to an inertial reference, i.e., north, is selected, then motion compensation can be applied. In this case the unit vector is rotated through the angular sector to be imaged. This is accomplished by changing the map heading angle  $H_M$ .

### **4.3 Radar Control Mechatronical System**

To ensure the performance for a radar system working on the sky, a control system should be used to drive the radar gimbals. The preliminary job for this is to establish the radar gimbals and do the best to simulate every situation of an aircraft on the ground to substitute for occurring on the sky. PC-based controller is the best choice for high speed calculation, real-time operation, easy



programming, expansion ability, and good feasibility. Compact PC is less weight and can be carried movably.

Below we introduce the all radar control system consist of a host computer, motion control card, motion detected sensor, radar gimbals mechanism, drivers, and the mechatornical system on it.

### 4.3.1 Radar Mechanism

The gimbals in [Figure 4-6](#) and [Figure 4-7](#) is the prototype of radar gimbals designed by our laboratory (senior W.Z. Yu and peer Y.C. Tong). Because of the low power limitation (about 500W on the plane), the mechanism called tuning block as [Figure 4-6](#) is designed for the purpose of high efficiency and least power loss in a small workspace. That's just suitable for airborne side-looking SAR. We use the stepper motor with high resolution of 25000 steps to drive the antenna and give the feedback encoder of 2500 counts with 4 times ratio frequency, 10000 counts, through the PWM drivers. The inverse kinematics of [Figure 4-6](#) is

$$S_1 = f(T(\theta), S_0, R, L) \quad (4-28)$$

where  $S_1$  is the extended length of the linear actuator. [Figure 4-8](#) shows the fourth generation radar gimbals designed in our laboratory (Y.C. Tong). The mechanism is like the universal joint with cross two axes.

### 4.3.2 Motion Control Card

The motion control card we used is National Instrument 73series control card. The 7344 controllers are a combination of servo and stepper motor controllers for PCI, PXI, and 1394 bus computers. The 7344 controllers are

exclusively stepper motor controllers for PXI bus computers and 7334 controllers are PCI bus compatible. Figure 4-9 exhibits the NI 7344 PCI motion control card and its extending board. The utility of extending board may communicate between PC and encoders, limit switches or other sensors on gimbals. Then stepper axes on it control stepper motors. These can operate in open or closed-loop. The use quadrature encoders or analog inputs for position and velocity feedback (closed-loop only), and provide step direction or clockwise and counter-clockwise digital command outputs. All stepper axes support full, half, and micro-stepping applications in this controllers of 73series<sup>[13]</sup>. Figure 4-10 shows the digital command and sensor signal flows from the extending board and the power supplier. Figure 4-11 displays the console programming by Microsoft Visual C and its user interface edited by GPE of WinPC32.



### 4.3.3 Radar Control Using Tracking Algorithm

Our aerial carrier for airborne SAR is a pilotless plane called Unmanned Aerial Vehicle (UAV). UAVs are valuable tools for collecting information in high-threat areas where the risk is great for manned platforms. Table 4-1 lists the UAV characteristics by analyzing the model of aerodynamics but has the assumption of a constant level flight speed 70 knots (about 130 kilometers per hour). From Table 4-1, we assume that the UAV's motion frequency is under 5Hz for simulation later. Because of the antenna deviation caused by maneuvers, atmospheric gust, the antenna must be stabilized for always pointing the same direction during the integration time. For a SAR carrying out a task of strip map or squint map, the antenna will draw a straight line called central reference line (CRL). Actually, the central reference line and the aircraft flight path are given

before airplane taking off. In our gimbals, the axes have been specified the fixed angular velocity 20 degrees per second. For antenna stabilization, this is not fast enough to compensate the motion variation. Hence, a tracking technique for predicting the antenna's angular position is used. The method is polynomial curve fitting.

According to  $N$ th order polynomial as following, the position at time  $t$  is

$$f_x(C, t) = c_0 + c_1t + \dots + c_Nt^N \quad (4-29)$$

or can be written as

$$f_{x,k}(C_k, t) = \sum_{n=0}^k c_n t^n \quad (4-30)$$

where  $t = kT$  and  $k = 0 \sim N$ ,  $T$  is sampling time.

To solve the parameter of  $C$  with  $n$ th order polynomial, we must have  $k$ 's equations, that is,  $(n+1)$ 's equations. See Figure 4-12.

$$\begin{bmatrix} p(0) \\ p(1) \\ p(2) \\ \vdots \\ p(n) \end{bmatrix} = \begin{bmatrix} 1 & 0 & 0 & \dots & 0 \\ 1 & T & T^2 & & T^n \\ 1 & 2T & (2T)^2 & & \\ \vdots & \vdots & & \ddots & \vdots \\ 1 & nT & (nT)^2 & \dots & (nT)^n \end{bmatrix} \begin{bmatrix} c_0 \\ c_1 \\ c_2 \\ \vdots \\ c_n \end{bmatrix} \quad (4-31)$$

$$P = TC \quad (4-32)$$

we can determinate the matrix  $C$  by

$$C = T^{-1}P \quad (4-33)$$

and the extrapolated point  $p(n+1)$  can be estimated by

$$p(n+1) = \begin{bmatrix} 1 & (n+1)T & ((n+1)T)^2 & \dots & ((n+1)T)^n \end{bmatrix} C \quad (4-34)$$

The first gyroscope we used is produced by InterSense as the picture of Figure 4-13. Figure 4-14 represents the InterSense gyroscope data with

sampling frequency 100Hz. Figure 4-15 shows the simulation of tracking trajectory by using MATLAB. It is a 3<sup>rd</sup> order polynomial curve fitting method. Certainly, this tracking algorithm is based on the absence of high frequency disturbances or noise. The tracking error is presented in Figure 4-16 and the root mean square (RMS) error of tracking is 0.8655° in yaw, 1.1070° in pitch, and 1.0077 in roll. It is rough precision for antenna stabilization caused by sensor measurement noise. Figure 4-17 shows the frequency spectrum of this gyroscope. A Butterworth lowpass filter is proposed due to its outstanding lowpass properties. Note that the multiplication of all poles of this Butterworth lowpass filter<sup>[14]</sup> is unity, which guarantees the magnitude of the low frequency parts of the input signal almost unvarying. A 3<sup>rd</sup> order low-pass Butterworth filter with transfer function expressed as below is used here.

$$T(z) = \frac{0.2706z^3 - 0.1858z^2 - 0.259z + 0.1974}{z^3 - 2.374z^2 + 1.929z - 0.5321} \quad (4-35)$$

Unlike other lowpass filter, the equation (4-35) is one to subtract 3<sup>rd</sup> order highpass Butterworth filter because of avoiding phase delay, as Figure 4-18 shown. Phase delay may cause distortion from original gyroscope data. Without phase delay, the (1- highpass) would amplify the magnitude around the cut-off frequency. The trade-off occurs between phase delay and amplification around the cut-off frequency. After filtering the measurement noise, tracking performance has been improved and the root mean square (RMS) errors of yaw, pitch, and roll are 0.1058°, 0.1360°, and 0.1241°, respectively. The RMS error developed about one-tenth times.

As above description, using IMU to test the tracking algorithm in 4<sup>th</sup> generation gimbals. Since the IMU integrating with the INS which has Kalman

Filter in it, the simulation without software programmed filter also works well. [Figure 4-19](#) shows the IMU data sampling in 100Hz to simulate the transfer update data rate. As [Figure 4-20](#) showing, the spectrum compared with [Figure 4-17](#) is excepted from higher frequency of about 10Hz. The spectrum of InterSense gyroscope in range from 15Hz to 50Hz is disorderly and confused because of high measurement noise folding in. The 100Hz sampling frequency limited to about 200Hz by Nyquist low. But in IMU, the spectrum of motion always lies in 15Hz. This verifies the motion of the airplane based on assumption of less than 5Hz. Tracking results and its errors are showed in [Figure 4-21](#) and [Figure 4-22](#), respectively. The RMS of tracking errors of yaw, pitch, roll are  $0.0520^\circ$ ,  $0.0249^\circ$ ,  $0.0088^\circ$ , respectively, and better than InterSense tracking data after filtering. All computational RMS errors of tracking points in each situation list in [Table 4-2](#).

Summary, high order polynomial has higher sensitivity with respect to noise but more precise for tracking. A designed filter must efficiently filter out high frequency measurement noise to achieve polynomial tracking for simulation and implementation. A prerequisite of motion compensation is based on a good performance sensor even processes signal-based motion compensation. In fact, the 4<sup>th</sup> generation gimbals with IMU stabilizes the antenna co-operation very well on the aircraft. At least, the flight test in Pingtong acquires some good images to stride forward a big step on remote sensing for future.

## Chapter 5 Signal-based Motion Compensation

The motion compensation in signal measurement is frugal of navigation computation or accuracy sensors in airborne application of radar system. Successful formation of well focused images in an aperture synthesis imaging system requires precise phase stability and coherence over the synthesized aperture. Unknown phase errors across this aperture can have a disastrous effect on image quality. Therefore, phase error compensation is a problem common to all such imaging systems. Specifically, such aperture phase errors can arise due to numerous natural and measurement, induced sources. In SAR, uncompensated platform motion errors imaging primarily cause the source of these propagation effects to come into view of images. Tropospheric turbulence is predominant in these speckle imaging. Aperture synthesis radio astronomy suffers from both propagation effects and problems associated with maintaining phase coherence over widely separated receivers<sup>[15]</sup>. Motion Compensation of such these pulse-Doppler systems stands supreme station of its image formatting processing<sup>[16]</sup>. In this section, the topics in doing motion compensation without any measurement sensor and just using the signal history to estimate phase error function are called signal-based motion compensation.

### 5.1 Autofocus

In some cases, it is possible to instrument and measure some sources of phase errors or to use an existing phase reference to maintain coherency over the entire aperture without sensors. However, such phase errors manifest themselves as redundant information in the reconstructed image. This invites the

use of a data driven algorithm to estimate the phase error function and perform the restorative deconvolution. Phase errors present in a SAR signal history at the time of the final Fourier transform operation degrade image quality in several ways. The most serious degradation is often image defocus caused by the presence of uncorrected quadratic and higher order phase errors. Uncompensated motion between the SAR antenna phase center (APC) and the scene being imaged is a primary source of phase errors. Other sources include algorithm approximations, hardware limitations, and propagation effects.

Autofocus techniques improve image focus by removing a large part of any phase errors present after conventional motion compensation and data formatting procedures. Autofocus with respect to SAR imagery refers to the computer-automated estimation and subsequent removal of these residual phase errors. Autofocus generally encompasses two distinct steps of error estimation and error compensation. There are five kinds of autofocus techniques including mapdrift (MD), multiple aperture mapdrift (MAM), phase difference (PD), prominent point processing (PPP), and phase gradient autofocus (PGA). In a simple realization, PPP is also a space-invariant focusing technique. In more refined applications, PPP provides a full motion compensation capability that includes the ability to determine the scene rotation rate for SAR and ISAR applications. The topic of our signal-based motion compensation will focus on the PGA to perform by next.

## **5.2 Phase Gradient Autofocus Algorithm**

The phase gradient autofocus (PGA) algorithm for estimating higher order phase errors first appeared in the SAR literature in 1989<sup>[17][18]</sup>. PGA represents a significant departure from previously published autofocus techniques in several



ways. It is non-parametric and takes advantage of redundancy of phase error function by averaging across many range cells, and it is derived using one of the methods of formal optimal estimation theory known as maximum-likelihood estimation<sup>[19]</sup>. The PGA algorithm exploits this redundancy to obtain a linear minimum variance estimator of the phase error. It has been demonstrated to be robust, computationally, efficient, and easily implemented in standard digital signal processing hardware.

The algorithm is unique in that it is not model-based; implementation does not require explicit selection of a maximum order for the phase error being estimated. The PGA algorithm has a well-deserved reputation as a superior algorithm for higher order autofocus. It accurately estimates multicycle phase errors in SAR signal data representing images over a wide variety of scenes<sup>[20]</sup>. The PGA performs images as well as any estimation scheme possibly can. This is accomplished by comparing the performance of PGA to the so-called Cramer-Rao lower bound on estimator variance. As will be demonstrated, the estimator used in PGA works very well even if all the targets used in the estimation have signal-to-clutter ratios that are less than unity. The PGA algorithm consists of several critical steps that include center (circular) shifting, windowing, phase difference estimation, and iterative correction. These algorithmic steps are shown in the diagram of [Figure 5-1](#). In the following subsections, we demonstrate how each processing step contributes to robustness of the PGA autofocus methodology<sup>[20][21]</sup>.

### **5.2.1 Center Shifting**

From [Figure 5-1](#), the first step of PGA emphasizes that the input data must be complex image domain data. Sometimes, we propose that input can be after



range compressed data for some applications like real time SAR. The fundamental concept of the PGA algorithm is to average information across many targets for determining the phase error estimate. To this end, the algorithm attempts to isolate a number of single targets in the image for use in the estimation process. A nominal procedure for selecting targets is to choose one on each range line. In the input image, strong targets relative to the surrounding clutter naturally provide better potential for phase estimation than do targets with strength only on the order of the clutter. PGA selects the strongest target on each range line and circularly shifts it to the scene center. This circular-shifting operation preserves the effects of the phase error on the selected target while simultaneously removing any linear phase component in the azimuth dimension associated with that target. The removal of the linear phase component is desirable when the common aperture phase error function is estimated using integration across the range dimension. The shifting operation in essence creates a new image wherein all the targets to be used in the estimation process are aligned and stacked in the center of the scene.

[Figure 5-2](#) is the input data for simulation. That is an ISAR image of Boeing 727 transporter. The image has a high signal-to-noise ratio (SNR) for simulation. [Figure 5-3](#) does circular shifting operation of image in [Figure 5-2](#).

### **5.2.2 Windowing**

After center shifting, the next step in PGA is a windowing operation. The intent of windowing is to preserve the information contained in the center-shifted targets that describes the blurring kernel, while simultaneously rejecting information from all other surrounding clutter and targets. The PGA algorithm simply applies a rectangular window to the center-shifted data. In this

operation, the difficult part is to determine the width of windowing. If the window is too wide, an unnecessarily large amount of noise is admitted. On the other hand, it is important to capture all the center-shifted target energy so that none of the defocus effect on the selected target is lost. One method for automatic determination of the window width uses non-coherent averaging. The window width is estimated by simply summing the magnitude of the image data in the range direction for every cross-range position. This is described by

$$s(n) = \sum_{k=1}^N |g(k, n)|^2 \quad (5-1)$$

where  $g(k, n)$  is the circularly-shifted complex image data,  $N$  represents the total number of range lines, and  $n$  represents the image-domain cross-range position index. Because of the center-shifting process,  $s(n)$  will tend to achieve its maximum value at the center of the image and will typically exhibit a plateau having approximately the same width as the blur footprint. Thus, the blur width can be estimated by thresholding  $s(n)$  at some chosen level below its peak. The non-coherent average shown in Figure 5-4(a) displays the  $s(n)$  of the center-shifted image of Figure 5-3 and Figure 5-4(b) is chosen as the window width of 20dB below the peak. Low-order phase errors cause a distinct broadening of the mainlobe of the point target response (IPR). High-order phase errors, however, do not significantly broaden the mainlobe of the IPR; instead, they raise its side lobe. Usually, for high SNR image, we propose the wider (high dB values) window width, and for low SNR image, the narrower (low dB values) window width may be better.

### 5.2.3 Phase Estimation

That the circular-shifting operation will not change the frequency domain value of cross-range image lines matches the next fast Fourier transformation (FFT). The model for the transformed data is then taken to be

$$G(k, m) = a(k)e^{j\phi(m)} + \eta(k, m) \quad (5-2)$$

where  $k$  represents the range lines, and  $m$  is the aperture position index.  $a(k)$  is the different for each range line. The noise term  $\eta(k, m)$  models the interfering clutter that surrounds a selected point target. In particular, the noise  $\eta(k, m)$  is assumed to be zero mean, white Gaussian, and independent of the signal term  $a(k)$ . In short, it is assumed that within the image-domain window, the target is a point reflector surrounded by clutter targets, which are modeled as independent identically distributed (iid) white Gaussian noise.

A direct approach to the phase estimation problem is to use all data points to derive a maximum-likelihood (ML) estimation of  $\phi(m)$ . A simpler approach, and the one that has become the most widely used in real SAR systems, is to use data on two adjacent pulses at a time to estimate the phase difference between them. These differences may then be integrated to obtain an estimate for the entire  $\phi(m)$ . In the phase difference algorithm,  $\Delta\phi(m) = \phi(m) - \phi(m-1)$  is estimated for each value of  $m$ . Then the ML estimator of this adjacent-pulse phase difference is found to be

$$\Delta\hat{\phi}(m) = \underset{\Delta\phi}{\text{argmax}} \sum_{k=1}^N \{G^*(k, m-1)G(k, m)\} \quad (5-3)$$

where  $\Delta\hat{\phi}(m)$  denote the ML estimate of  $\Delta\phi(m)$ . Specifically, it is unbiased and is efficient over a broad range of signal-to-clutter ratios. Once the estimate

for  $\Delta\phi(m)$  is obtained for all  $m$ , the entire aperture phase error is estimated by integrating the  $\Delta\hat{\phi}(m)$  values. Mathematically, this is given by the expression

$$\hat{\phi}(m) = \sum_{l=2}^m \Delta\hat{\phi}(l), \quad \hat{\phi}(1) = 0 \quad (5-4)$$

Thus, the phase estimation portion of PGA consists of estimating the phase differences for all adjacent pulses using equation (5-3), followed by integrating or summing the results to get  $\hat{\phi}(m)$ . The angle between two complex numbers  $G(k, m-1)$  and  $G(k, m)$  can be obtained as  $\Delta\phi(m) = \angle\{G^*(k, m-1)G(k, m)\}$ .

By contrast, the ML estimator works extremely well even in situations when all the individual target-to-clutter ratios are well below 0 dB, which is the condition when the noise vector and the signal vector for an individual target are of similar size.



#### 5.2.4 Linear Phase Removal

Usually the autofocus processing is placed after sensor-based motion compensation as the description of chapter 4 such that the algorithm has been designed without linear phase problem. Ideally, no linear phase will be estimated in signal-based computation. But actually, estimation method like PGA or other autofocus will not apply any linear phase that will cause the image to shift. Some residual linear phase remaining in the processing should be removed. A simple regressive method proposes to be applied here. Assuming that the motion deviation can be written in Taylor Series Expansion form as

$$R(t) = R_0 + R'(t)t + \frac{1}{2}R''(t)t^2 + \frac{1}{6}R'''(t)t^3 + \dots \quad (5-5)$$

where  $R_0$  is constant,  $R'(t)$  is linear term,  $\frac{1}{2}R''(t)$  is quadrature term and others are higher order term. Constant phase does not affect the image at all, but linear phase will shift the displacement of the image and higher order term will degrade the image quality.

The regressive method to remove linear phase uses the results of the estimated phase as following

$$\hat{\Phi} = ax + b \quad (5-6)$$

or

$$\begin{bmatrix} \hat{\phi}_1 \\ \hat{\phi}_2 \\ \vdots \\ \hat{\phi}_m \end{bmatrix}_{m \times 1} = \begin{bmatrix} x_1 & 1 \\ x_2 & 1 \\ \vdots & \vdots \\ x_m & 1 \end{bmatrix}_{m \times 2} \begin{bmatrix} a \\ b \end{bmatrix}_{2 \times 1} \quad (5-7)$$

The suffix number means aperture position and let  $\mathbf{X} = \begin{bmatrix} x_1 & x_2 & \dots & x_m \\ 1 & 1 & \dots & 1 \end{bmatrix}^T$

and  $\mathbf{C} = \begin{bmatrix} a \\ b \end{bmatrix}$ , then the equation (5-6) can be replaced as

$$\hat{\Phi} = \mathbf{X}\mathbf{C} \quad (5-8)$$

Using the inverse matrix to find that

$$\mathbf{C} = (\mathbf{X}^T \mathbf{X})^{-1} \mathbf{X}^T \hat{\Phi} \quad (5-9)$$

The parameter  $a$  in matrix  $\mathbf{C}$  is the linear phase. [Figure 5-5](#) shows the image without linear phase removal.

### 5.2.5 Correcting Phase

The phase error estimates produced by equation (5-3) and (5-4) may now be

used to correct the degraded image. This process is identical for all phase correction algorithms and simply involves multiplying the degraded range-compressed data by the complex conjugate of the phase error estimated. Mathematically, this is given by the operation

$$G_c(k, m) = G_e(k, m)e^{-j\hat{\phi}(m)} \quad (5-10)$$

where  $G_c(k, m)$  denotes the corrected range compressed data. Substituting the corrupted range-compressed model, we have

$$G_c(k, m) = G(k, m)e^{-j(\hat{\phi}(m)-\phi(m))} \quad (5-11)$$

If the phase error estimate  $\hat{\phi}(m)$  is equal to the true phase error  $\phi(m)$ , the corrected range-compressed data are equal to the uncorrupted range-compressed data and the image will have been perfectly restored. All that remains is to transform the corrected range-compressed data to the image domain using one-dimensional inverse Fourier transformation. Figure 5-6 exhibits the image corrected by estimating phase error function.

### 5.2.6 Iterating

Of course, the phase error estimation is only as good as the assumptions that are used in its derivation. In practice, it is very difficult to precisely center shift the target when it has been degraded by a phase error function. This is because a phase-degraded target is smeared so that its true peak can not be located without some error. In addition, it is not unusual in real SAR imagery to have two strong targets on the same range line spaced sufficiently close together in cross-range that the windowing procedure captures a portion of the neighboring target. For these reasons, it is often necessary to execute the PGA

algorithm in an iterative manner, in an attempt to converge on the correct center shifting and target isolation. Therefore, after the image is corrected using the initial ML estimate of the phase error function, the entire process is repeated on this refocused image. A sequence of incremental phase error function is thus computed. On each iteration,  $\hat{\phi}(m)$  is updated by addition of the current incremental estimate. As  $\hat{\phi}(m)$  becomes more accurate, the targets become more compact and allowing more accurate center shifting and smaller windowing to be used with each iteration. The decreasing window width also decreases the probability of capturing undesired competing targets within the window. An estimated incremental phase error function with small total energy implies that the marginal benefit from the phase error produced at this iteration is negligible. The algorithm is terminated when the energy or rms value of the estimated incremental phase error function on any iteration falls below a prescribed threshold. The image in Figure 5-7(a) shows the center-shifting of image after a PGA procedure. The non-coherent average function in Figure 5-7(b) windows the image resulted in Figure 5-7(c) with 20dB width and yields a sharper peak than does the initial PGA. This is because the targets are now better focused. Usually the sharper peak indicates a smaller window can be used on this iteration. In general, as the iterations progress, the non-coherent average peak becomes much more defined, resulting in a decreasing window width. Figure 5-8 shows the corrected image after the second iteration. In many cases, the convergence occurs at once iteration just. Functions of applied phase error, first PGA estimation, and estimation after second iteration are illustrated by Figure 5-9. That can be compared with Figure 5-10 of the original image.

### 5.3 Low SNR Consideration of PGA

Even if the signal of SAR data received the low SNR to the clutter, PGA also works well. The reason is that the signal vector is obtained as a sum of smaller vectors of each range bins which correspond to the compressed domain information contributed by the center-shifted target on a given range line. As a result, they will add coherently to produce the signal vector larger than clutters or noises when averaging larger bins. It can be shown that for the case of large values of range bins, the noise or clutter becomes a small probability bloc at the tip of the summed signal vector. By contrast, simply averaging the phases of a set of targets all having poor SNR or signal-to-clutter ratio does not lead to a useful estimate of common phase. But in PGA, the ML estimator works extremely well even in situation when all the individual target-to-clutter ratios are well below 0 dB, which is the condition when the noise vector and the signal vector for an individual target are of similar size. In following, we will demonstrate such this performance via the simulations of SAR imagery. [Figure 5-11](#) shows the low signal-to-clutter image for simulation. The results of the steps of the second iteration are shown in [Figure 5-12\(a\)-\(h\)](#). [Figure 5-13](#) exhibits the final image after 2 iterations PGA in low SNR image. The estimated phase error functions plots in [Figure 5-14](#).



## Chapter 6 Conclusion

Airborne SAR systems possess remote information of real time obviating the weather and time of the day. Unlike Satellites SAR, airborne SAR must oppose against the perturbation motion on troposphere of the Earth. As great progress of the electronic technology today, precious and precise sensors acquire the motion to be redeemed. By these techniques, a generalized motion compensation approach applicable to all SAR mapping modes can be accomplishable. Beyond this, the antenna on the aircraft executes the stabilization automatically to avoid miss-pointing of the target. Integrating the inertial navigation and recommending antenna gimbals tie in with the motion cleverly to operate the front-end of motion compensation. Design of the antenna gimbals also plays an important role on this work. The photograph of antenna and gimbals used in this thesis was taken in [Figure 6-1](#).

In addition, the digital signal processing on radar system is another key to be concerned. The PGA algorithm has been shown to be an effective and robust tool for correcting radar phase errors in SAR imagery. It is also shown that it can accommodate phase error functions of arbitrary complexity spatial-frequency content. Currently, PGA is being adopted into a significant number of operational SAR systems even in other communication systems.

In future, there are many researches and developments in the topic of SAR. It takes a milestone in such topic and gives new challenges of radar system.

## References

- [1] George W. Stimson, Introduction to Airborne Radar, Second Edition, Scitech, New Jersey, 1998
- [2] Walter G. Carrara, Ron S. Goodman, Ronald M. Mfajewski, Spotlight Synthetic Aperture Radar, Signal Process Algorithms, Artech House, Boston/London, 1995
- [3] Roger J. Sullivan, Microwave Radar Image and Advanced Concepts, Artech House, 2000
- [4] Chris Oliver, Shaun Quegan, Understanding Synthetic Aperture Radar Images, Artech House, Boston/London, 1998
- [5] Giorgio Franceschetti, Riccardo Lanari, Synthetic Aperture Radar Processing, Boca Raton/London/New York/Washington D.C., 1999
- [6] G. J. A. Bird, Radar Precision and Resolution, John Wiley & Son , New York, 1974
- [7] Byron Edde, RADAR Principle, Technology, Applications, Prentice-Hall International, 2<sup>nd</sup> Editions, 1993
- [8] Bassem R. Mahafza, Radar Systems Analysis and Design Using MATLAB, Chapman and Hall/CRC, Boca Raton/London/New York/Washington D.C., 2000
- [9] Mehrdad Soumekh, Synthetic Aperture Radar Signal Processing with MATLAB algorithms, Wiley-Interscience Publication, 1999
- [10] Mohinder S. Grewal, Lawrence R. Weill, Angus P. Andrews, Global Positioning System, Inertial Navigation, and Integration, John Wiley & Sons, US, 2001
- [11] John C. Kirk Jr., Motion Compensation for Synthetic Aperture Radar, *IEEE*

*Transactions on Aerospace and Electronic Systems, Vol. AES-11, No.3, May 1975*

- [12] John C. Kirk Jr., SAR, ISAR and Motion Compensation, Goleta Engineering, February 1998
- [13] Motion Control, FlexMotion Software Reference Manual, National Instruments, November 1998
- [14] Alan V. Oppenheim, Ronald W. Schaffer, John R. Buck, Discrete-Time Signal Processing, Prentice-Hall, 2<sup>nd</sup> Edition, 1999
- [15] Jae Sok Son, Gabriel Thomas, Benjamin C. Flores, Range-Doppler Radar Imaging and Motion Compensation, Artech House, Boston London, 2000
- [16] Guy Morris, Linda Harkness, Airborne Pulsed Doppler Radar, Artech House, 2<sup>nd</sup> Edition, 1996
- [17] John C. Kirk Jr., Russ Lefevre, Randy van Daalen Wetters, Don Woods, Brendan Sullivan, Signal Based Motion Compensation, *IEEE international radar conference*, 2000
- [18] D. E. Wahl, C. V. Jakowatz, Jr., P. A. Thompson, D. C. Ghiglia, New approach to strip-map SAR autofocus, *Digital Signal Processing Workshop, 1994 Sixth IEEE*, pp.53-56, Oct. 1994
- [19] C. V. Jakowatz, Jr., D. E. Wahl, Eigenvector method for maximum-likelihood estimation of phase errors in synthetic aperture radar imagery, *Journal of the Optical Society of America, A*, vol.10 No.12, pp.2539-2546, December 1993
- [20] Charles V. Jakowatz, Jr., Daniel E. Wahl, Dennis C. Ghiglia, Paul A. Thompson, Spotlight-Mode Synthetic Aperture Radar, a signal processing approach, Kluwer Academic Publishers, Boston/London/Dordrecht, 1996

[21]歐彥甫, 航空雷達之運動補償, 碩士論文, 國立交通大學, 機械工程研究所, 2002

[22]Francois Le Chevalier, Principles of Radar and Sonar Signal Processing, Artech House, Boston/London, 2002

[23]Mehrdad Soumekh, Fourier Array Imaging, Prentice-Hall, New Jersey, 1994



## Figures

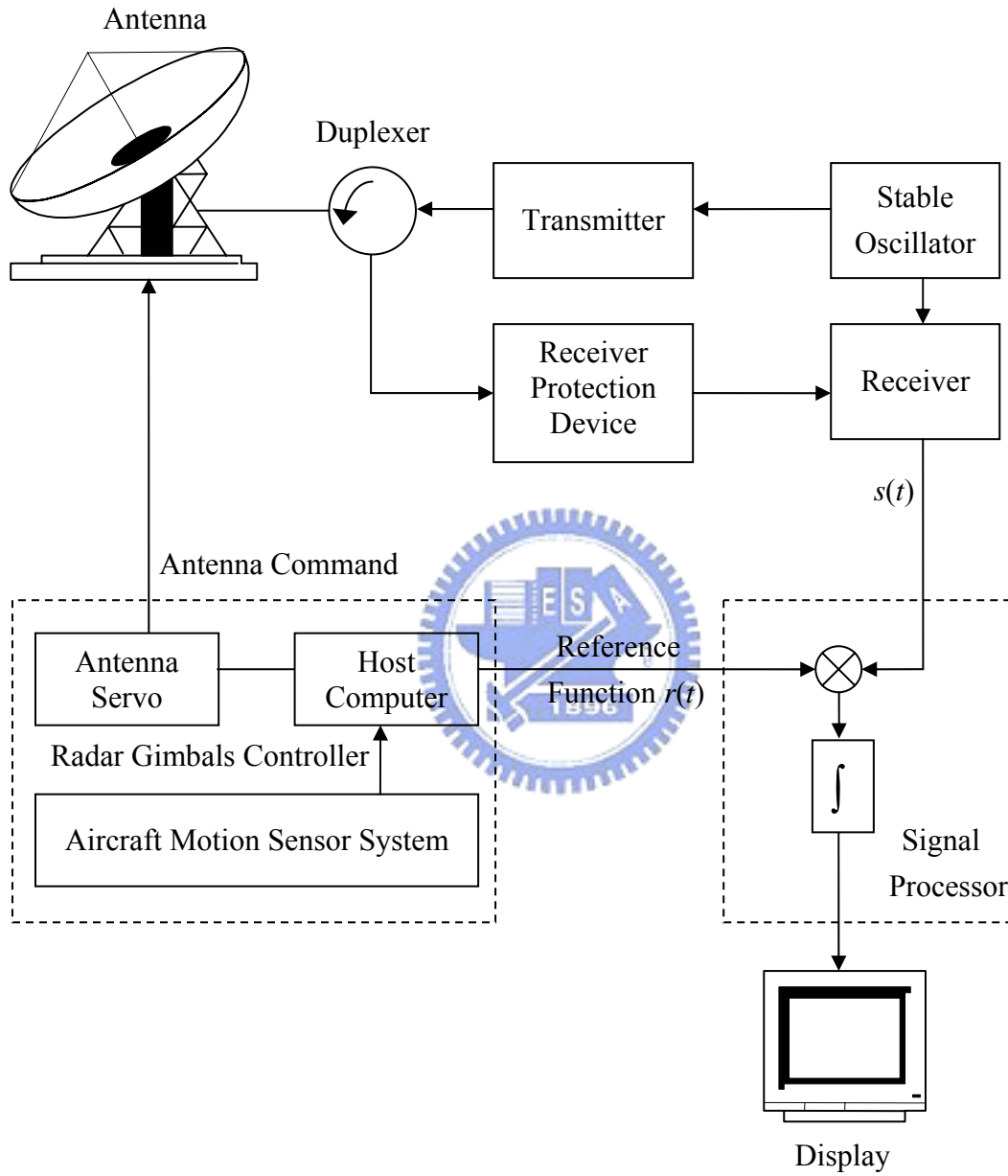


Figure 2-1 A Radar System Architecture

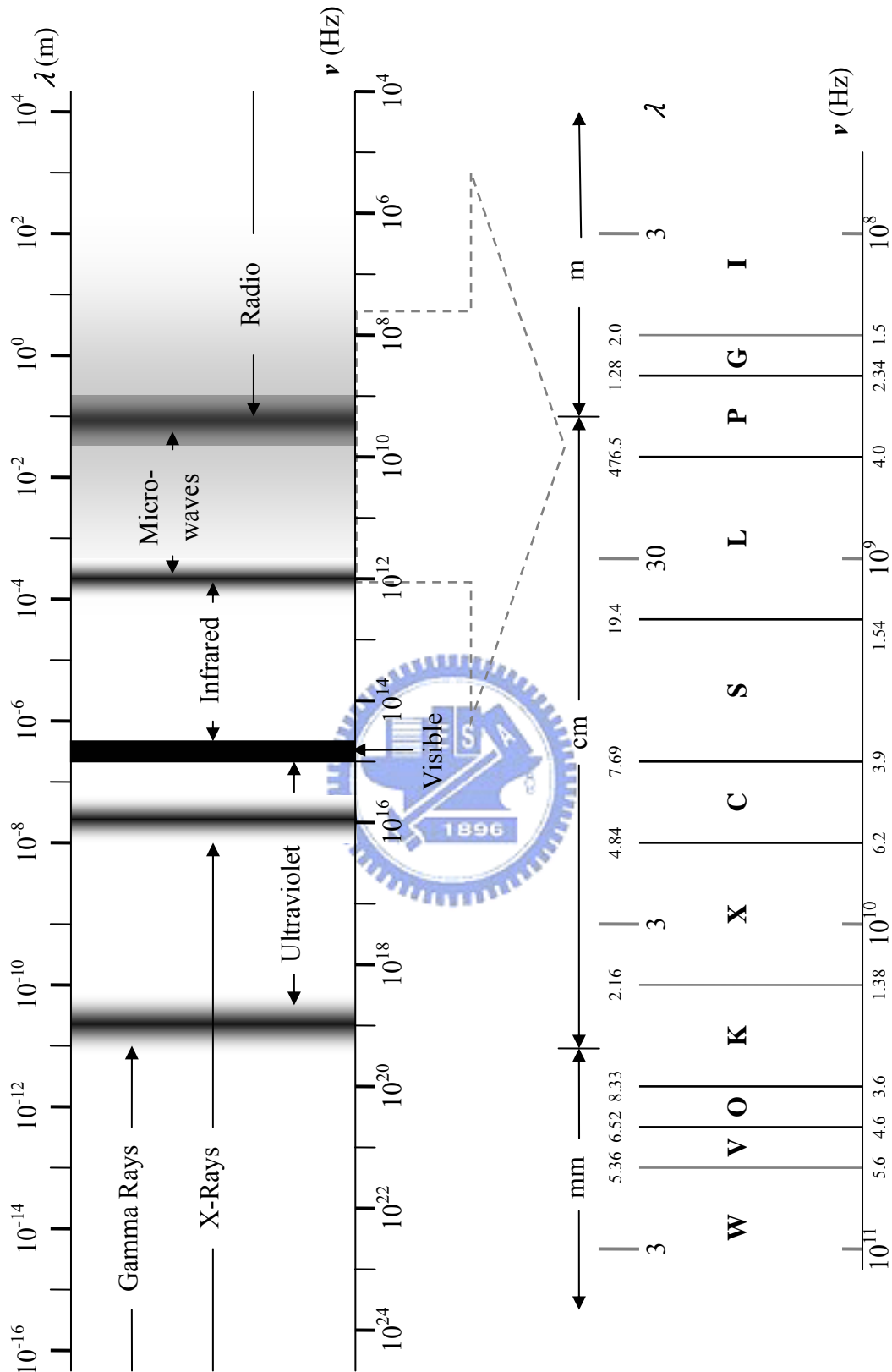


Figure 2-2 Electromagnetic Spectrum and Microwave Frequency Bands

Useful for Imaging

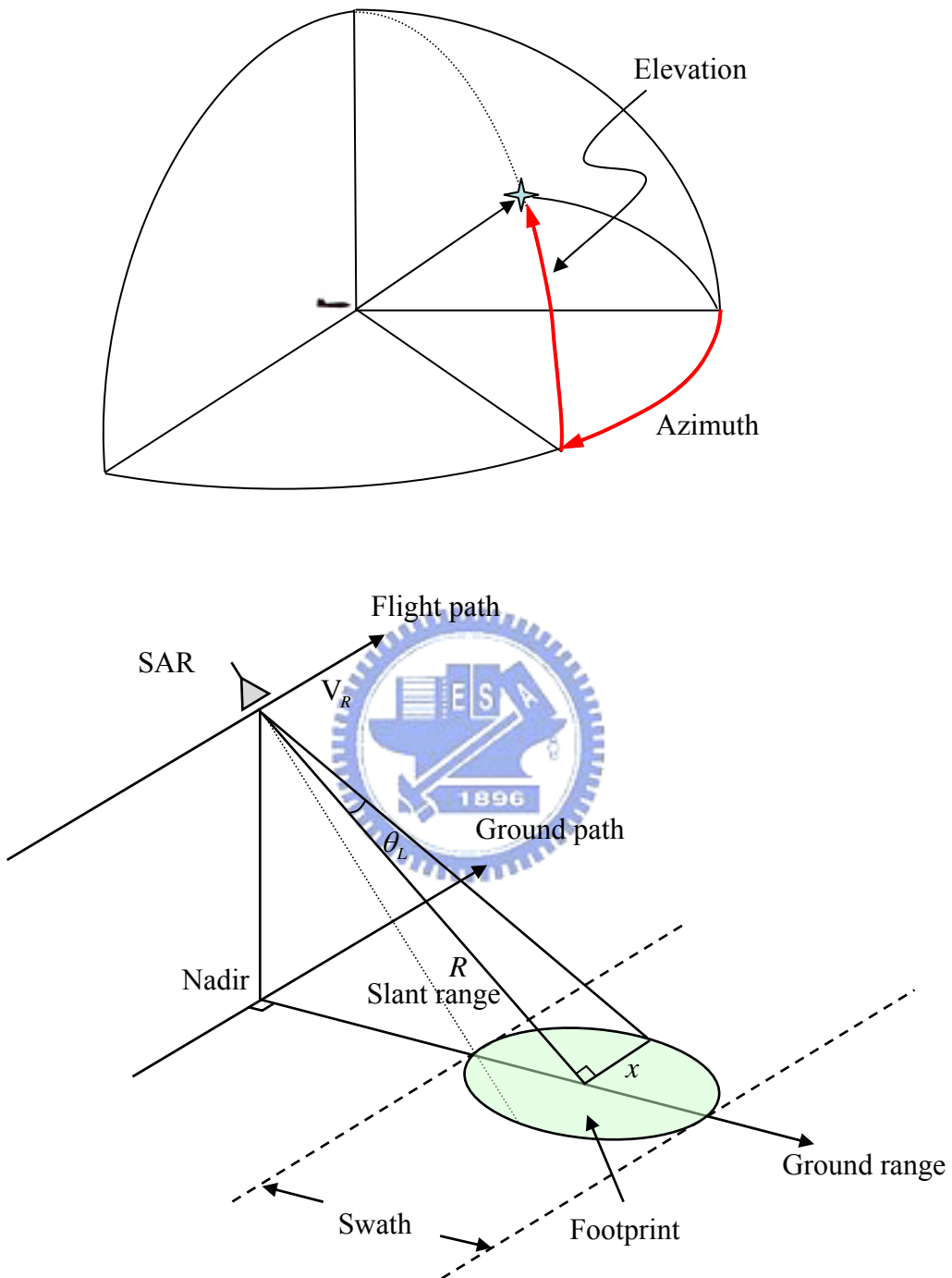


Figure 2-3 Geometry of SAR

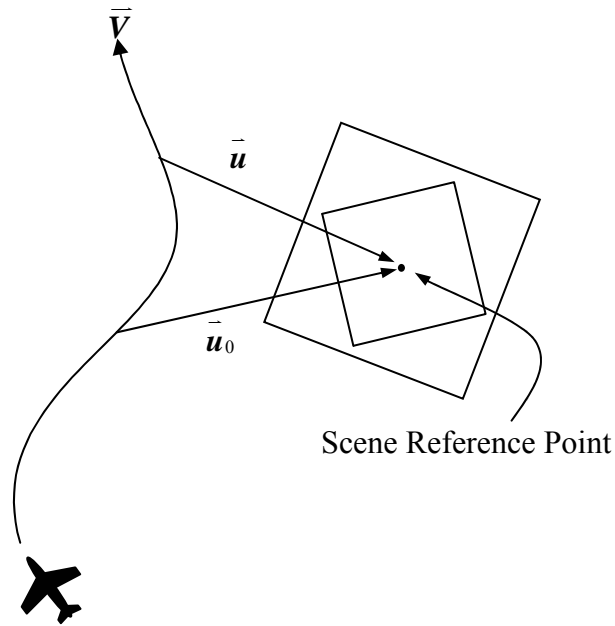


Figure 2-4 Spotlight Mapping

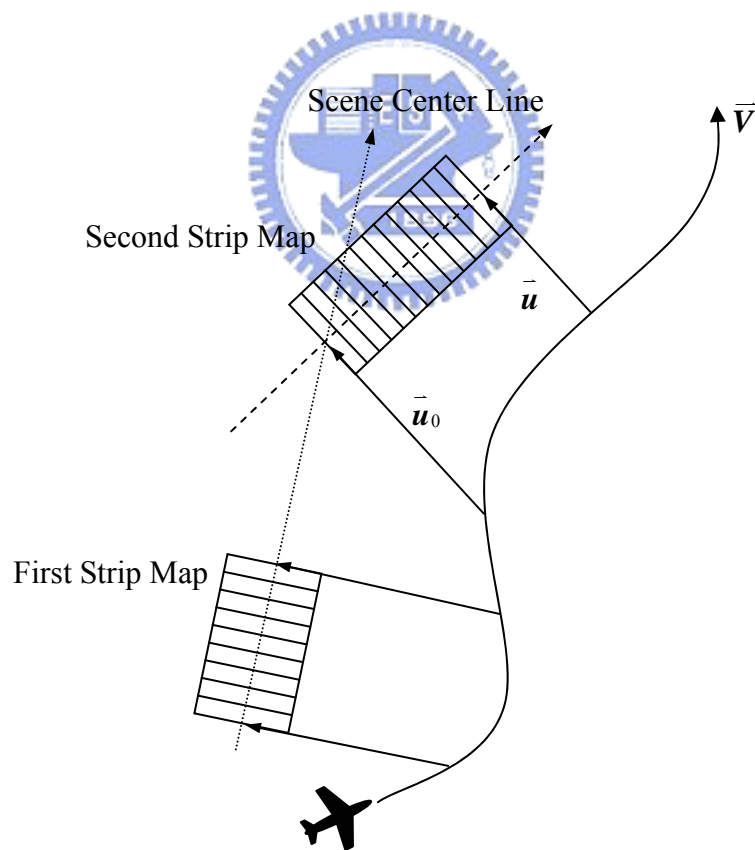


Figure 2-5 Strip Mapping



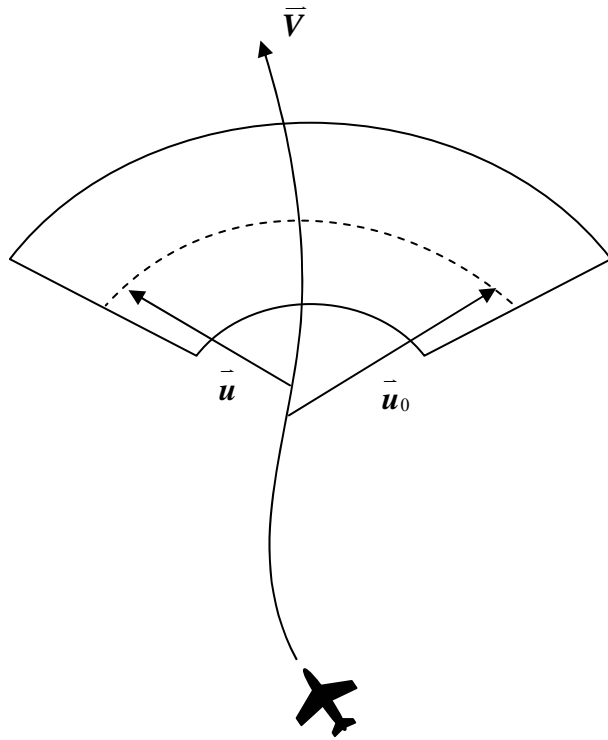


Figure 2-6 Doppler Beam Sharpening (DBS) Mapping

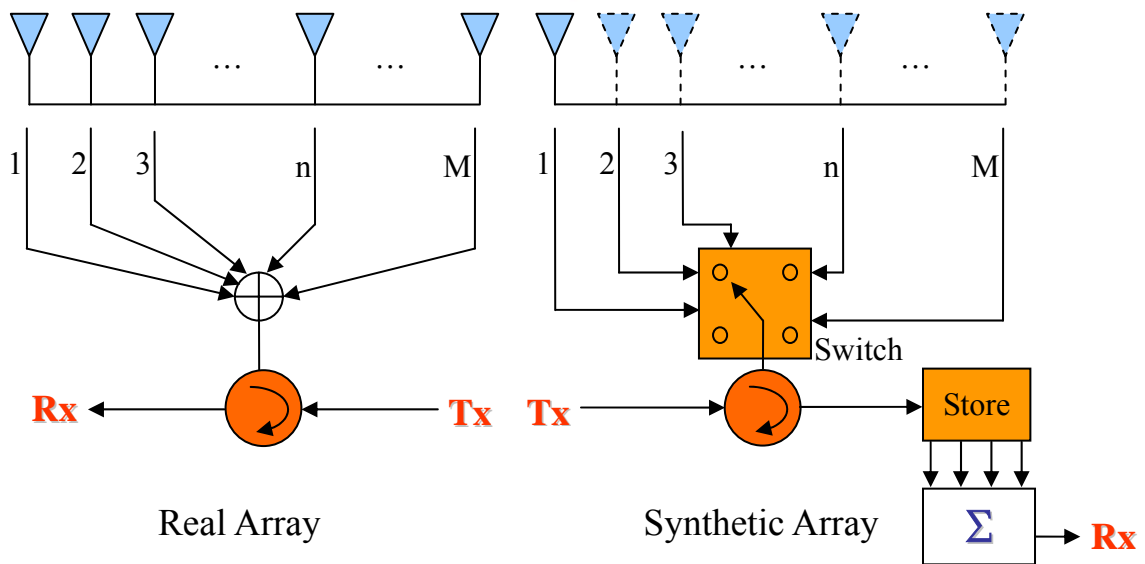


Figure 3-1 Synthetic Array and Real Array

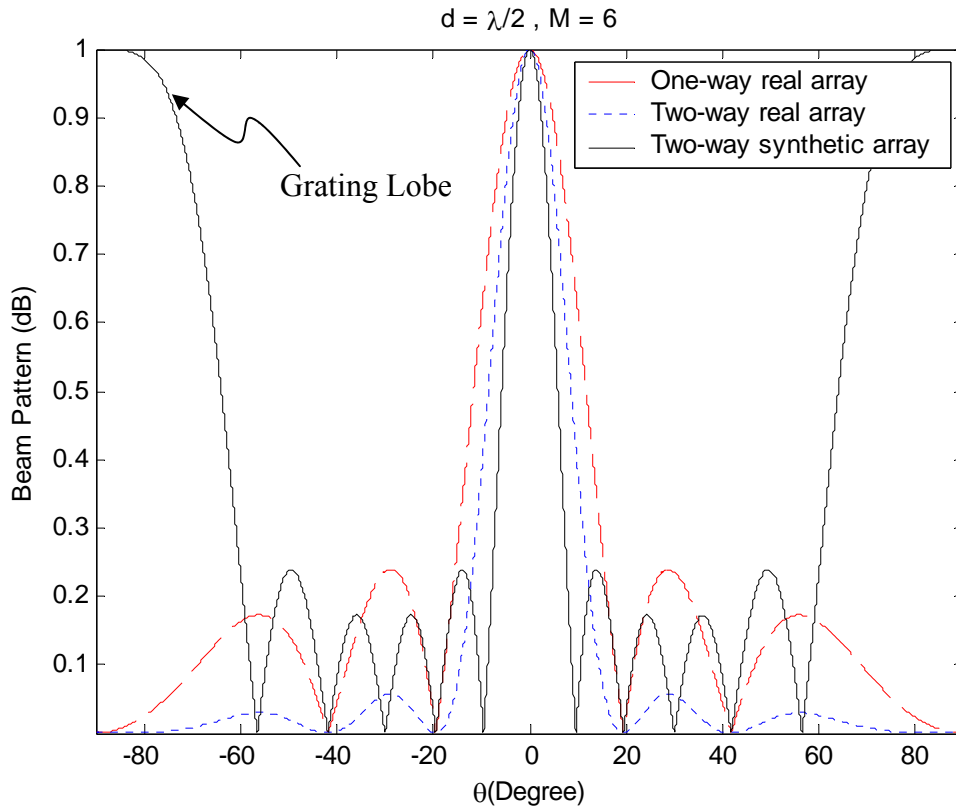


Figure 3-2 Beam Pattern in Synthetic and Real Array

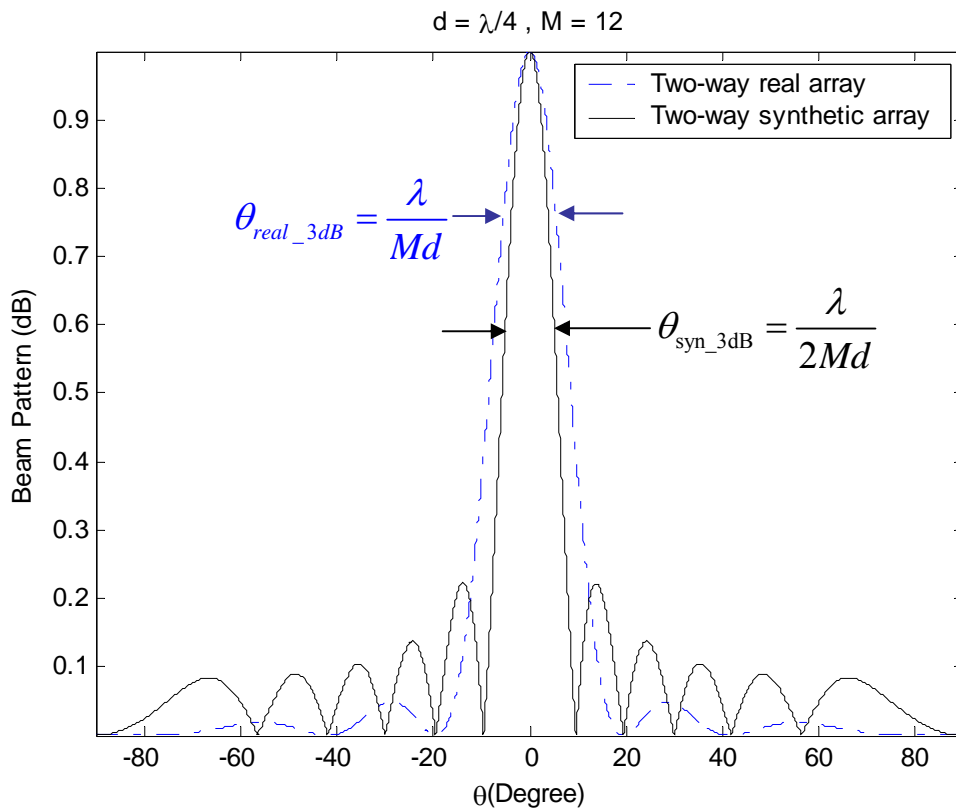


Figure 3-3 Beam Pattern of Removing Grating Lobe

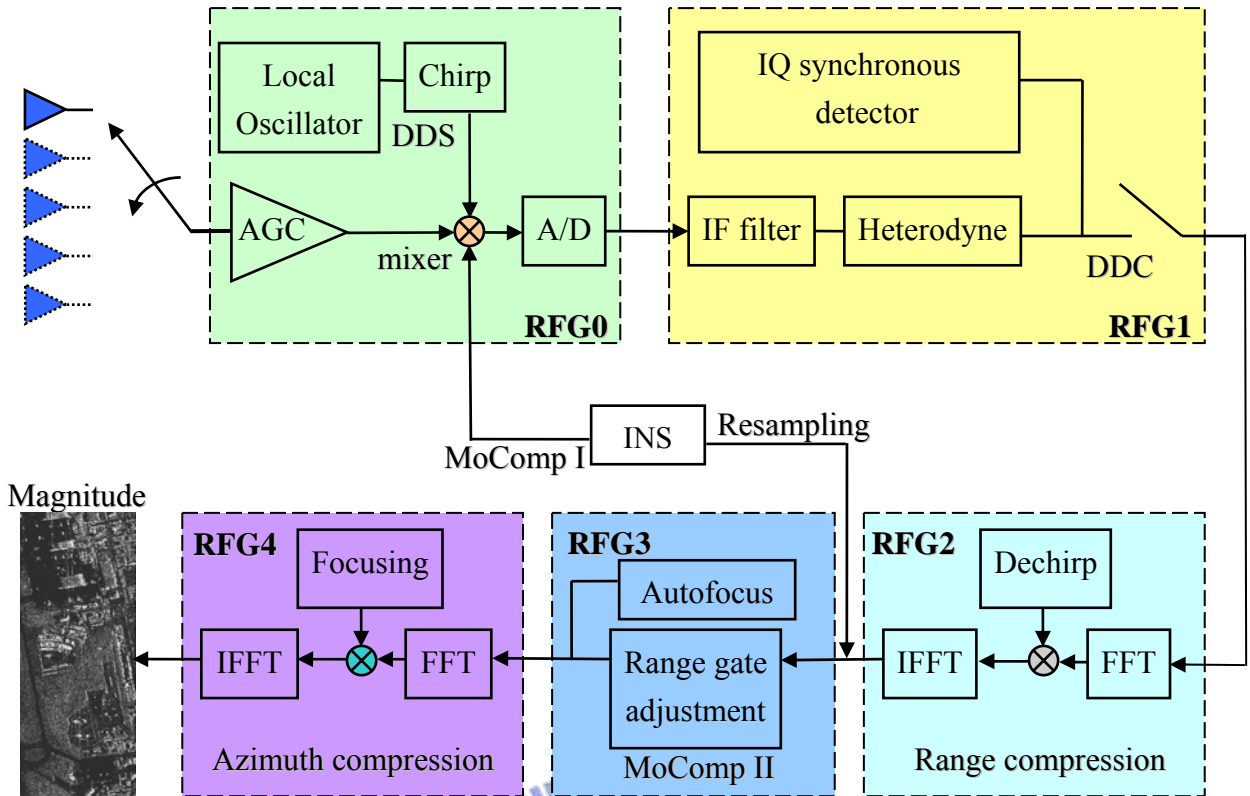


Figure 3-4 Signal Processing Function Block

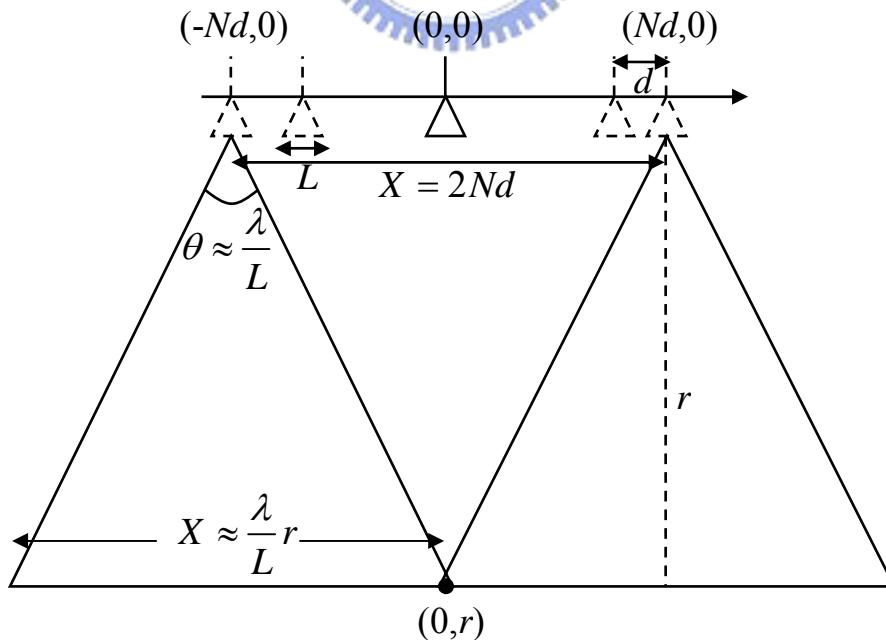


Figure 3-5 SAR Array Sampling Diagram

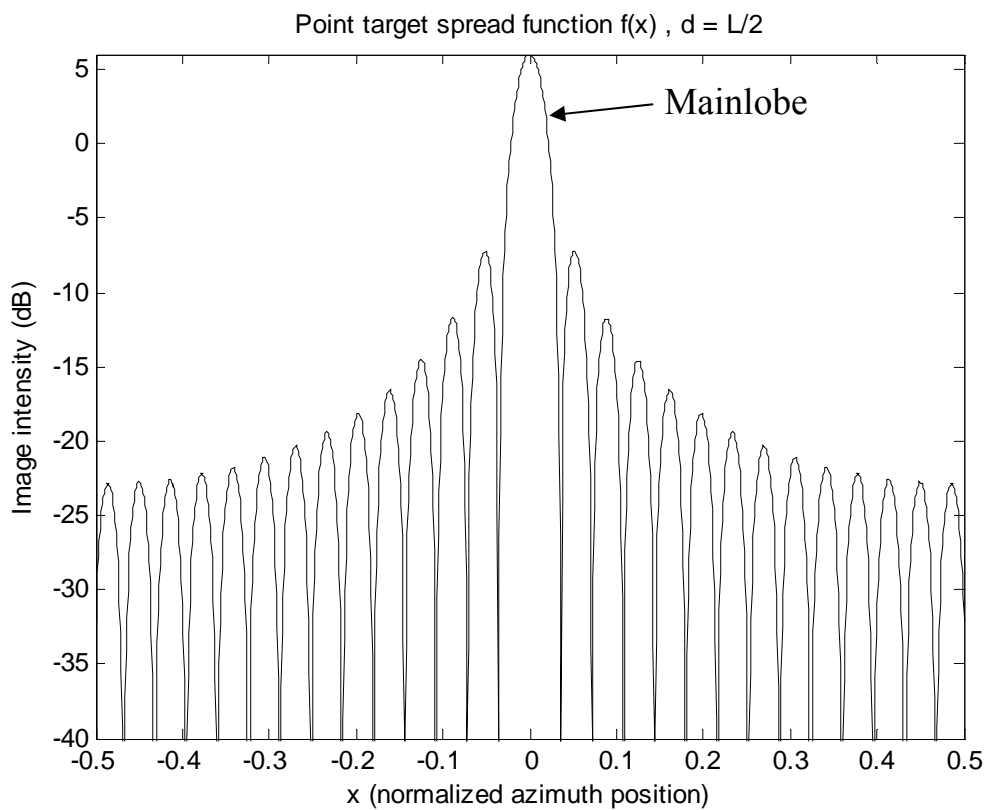
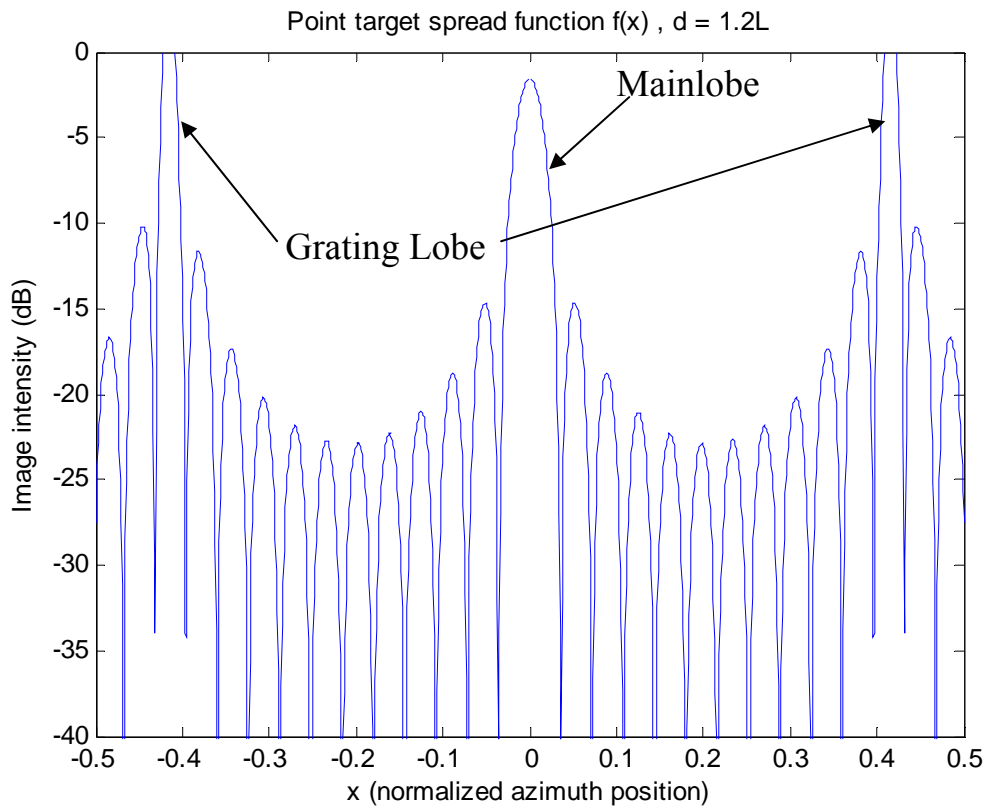


Figure 3-6 Point Target Spread Function in Azimuth Direction

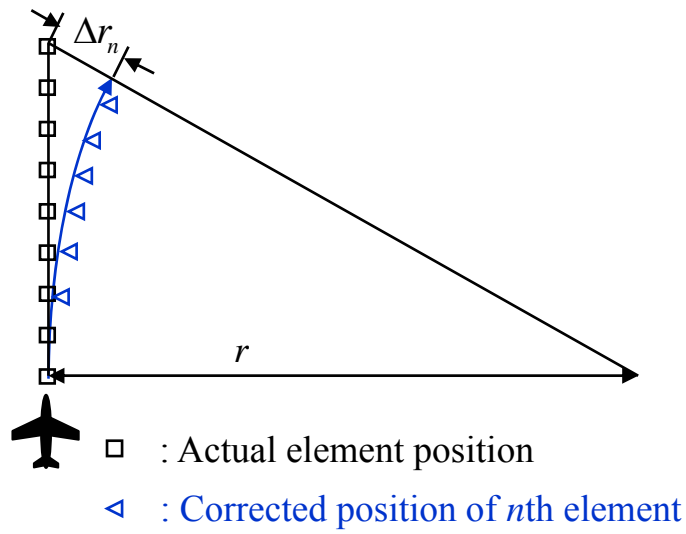


Figure 3-7 Focusing Diagram

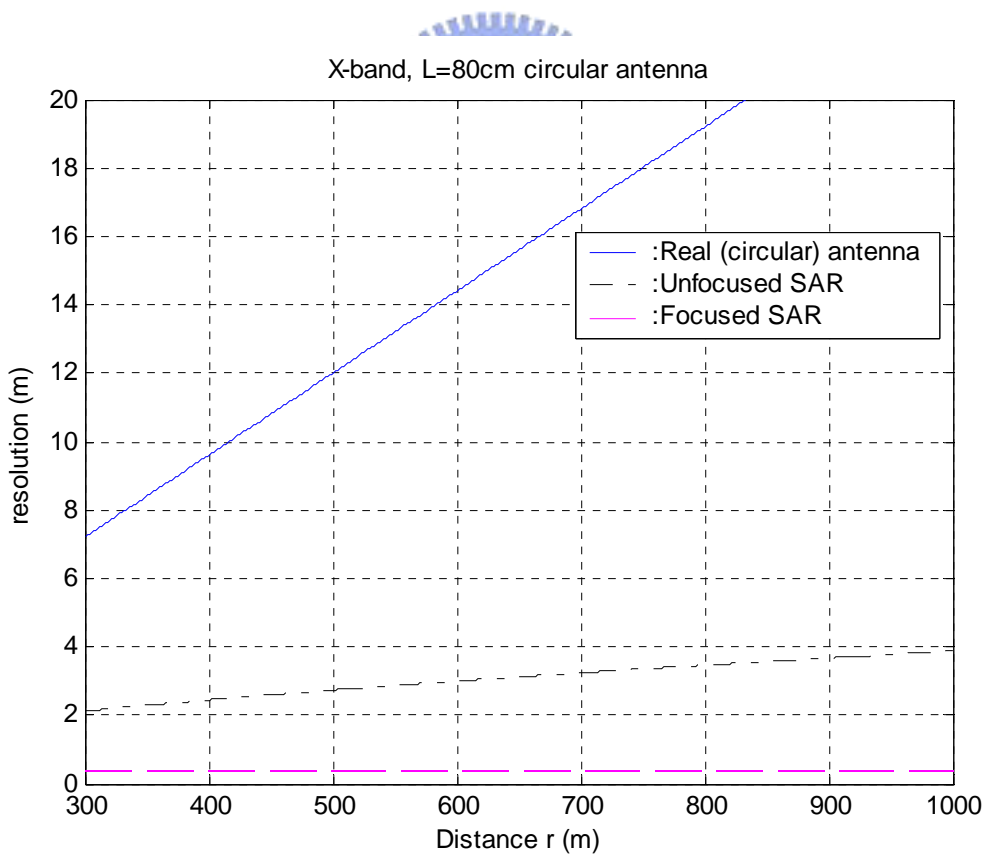


Figure 3-8 Resolution of Focused and Unfocused SAR

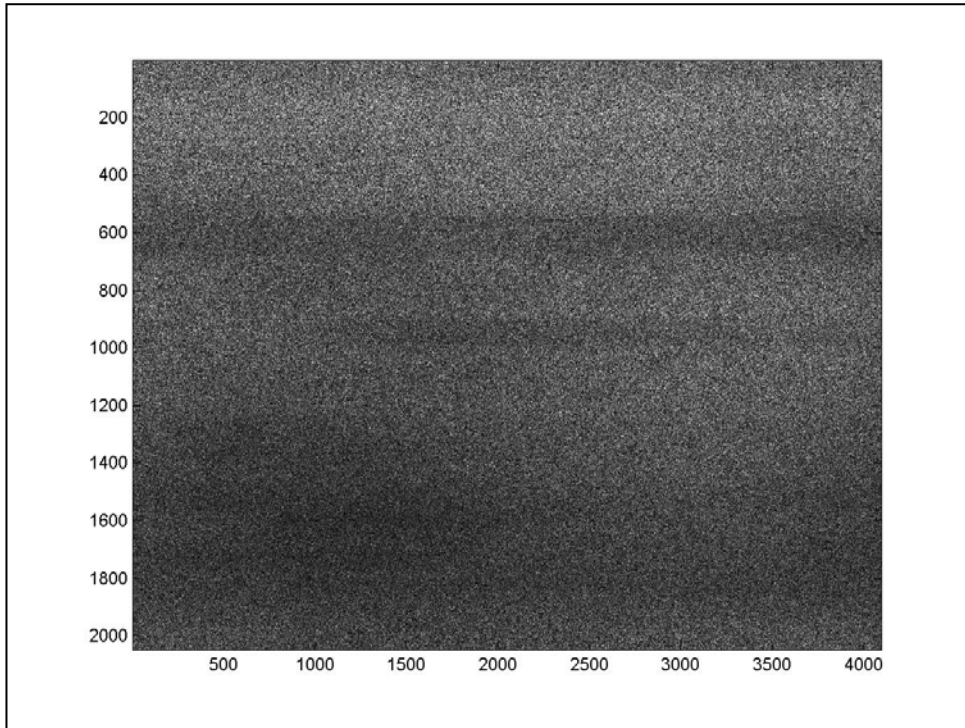


Figure 3-9(a) Raw data Image after Range Compression

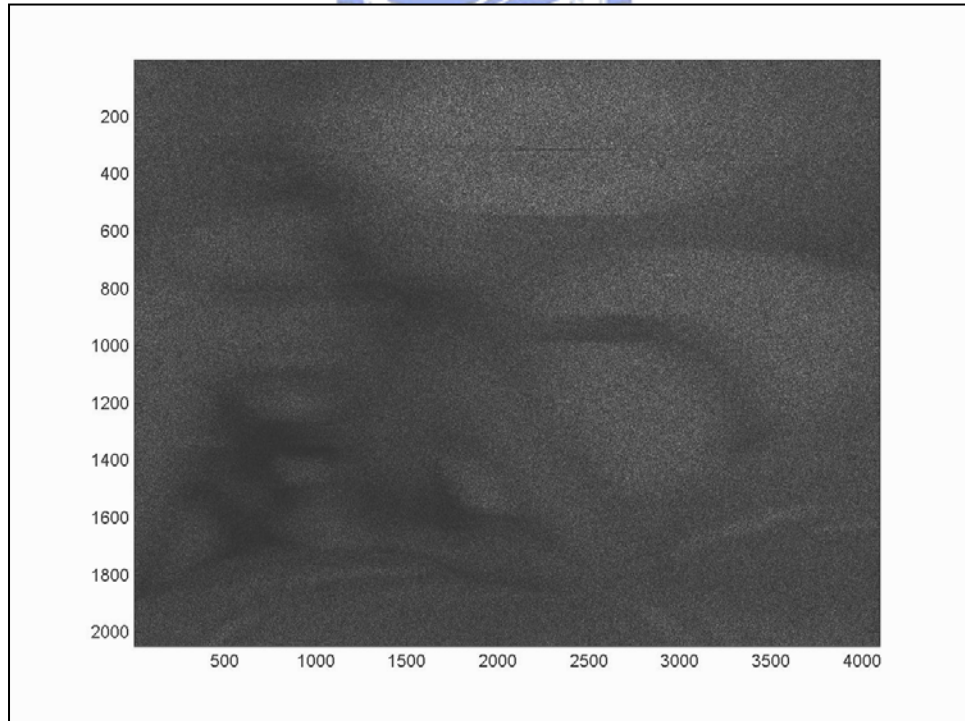


Figure 3-9(b) Azimuth Compression without Focusing

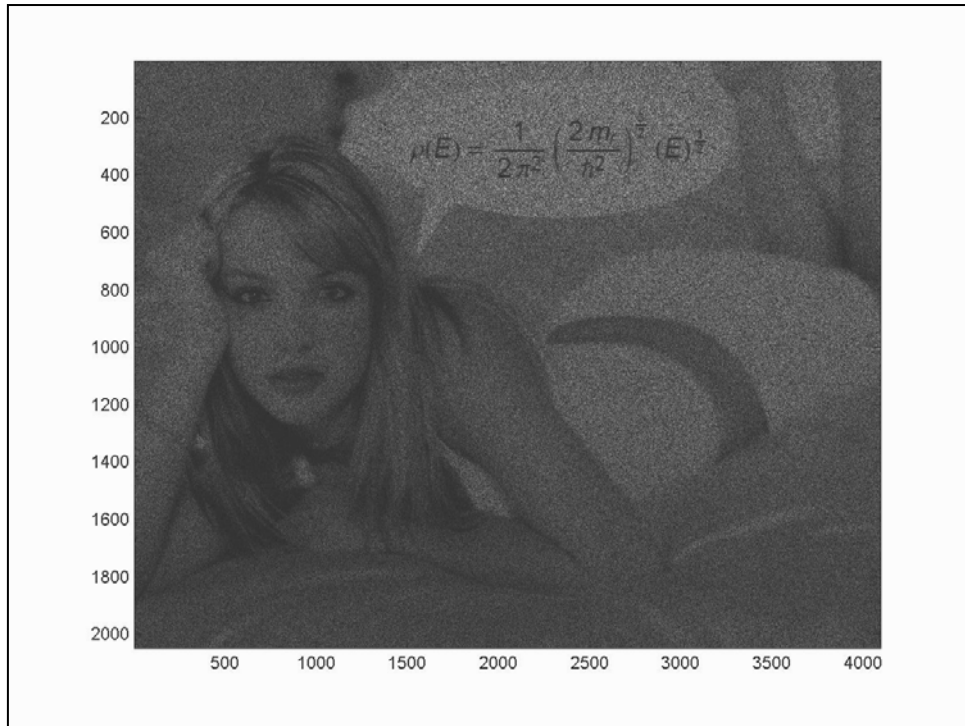


Figure 3-9(c) Azimuth Compression with Focusing

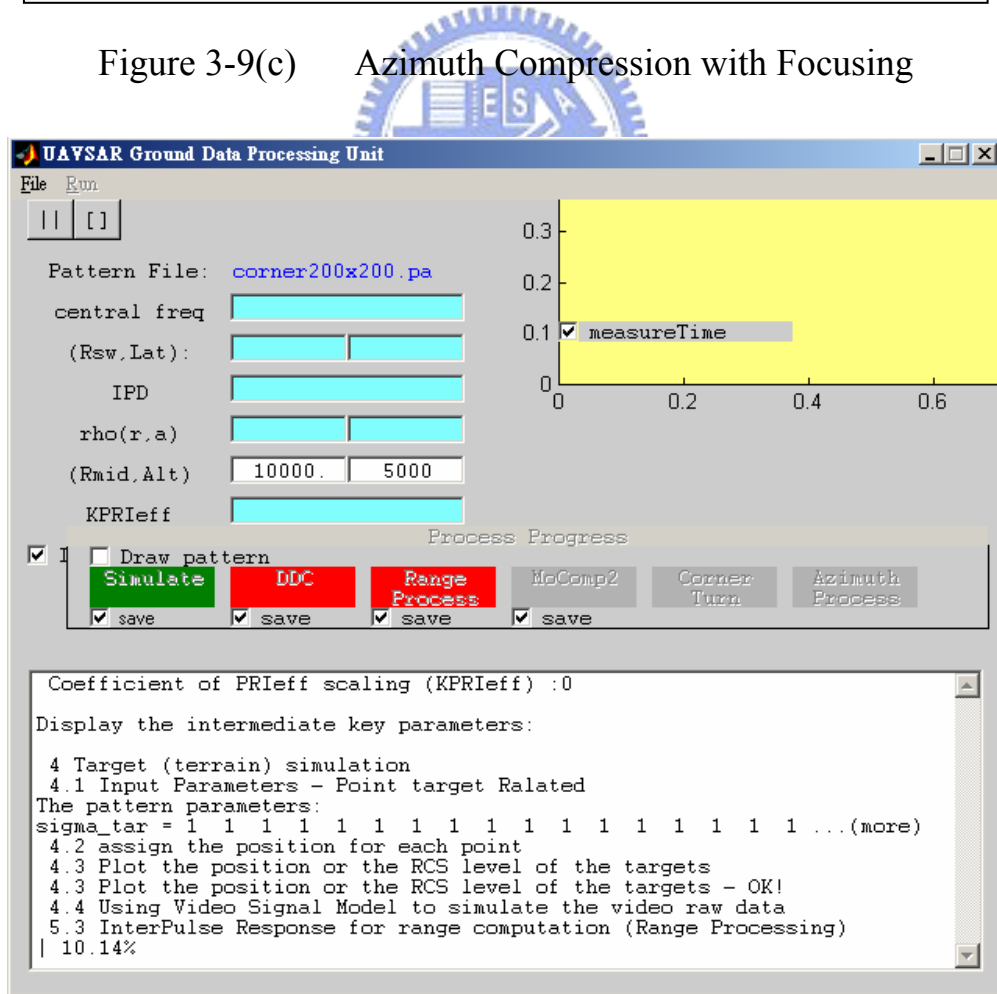


Figure 3-10 Ground Data Processing Unit Interface



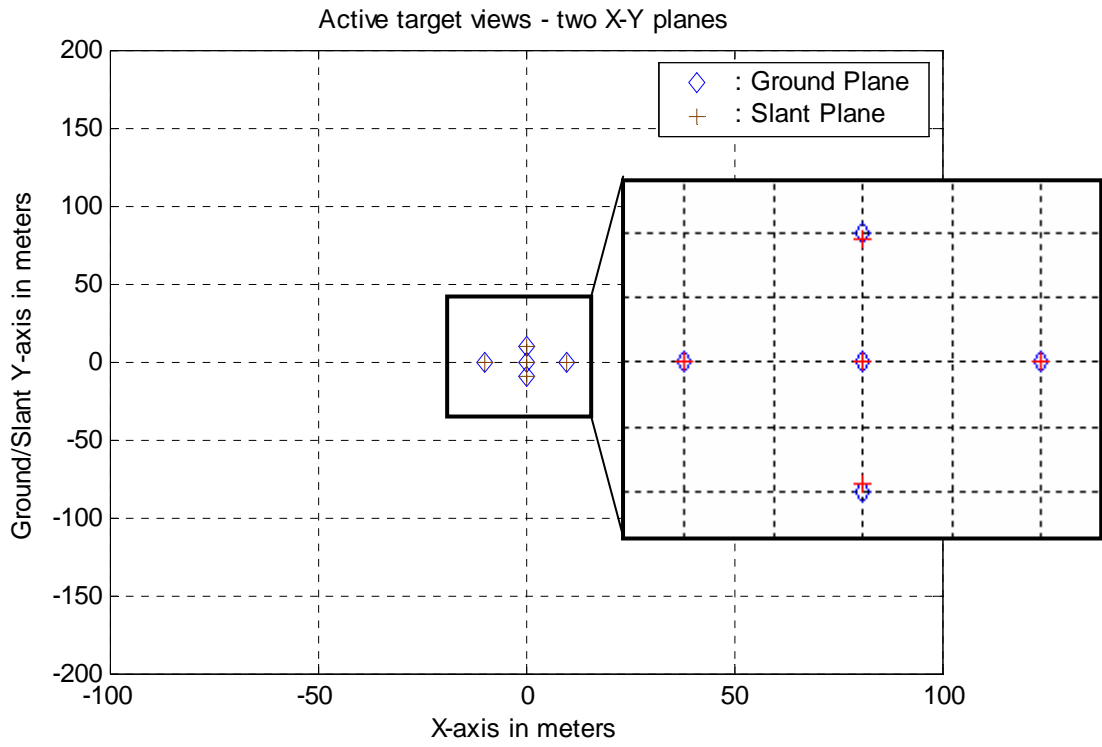


Figure 3-11 Targets on Ground and Slant Plane



video data of <1corner200x400.pat>

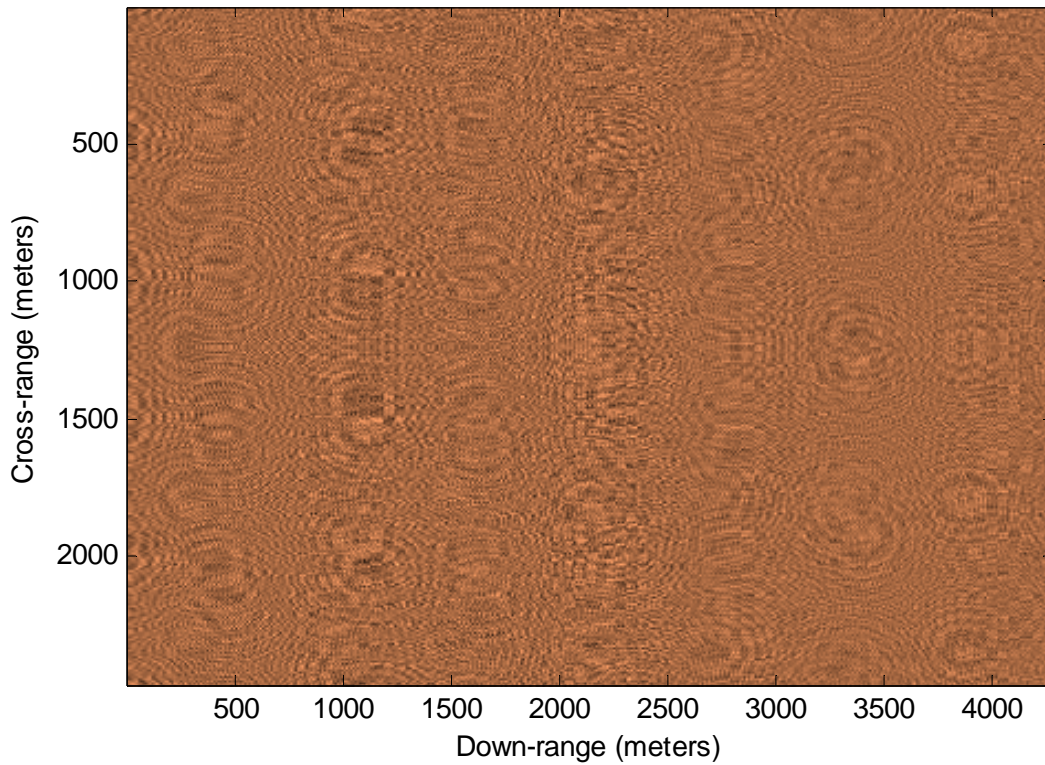


Figure 3-12 Video Data Image



DDC after video data of <1corner200x400.pat>

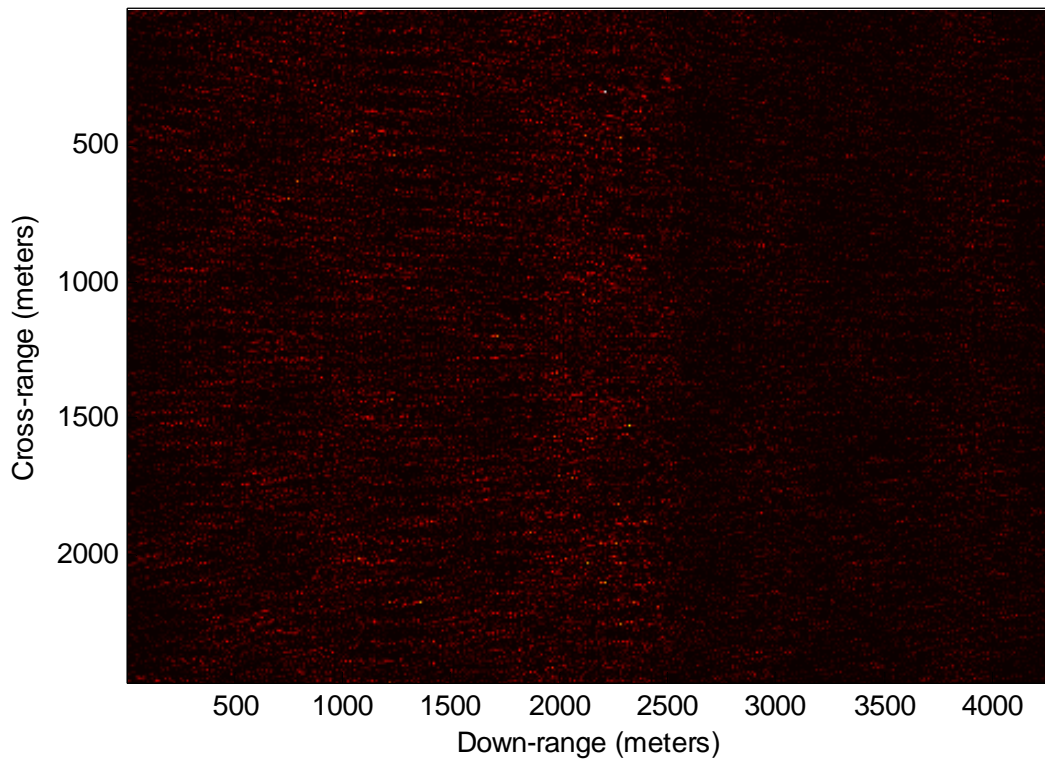


Figure 3-13 Image after DDC (RFG1)

video data of <1corner200x400.pat> after range processing

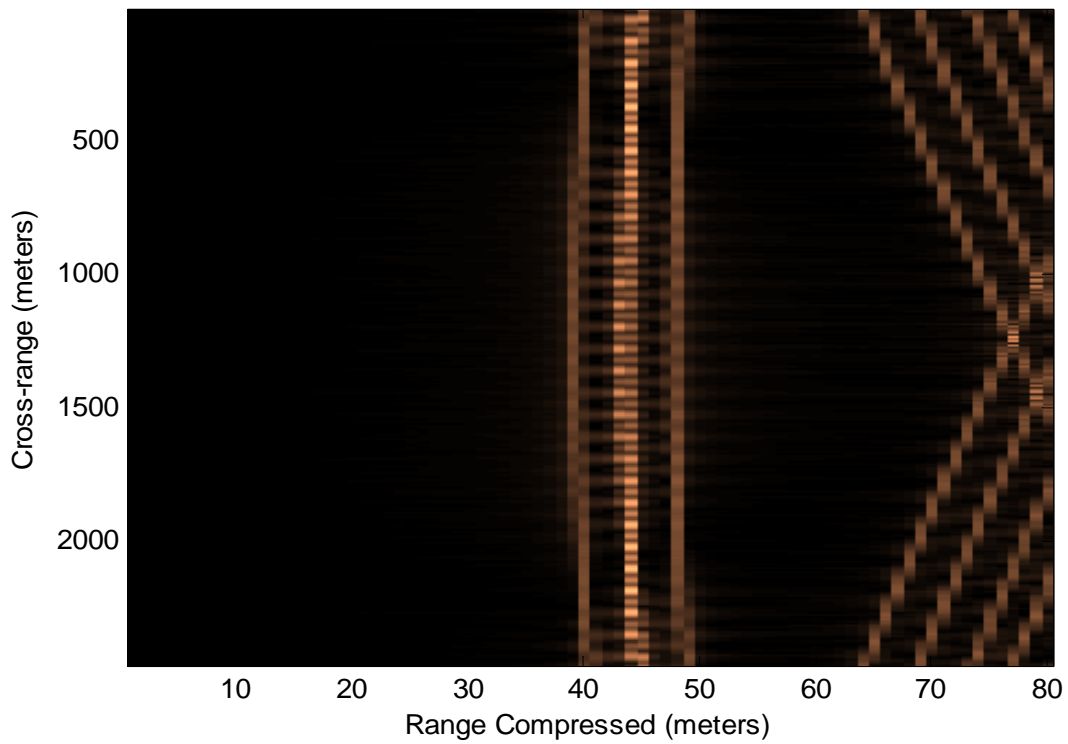


Figure 3-14 Image after Range Compression

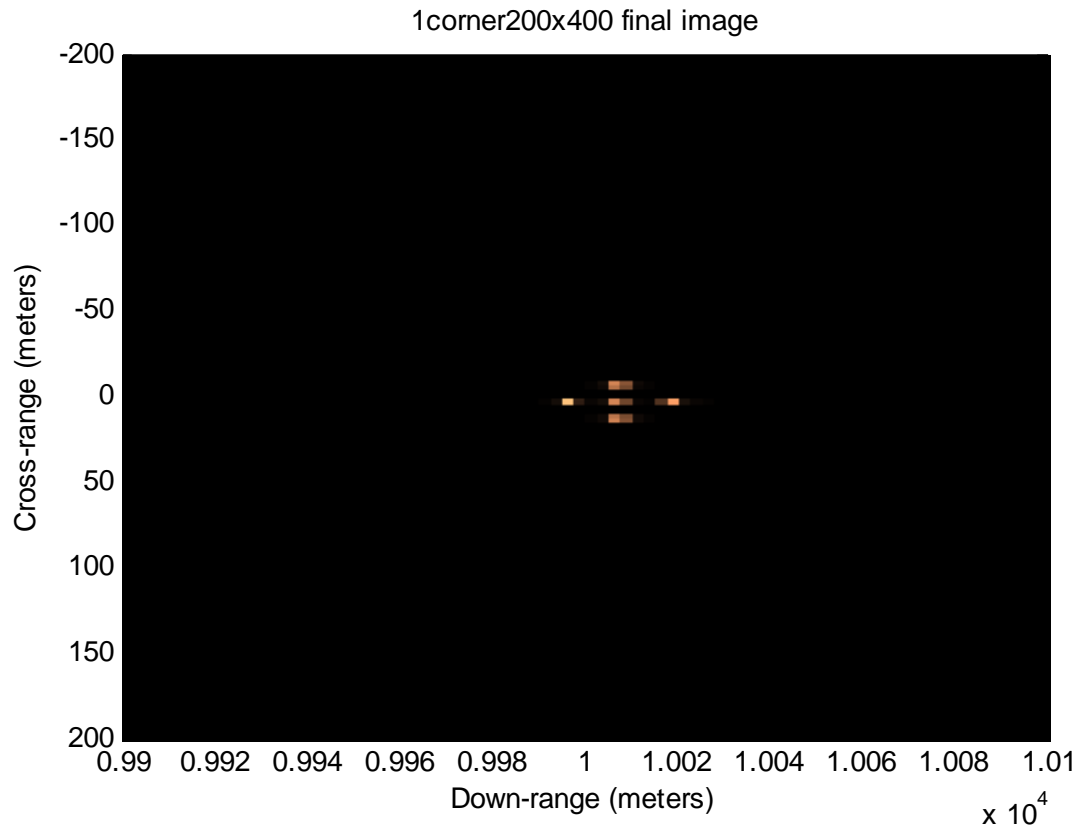


Figure 3-15 Processing Final Image

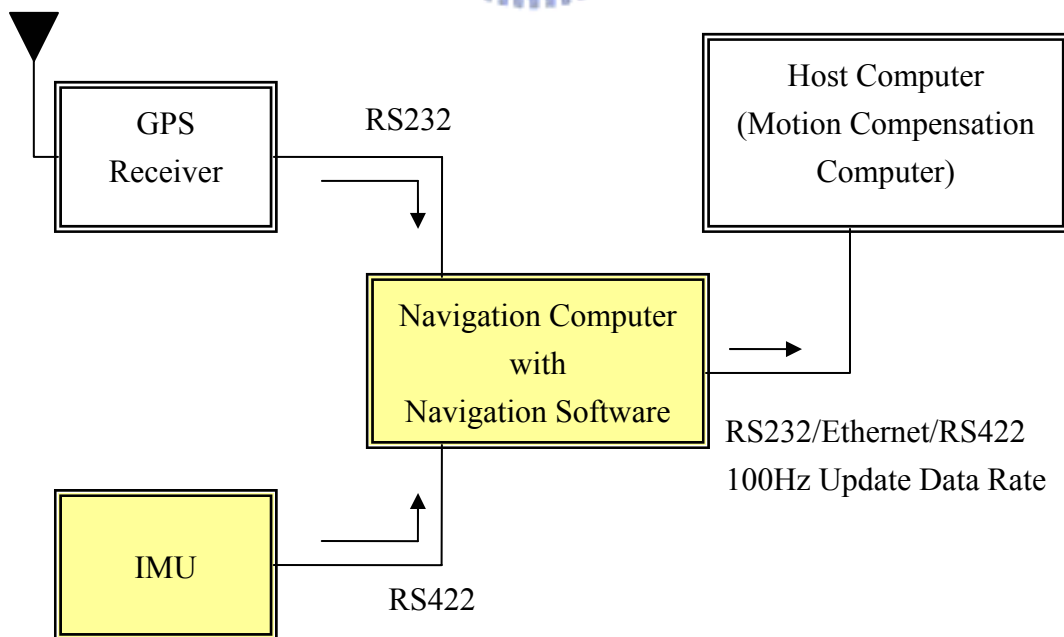
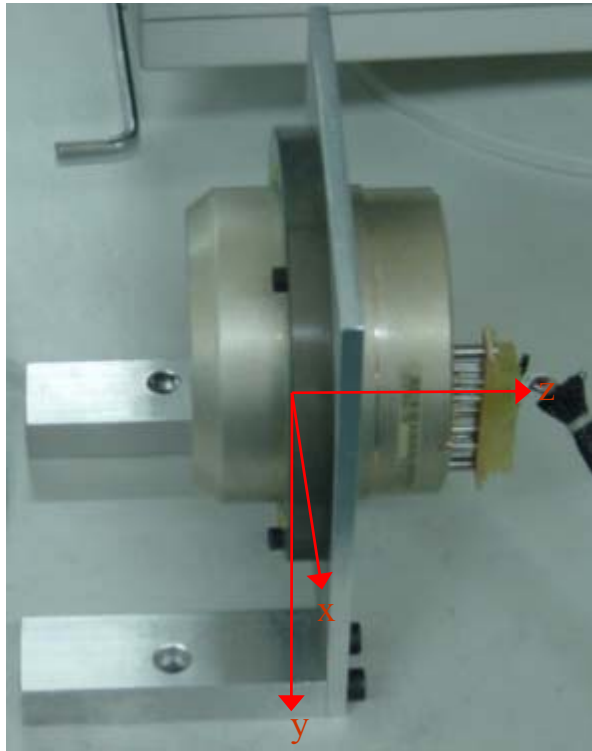


Figure 4-1 Motion Measurement System



(a) Inertial Measurement Unit (IMU)



(b) Navigation Computer

Figure 4-2 Actual Pictures of Motion Measurement System

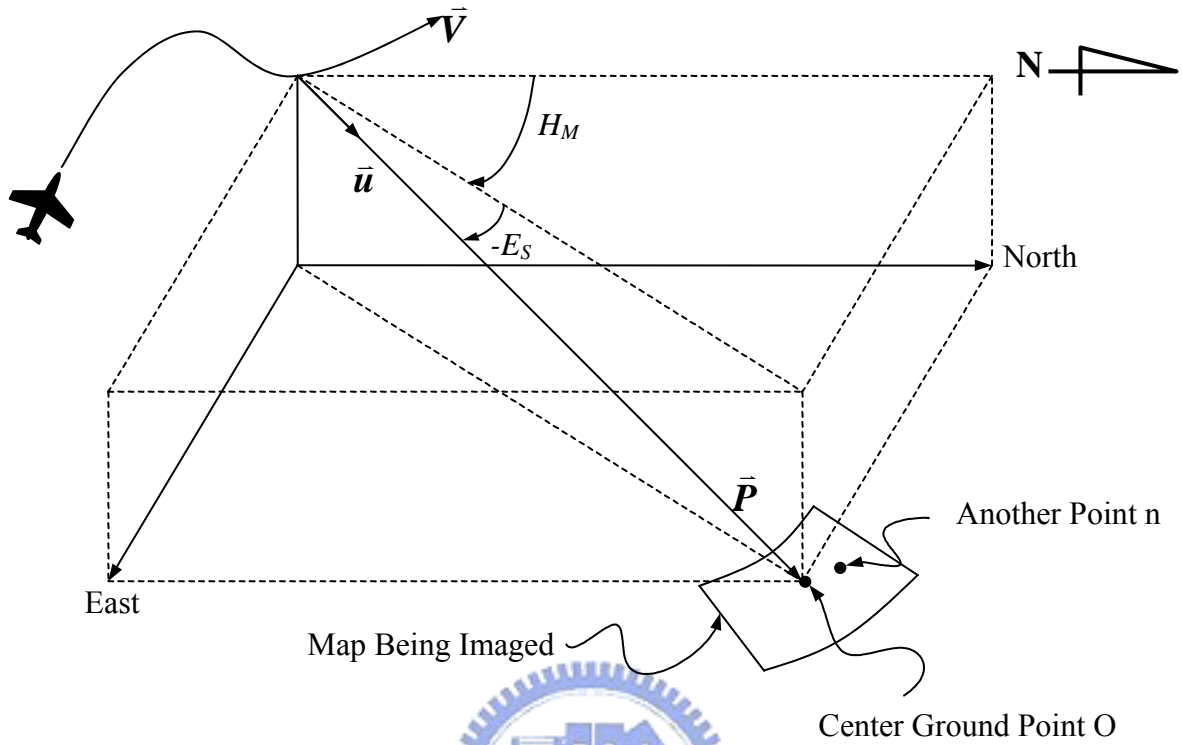


Figure 4-3 Mapping Geometry in Geographic Coordinates

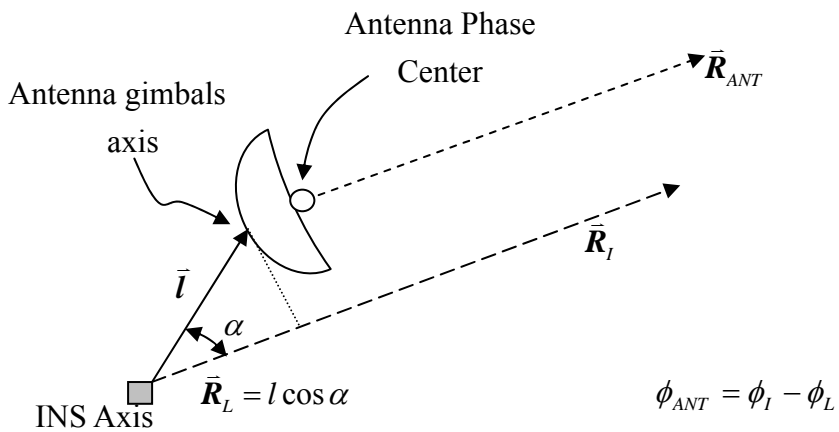


Figure 4-4 Lever Arm Phase Correction

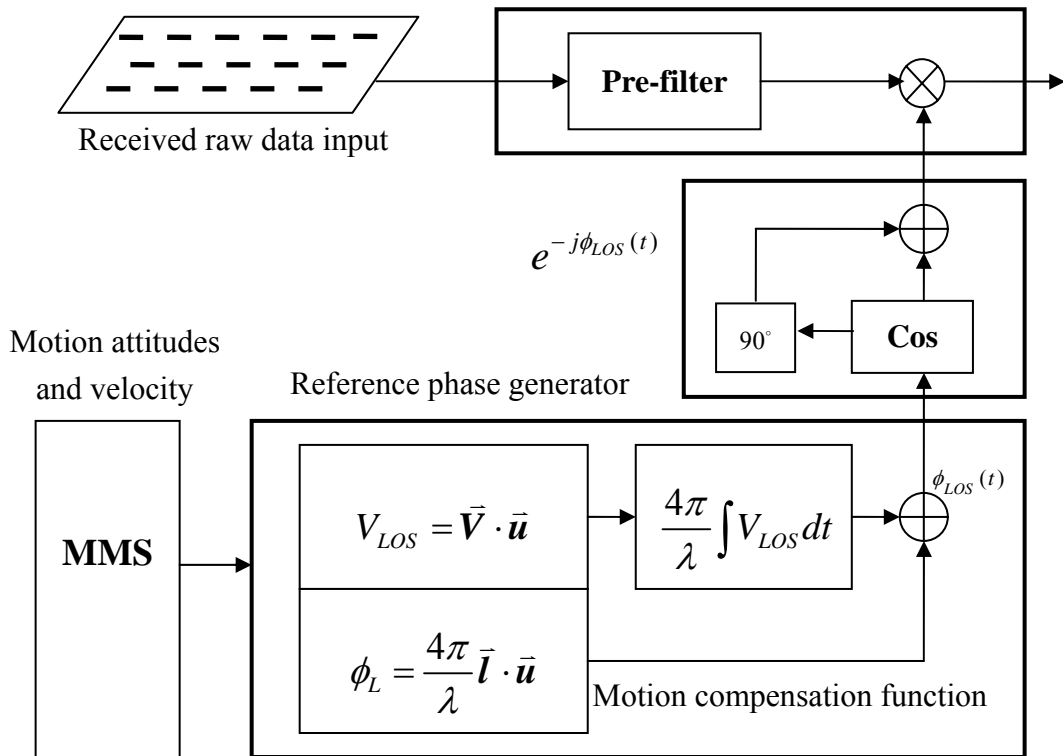


Figure 4-5 Hardware Implementation Diagram of Motion Compensation

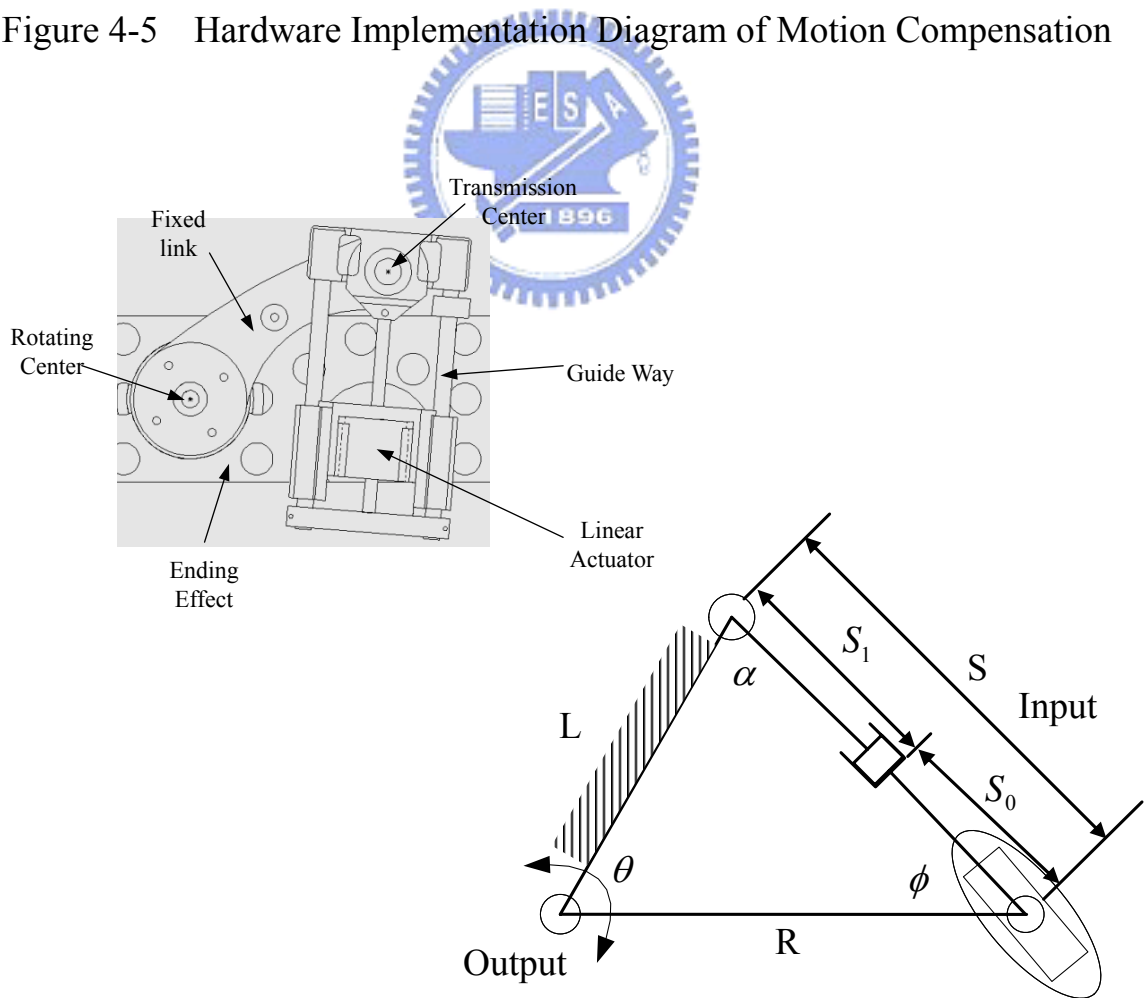
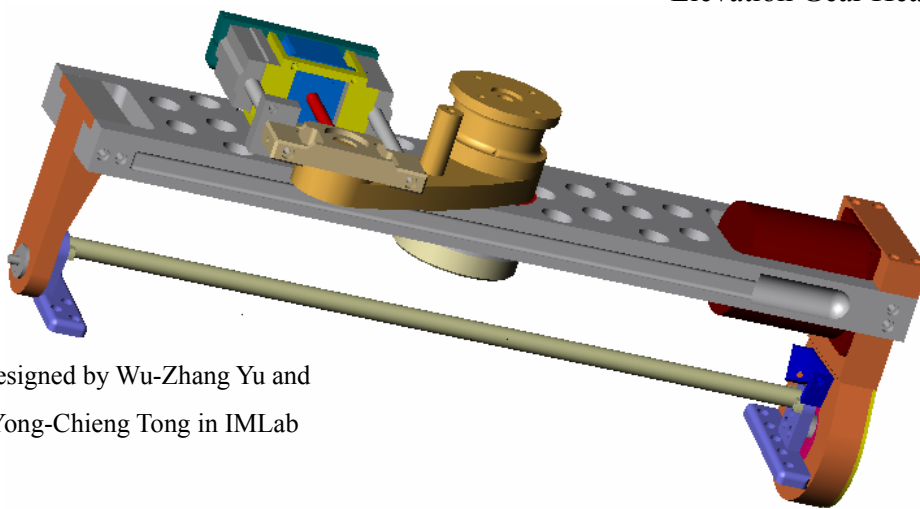
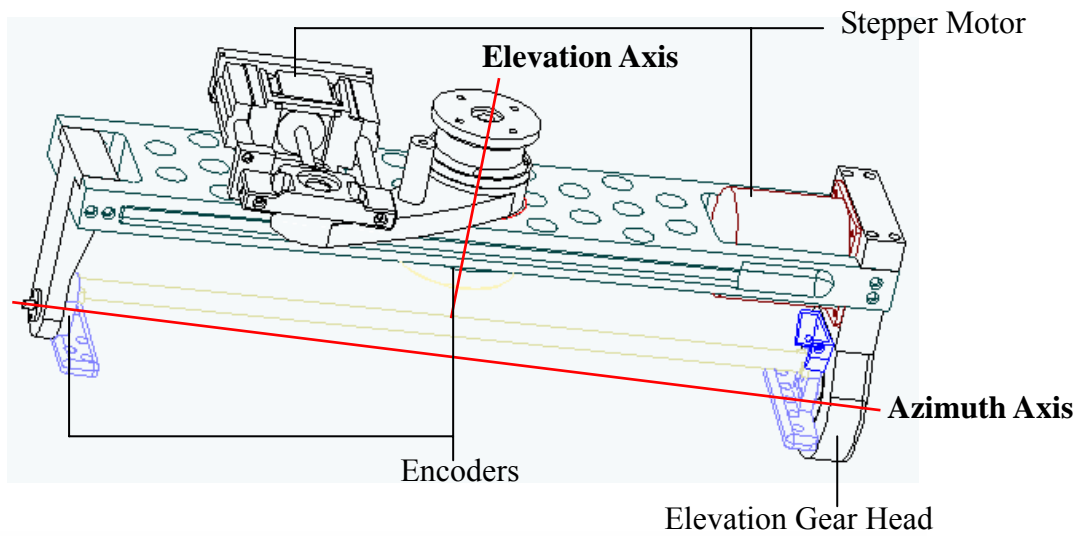


Figure 4-6 SAR Azimuth Mechanism Prototype



Designed by Wu-Zhang Yu and  
Yong-Chieng Tong in IMLab

Figure 4-7 SAR Antenna Gimbals 1<sup>st</sup>G Overview

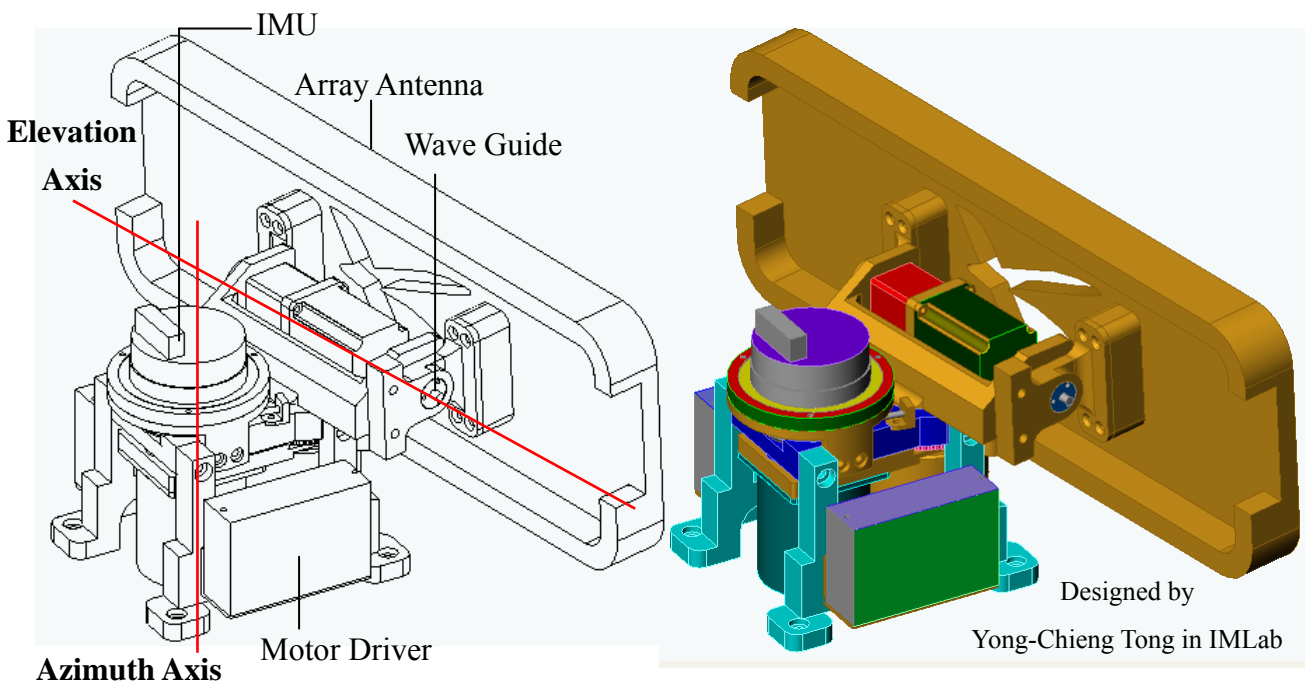


Figure 4-8 SAR Antenna Gimbals 4<sup>th</sup>G Overview



Figure 4-9 NI 7334 Motion Control Card and Extending Board

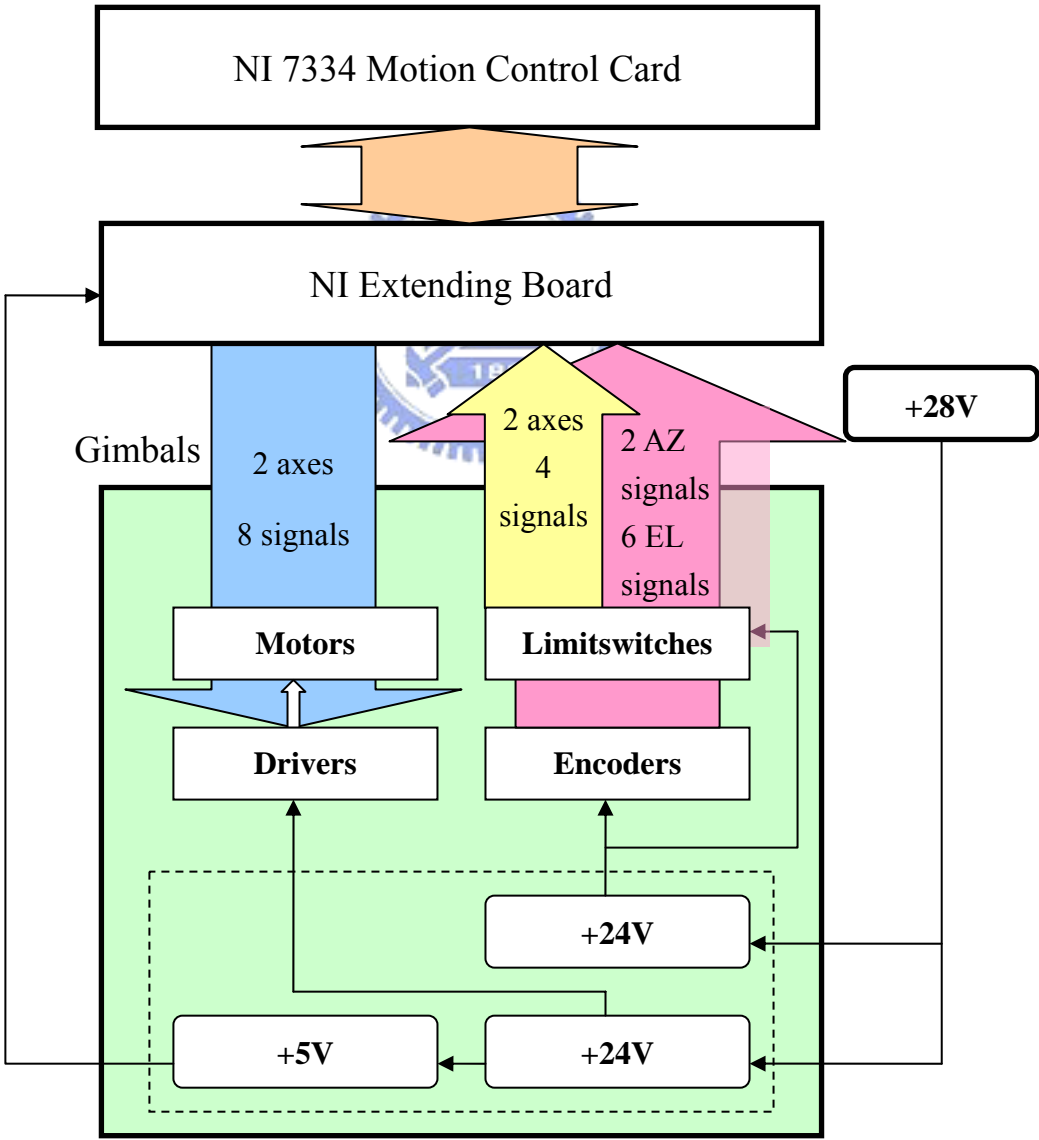


Figure 4-10 Power and Signal Flows of Antenna Gimbals



```

MS NIMotion
自動
===== [ Gyroscope ] =====
      Yaw :      -6.614      Roll :      24.011      Pitch :      -5.883
          9.385 Kbps
          MM timer is : 831531      117 Records/s
===== [ Positions ] =====
      Azimuth :      -79597      Elevation :      6434
Encoder AZ :      Encoder EL :
===== [ Dialog ] =====
Resetting positions to zero . . .
Energizing (halting) configured axes . . .
Enabling hardware limits . . .
Enabling home switches . . .
Setting operation mode . . .
Setting following error . . .
Loading velocity . . .
Homing finished!
Configuring inhibits . . .
===== [ Menu ] =====
[A] START      [S] STOP      [H] HOMING      [R] RESET      [X] EXIT

```

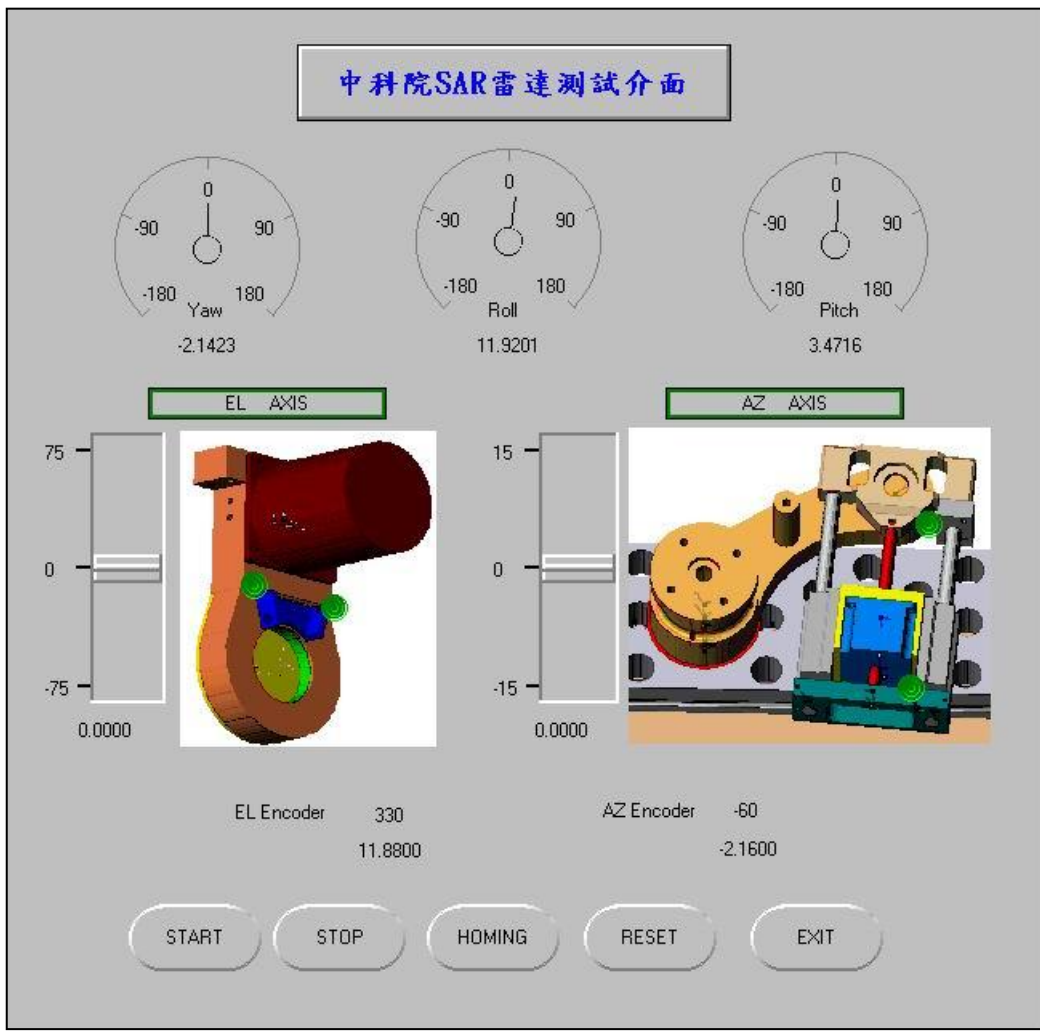


Figure 4-11 Console Program and User Interface of Antenna Gimbals



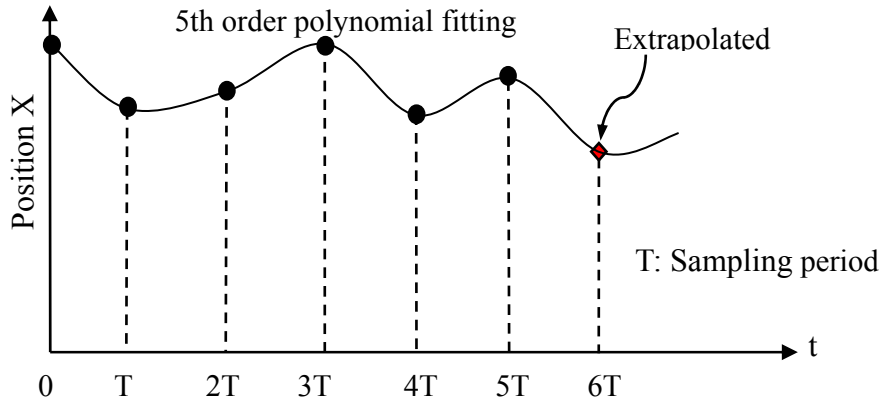


Figure 4-12 Polynomial Curve Fitting



Figure 4-13 InterSense Gyroscope

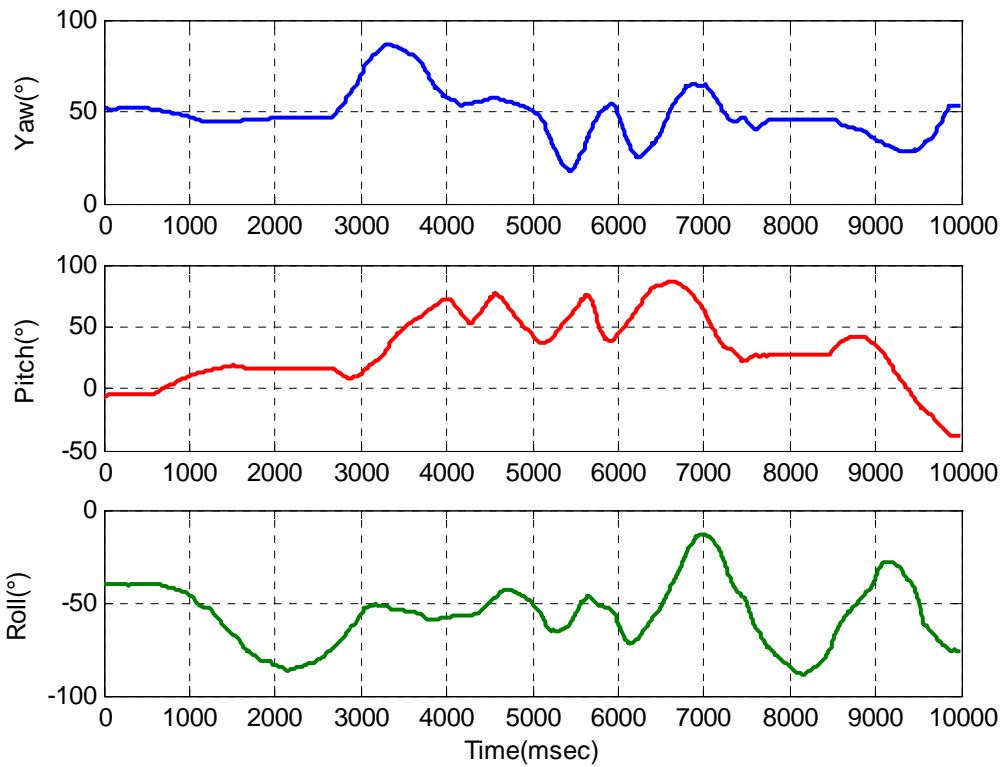


Figure 4-14 InterSense Gyroscope Data with Sampling Frequency 100Hz

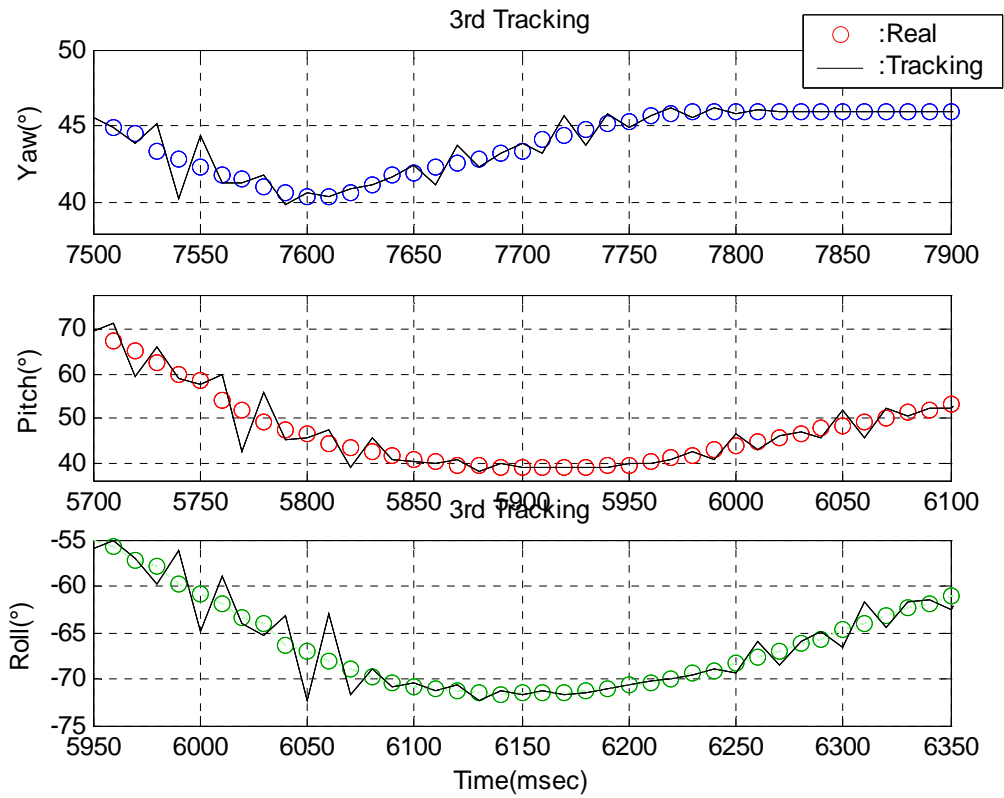


Figure 4-15 3<sup>rd</sup> Tracking in InterSense Gyroscope

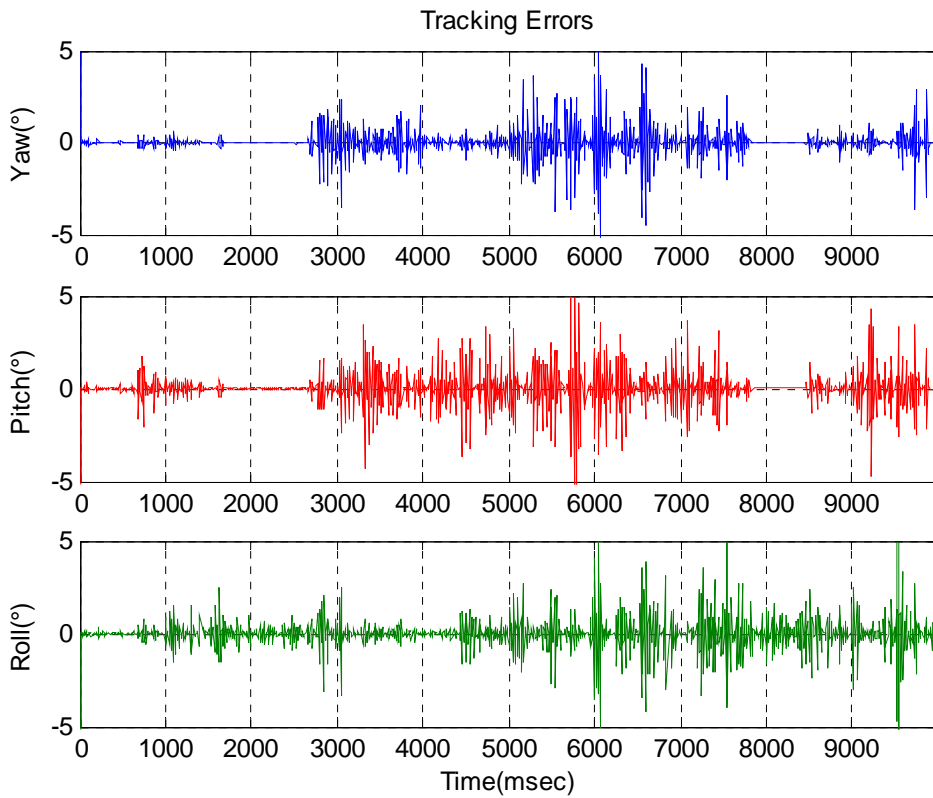


Figure 4-16 Tracking Errors of InterSense Gyroscope

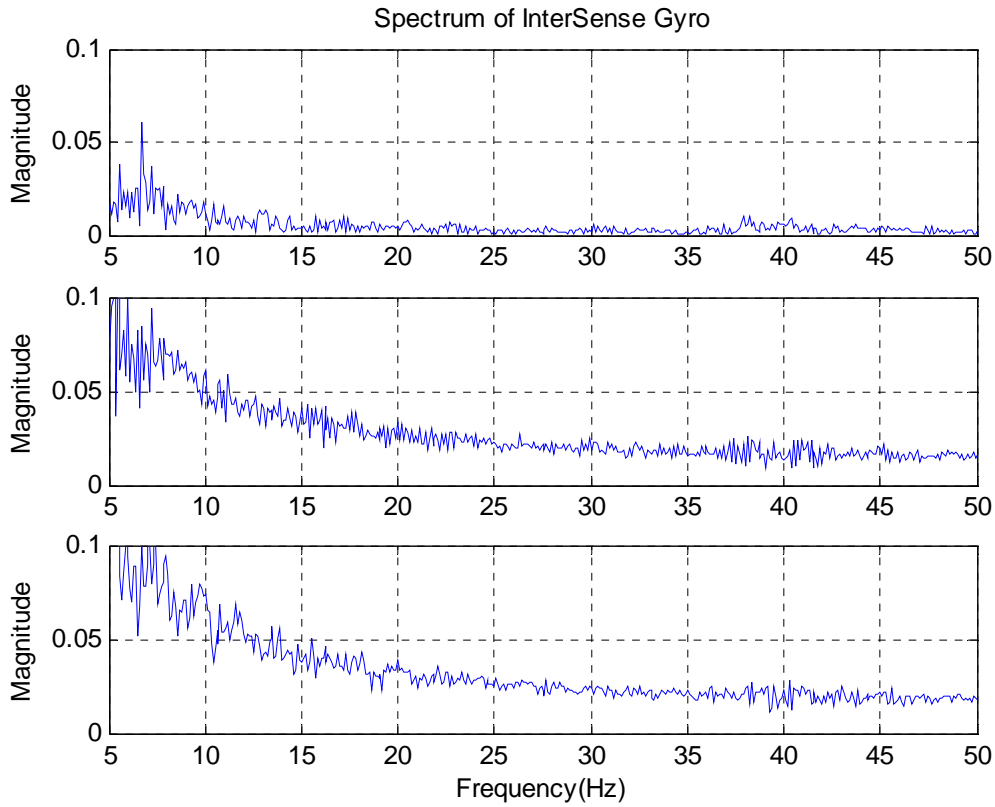


Figure 4-17 Spectrum of InterSense Gyroscope

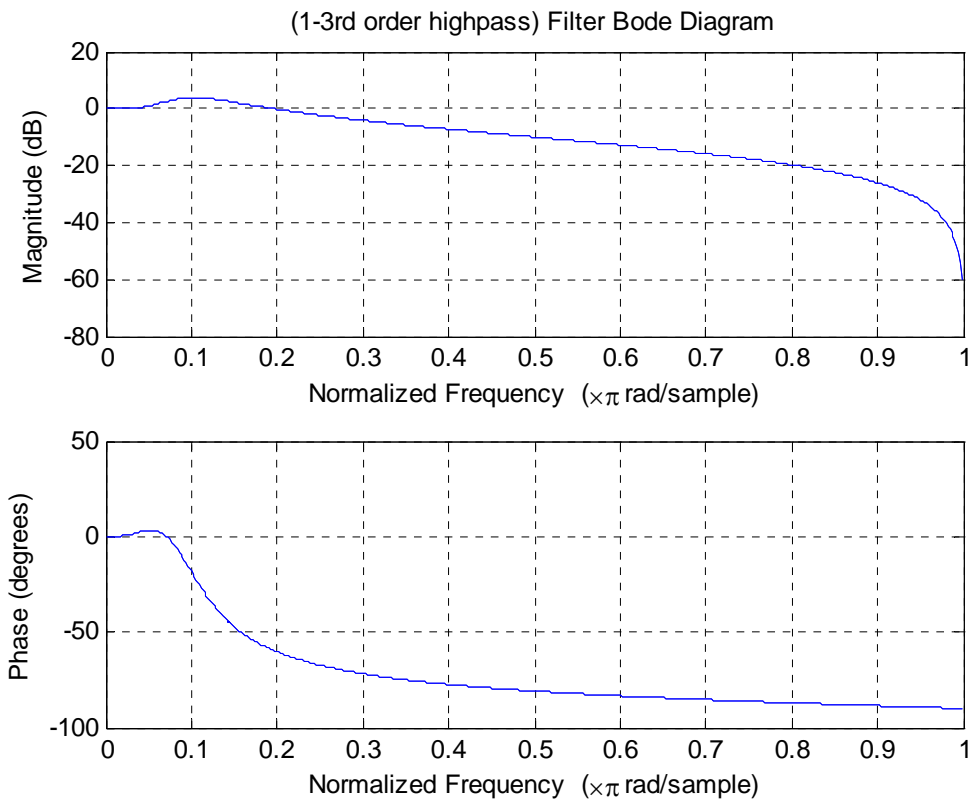


Figure 4-18 Bode Diagram of (1-3<sup>rd</sup> Order Highpass) Butterworth Filter

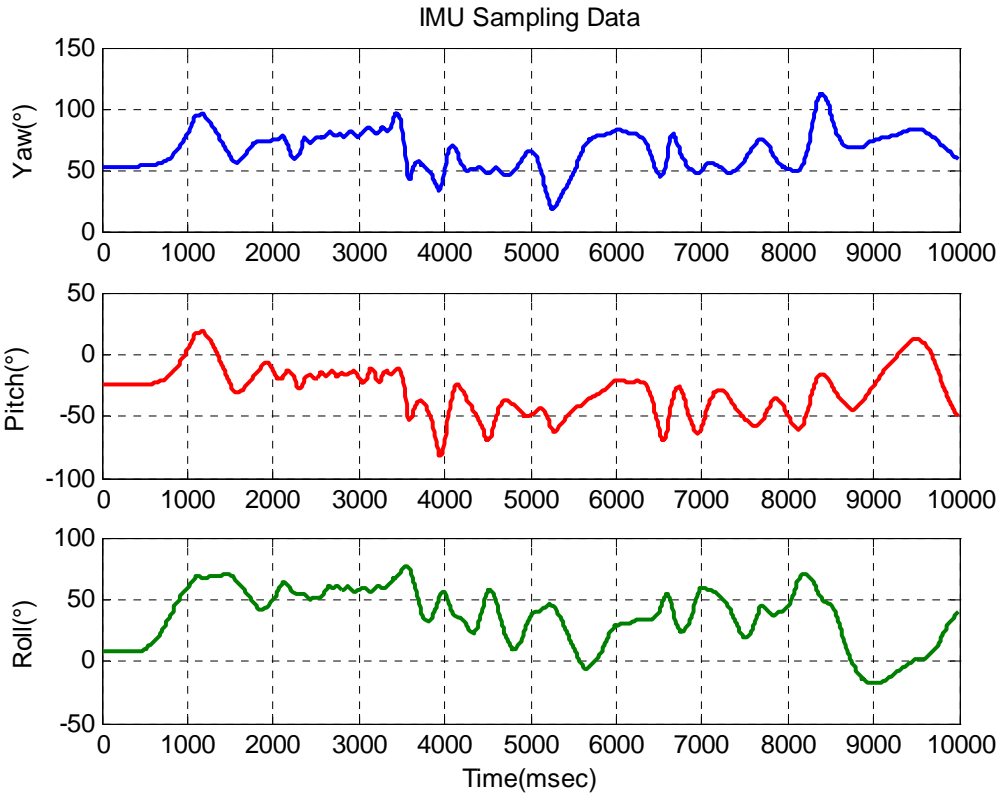


Figure 4-19 IMU Sampling Data with 100Hz Sampling Frequency

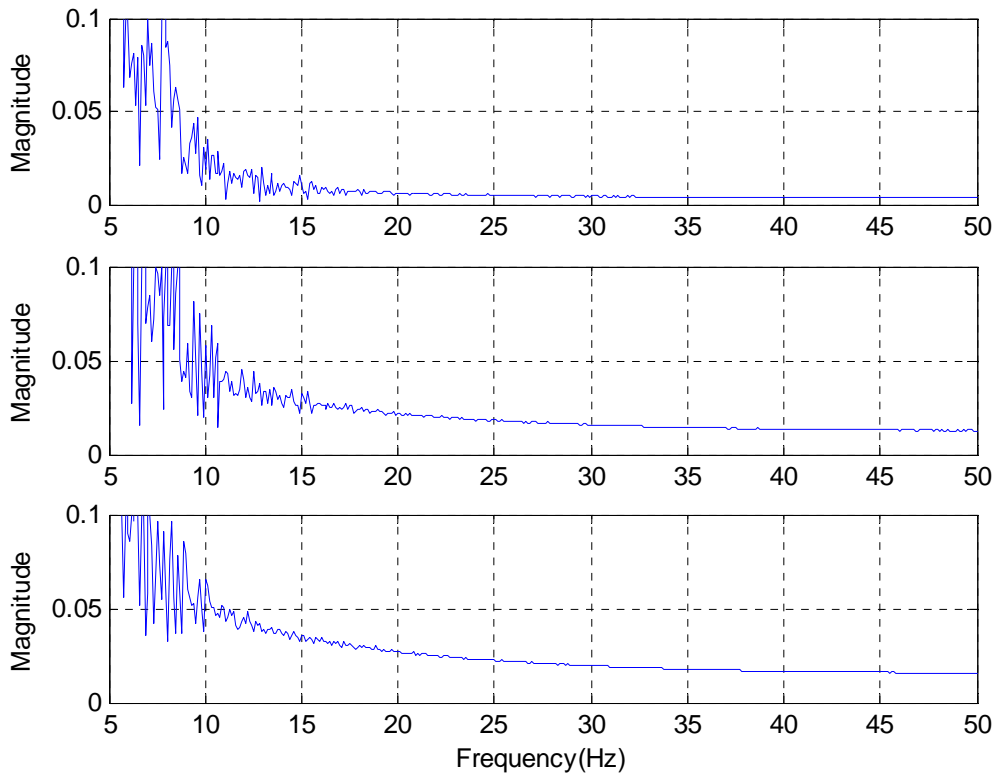


Figure 4-20 Spectrum of IMU

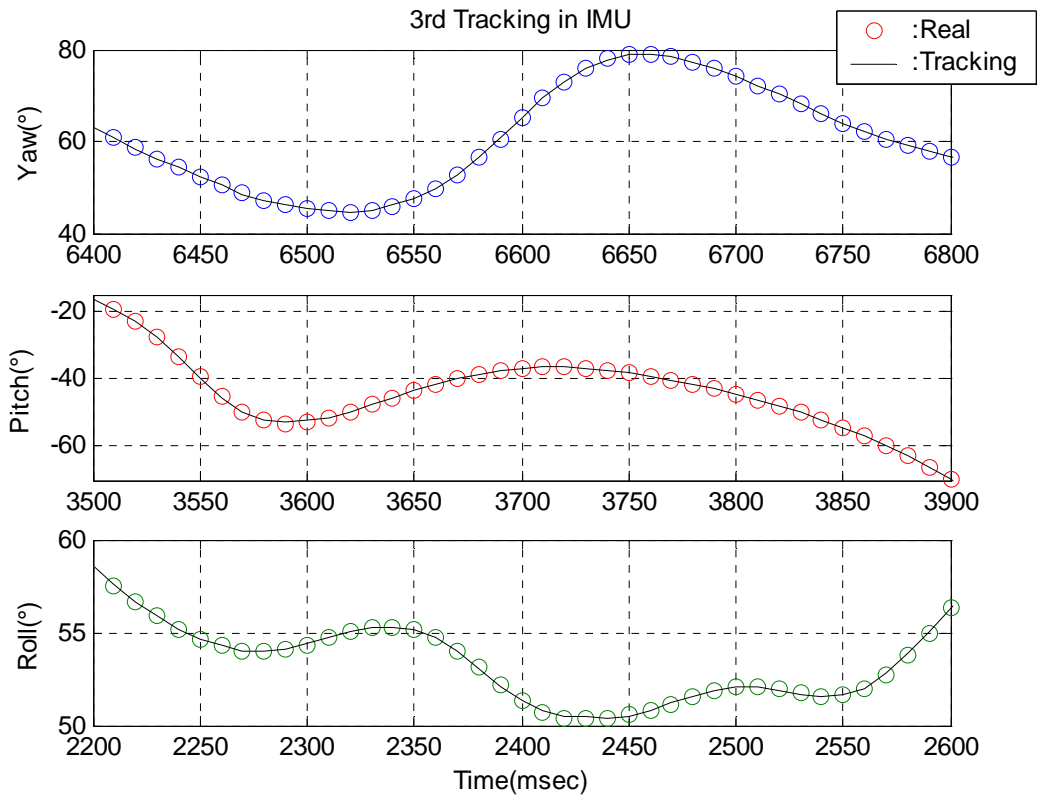


Figure 4-21 3<sup>rd</sup> Tracking in IMU

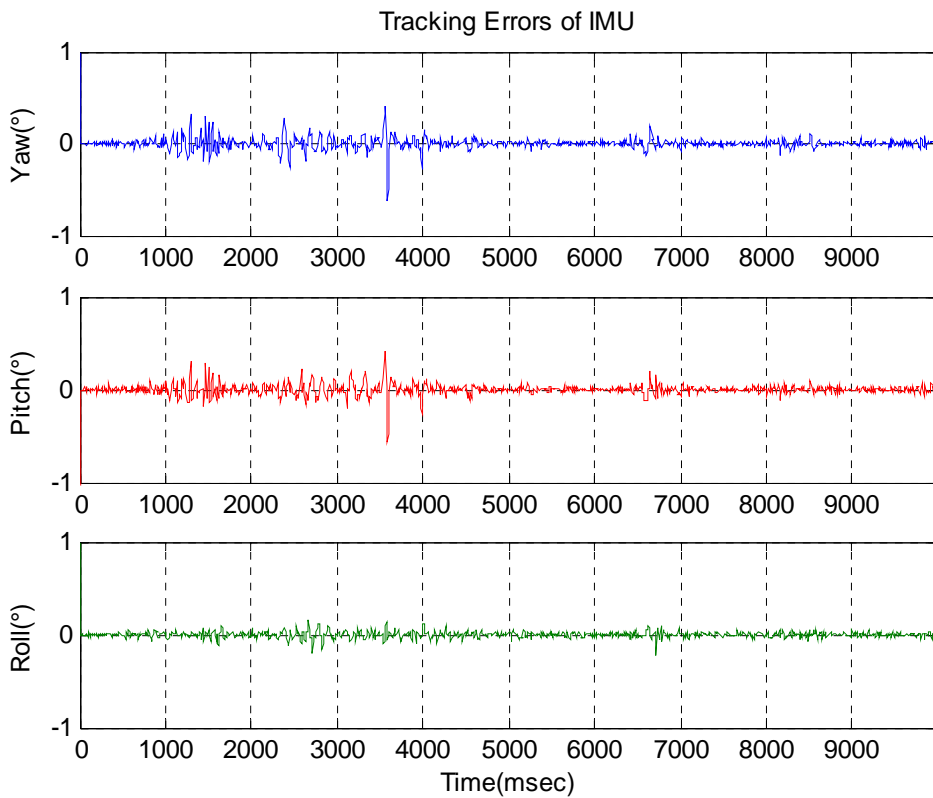


Figure 4-22 Tracking Errors of IMU

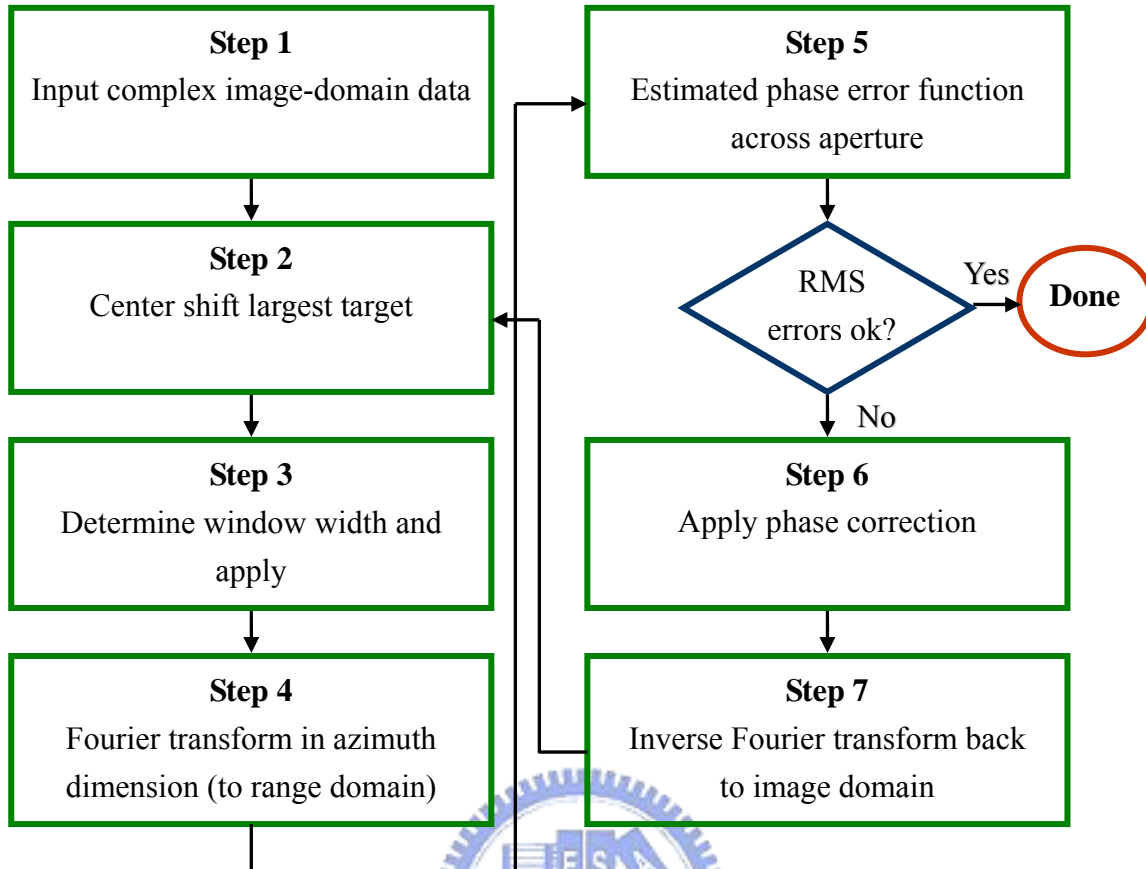


Figure 5-1 Algorithmic Steps in PGA

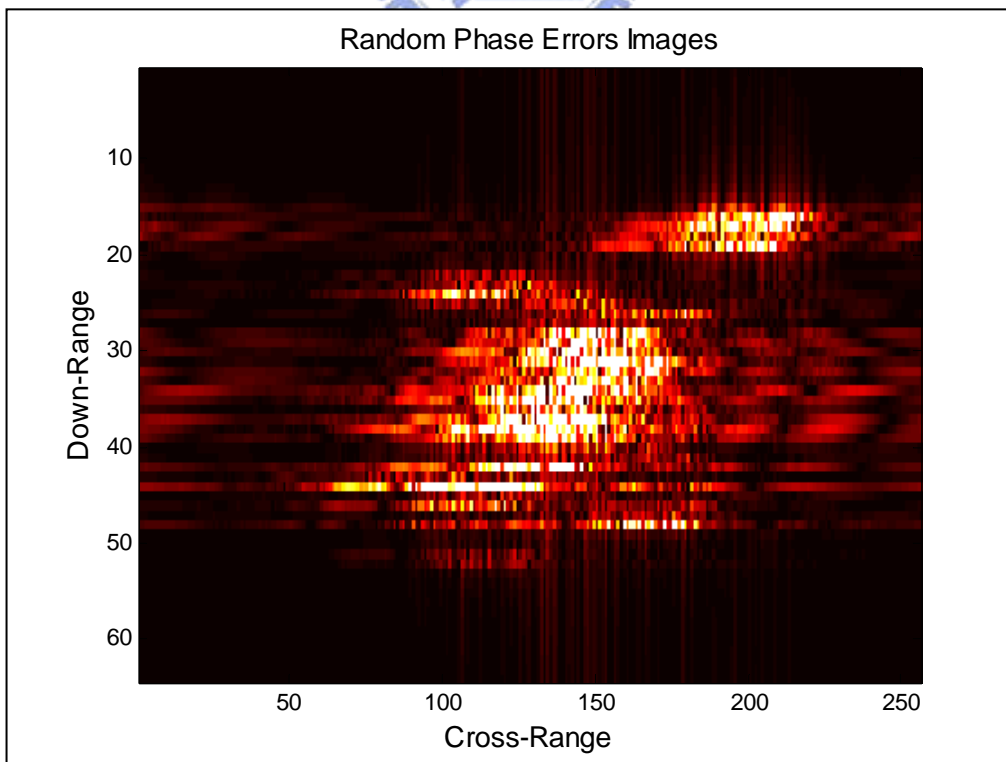


Figure 5-2 Input Image of PGA

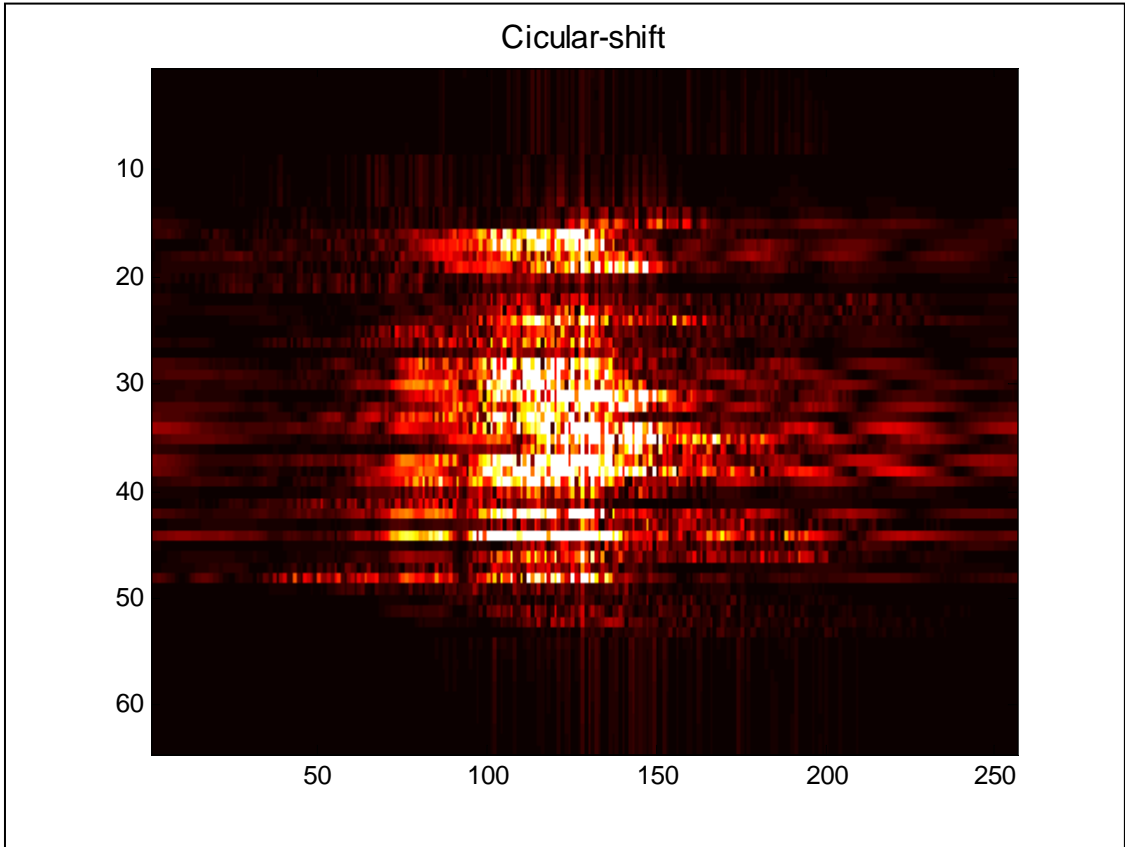


Figure 5-3 Center-shifted Image

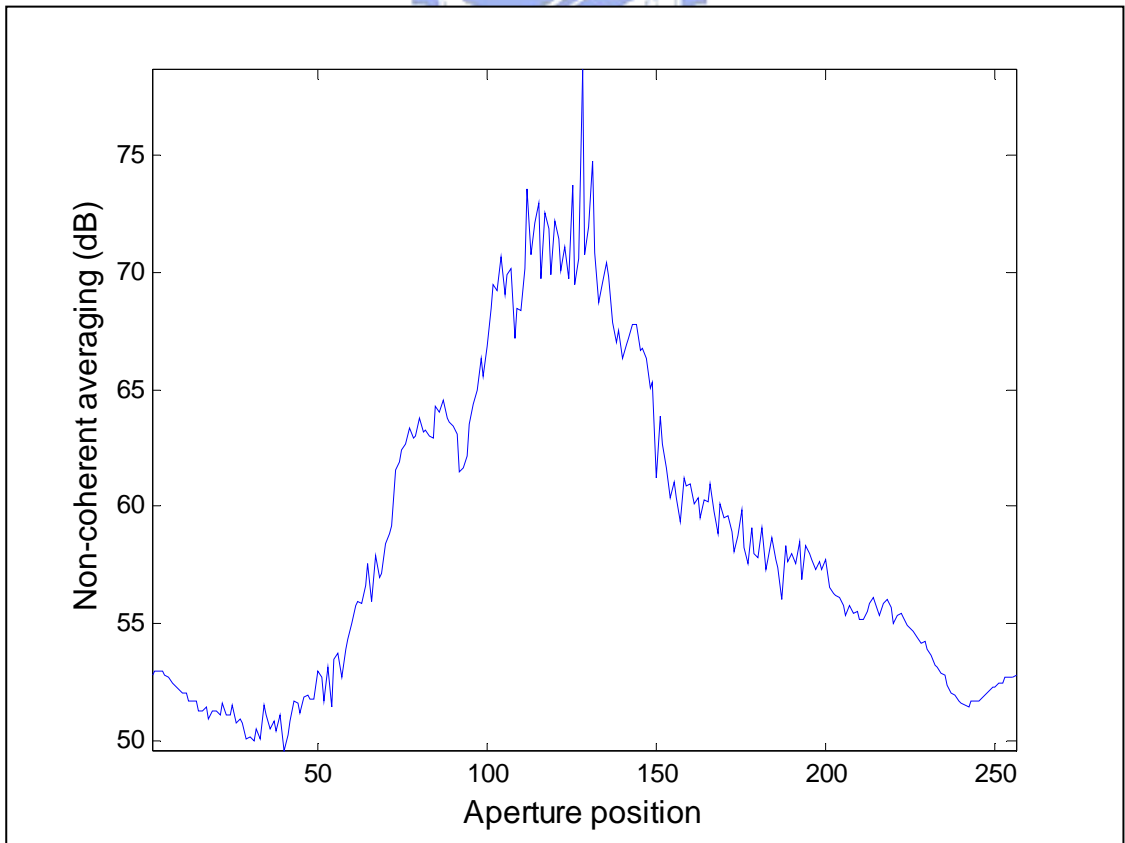


Figure 5-4(a) Non-coherent Average

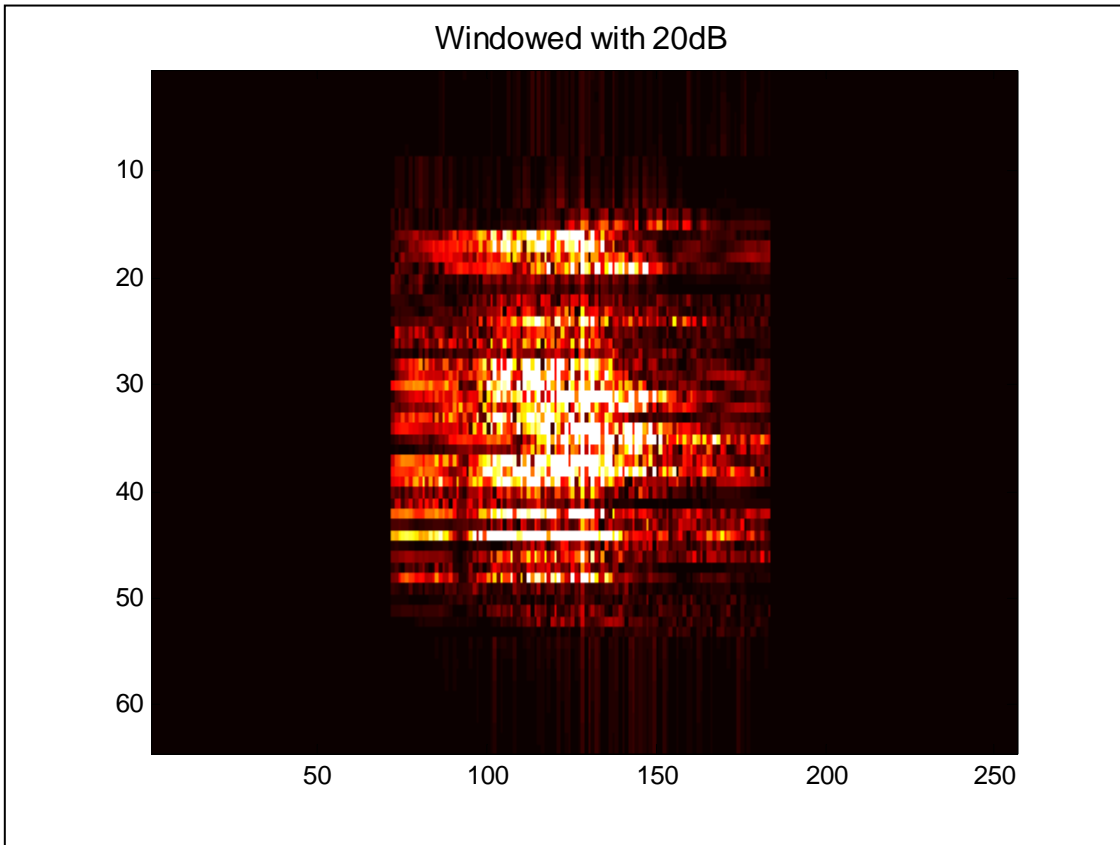


Figure 5-4(b) Windowed Image by 20dB

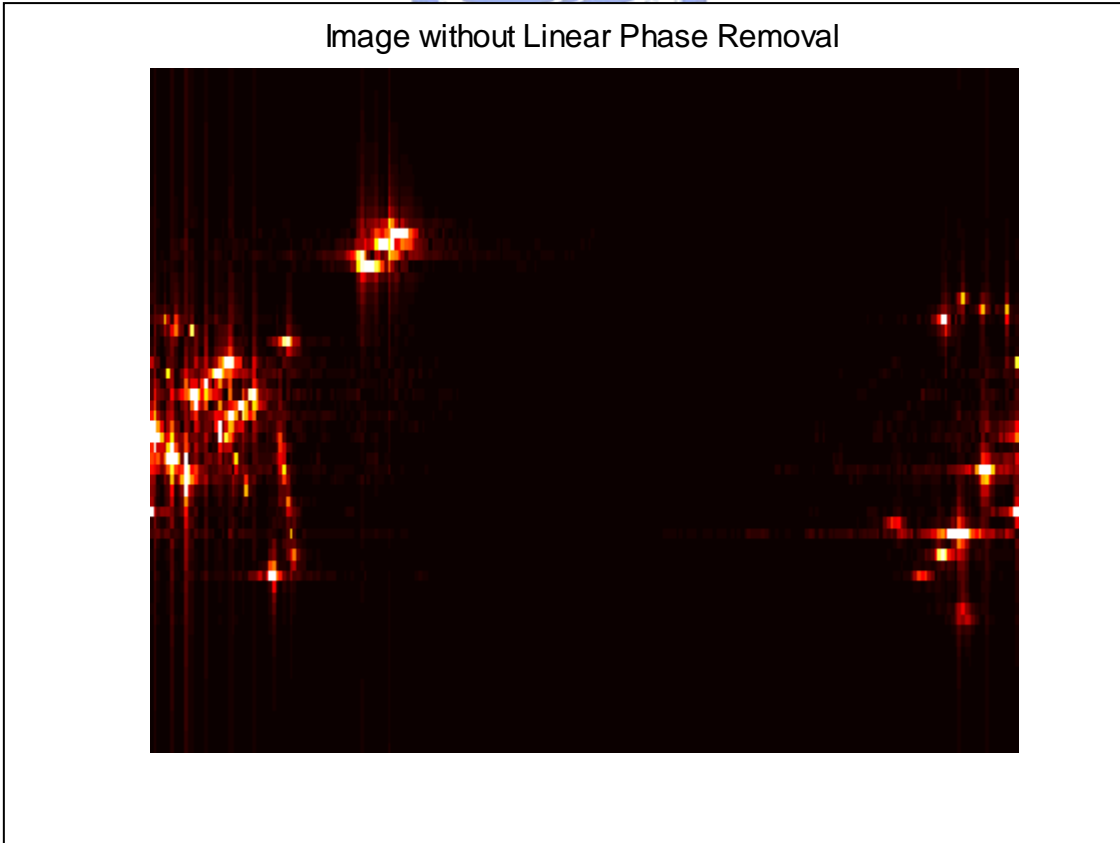


Figure 5-5 Image without Linear Phase Removal



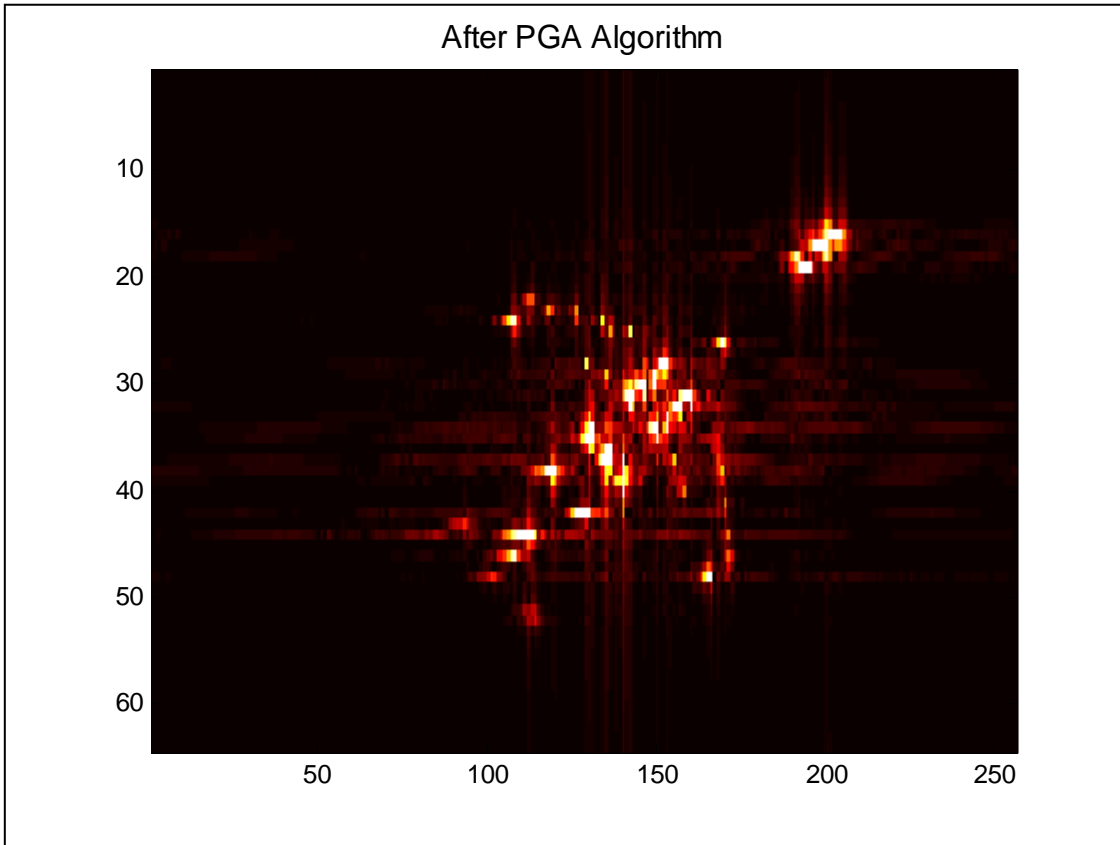


Figure 5-6 Corrected Image with Estimating Phase by PGA

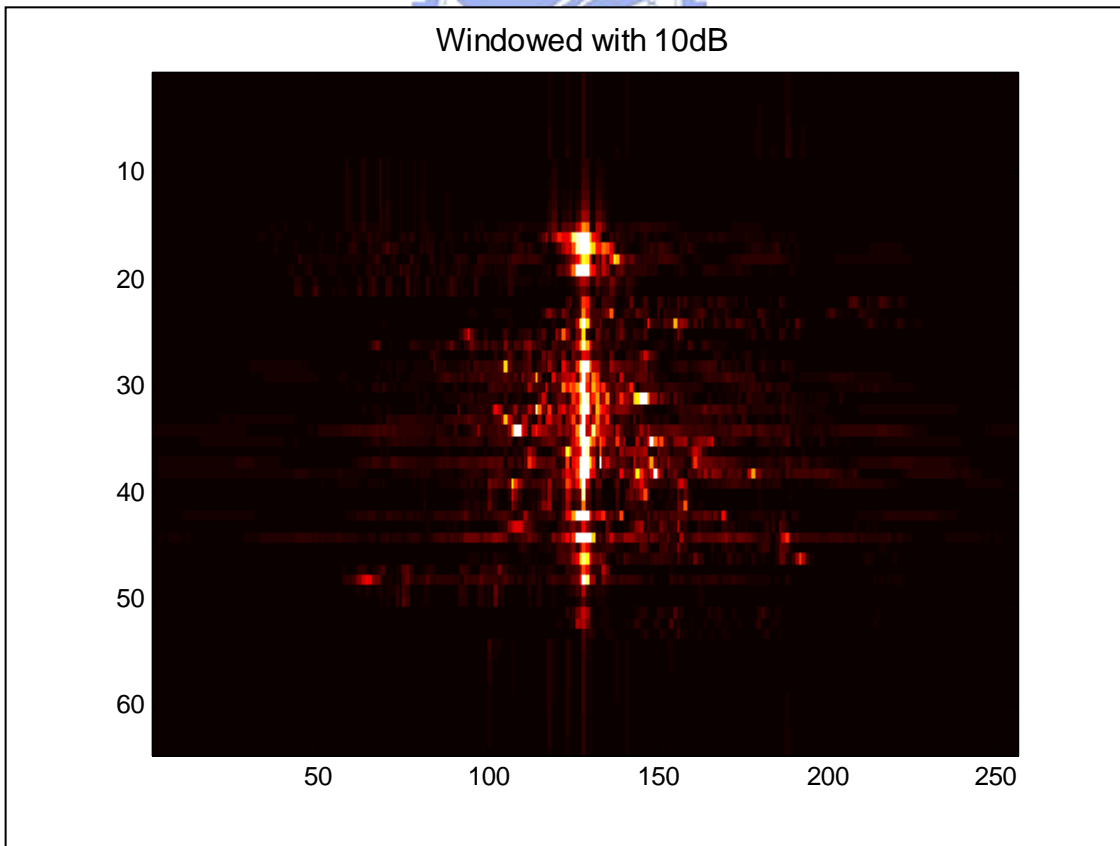


Figure 5-7(a) Center-shifting after PGA

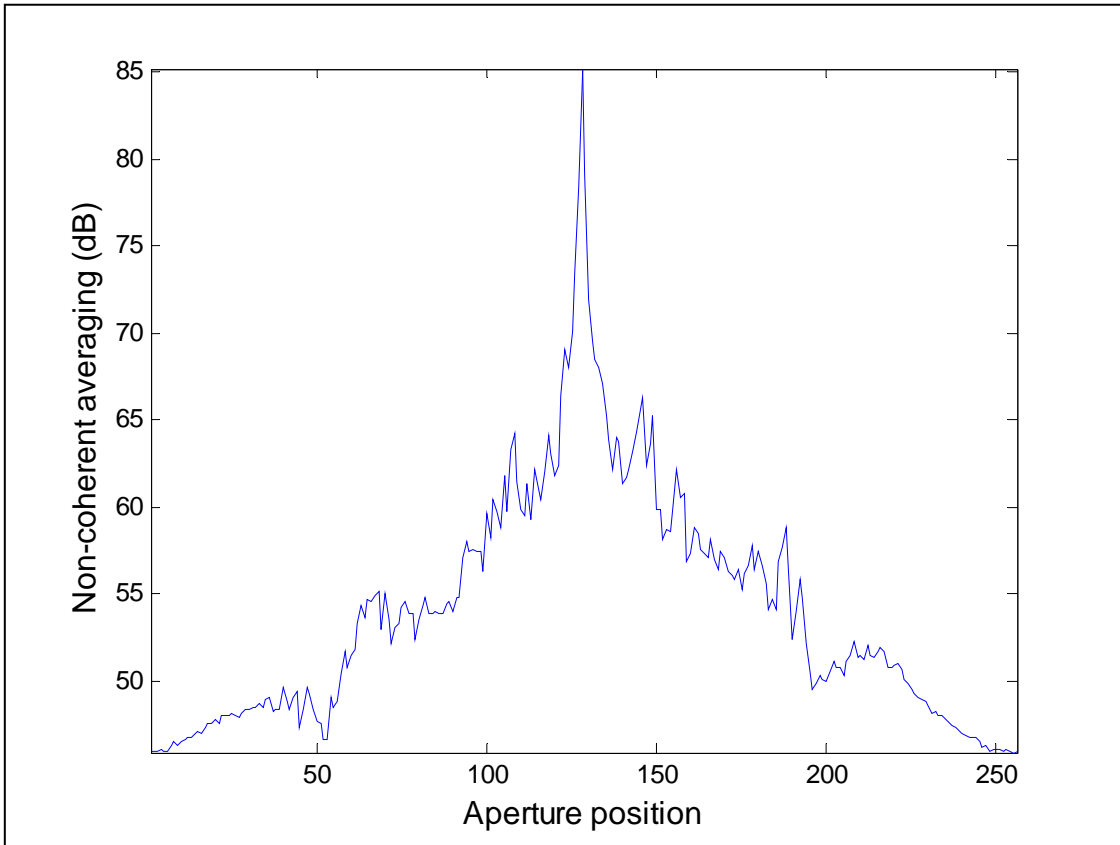


Figure 5-7(b) Non-coherent Average after PGA

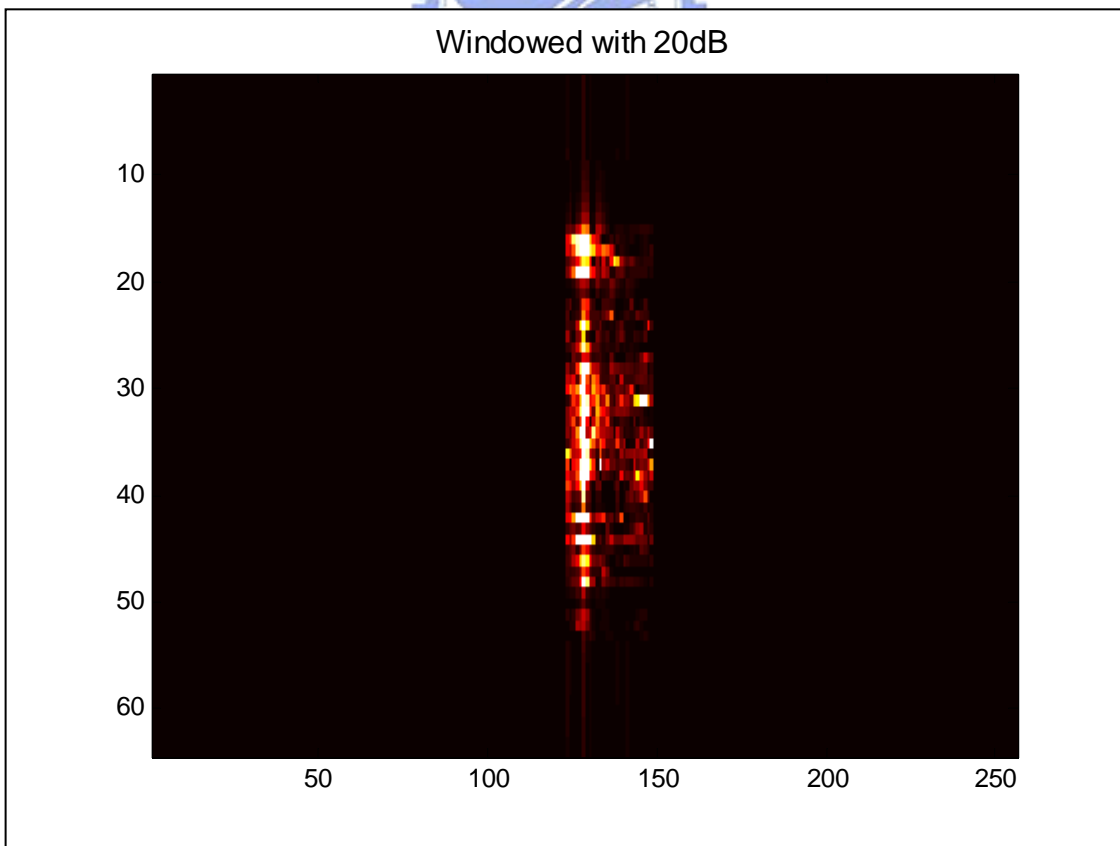


Figure 5-7(c) Windowed Image by 20dB after PGA

Image after PGA again (Iteration = 2)

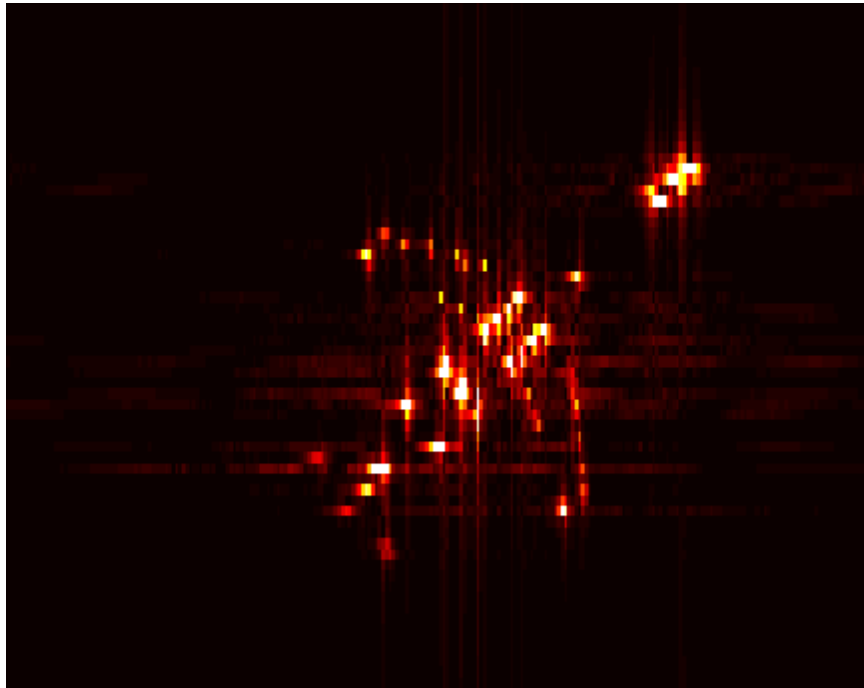


Figure 5-8 Corrected Image by Second Iteration of PGA

Boeing B727 Transportor

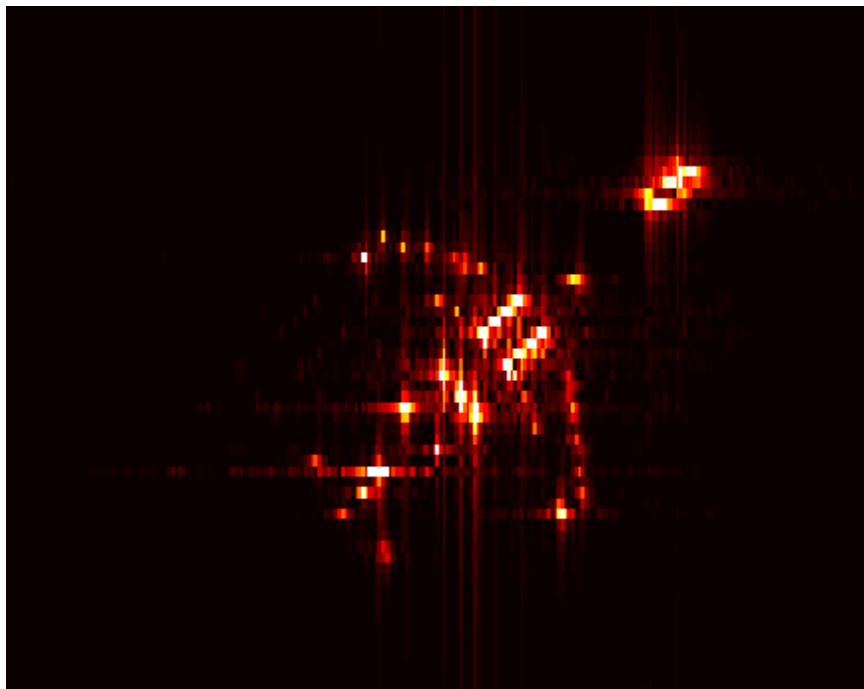


Figure 5-9 Original Image

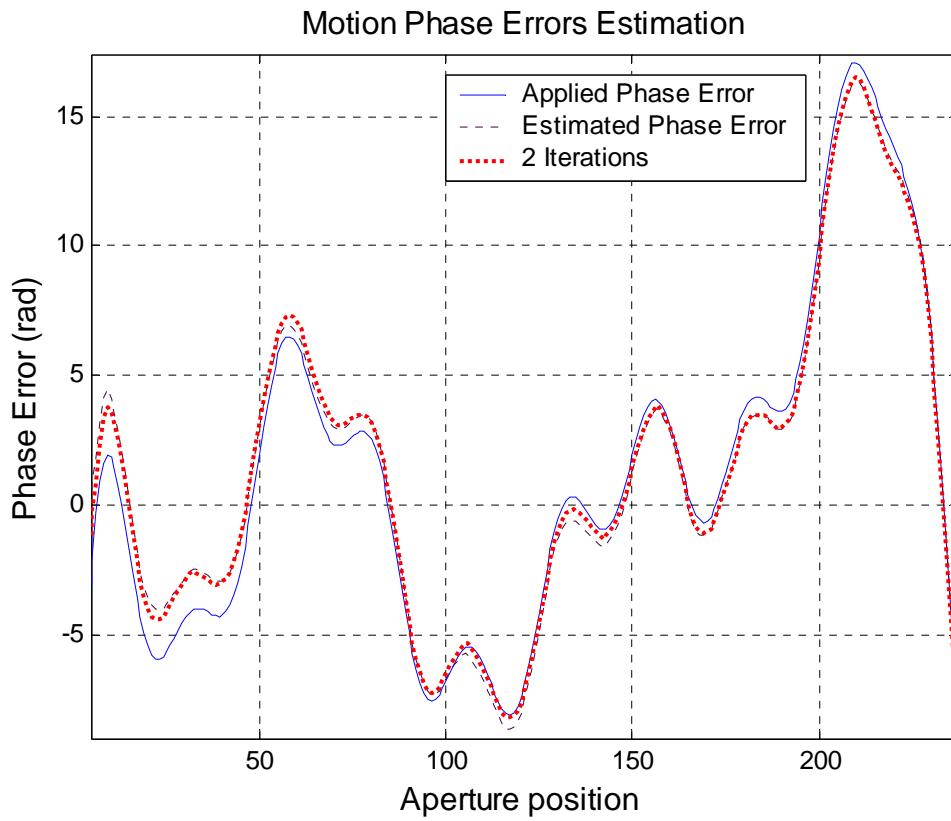


Figure 5-10 Estimated Phase Error Functions

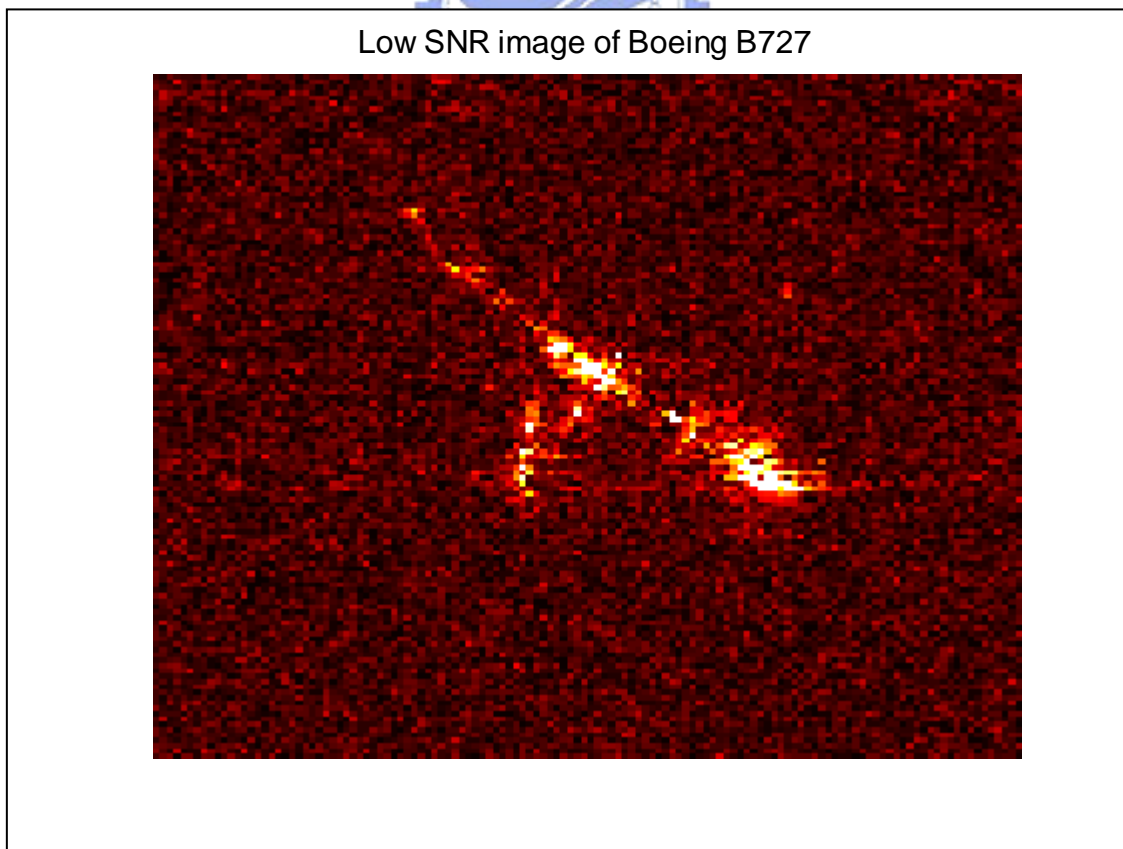


Figure 5-11 Low SNR Image for PGA Simulation

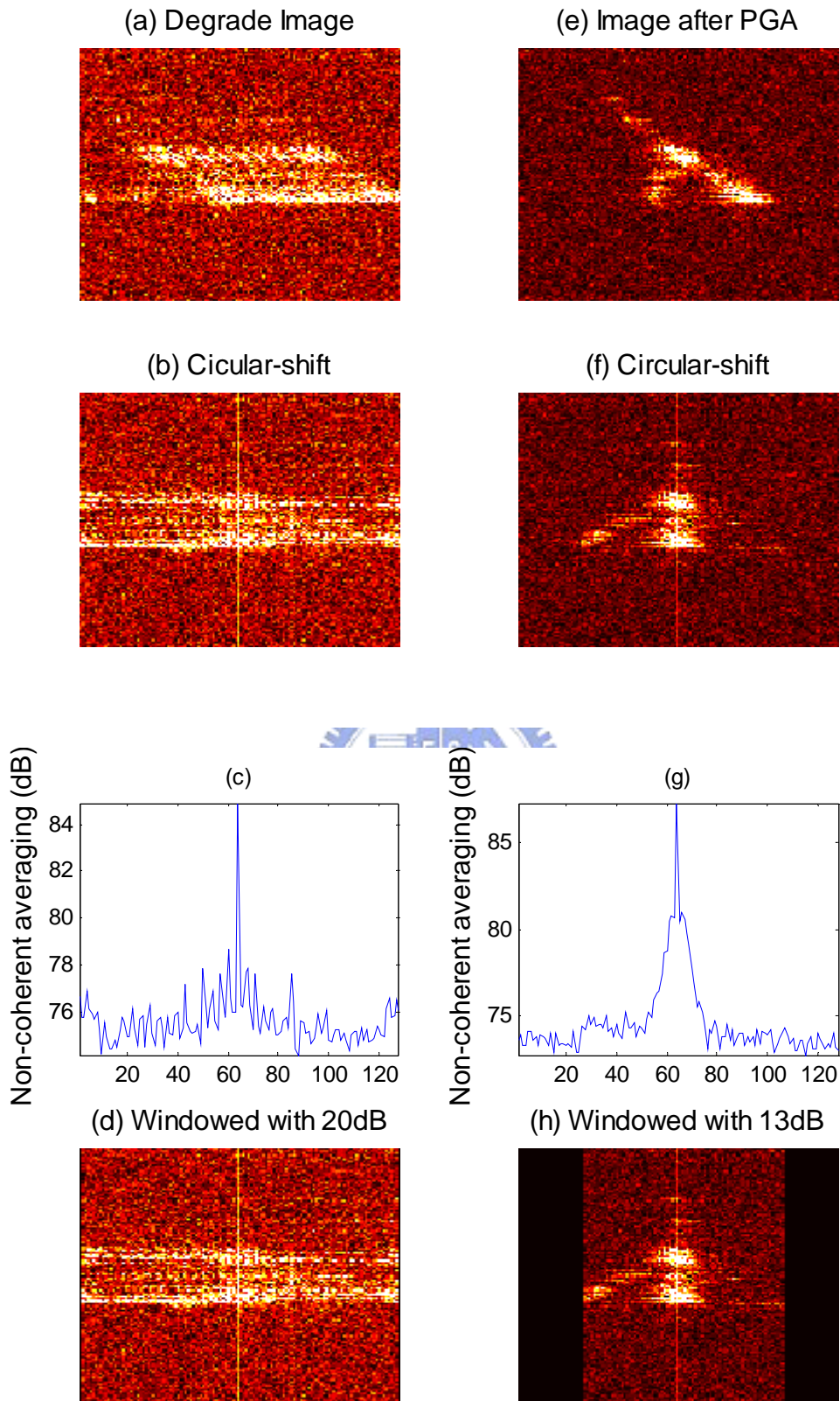


Figure 5-12 PGA Steps

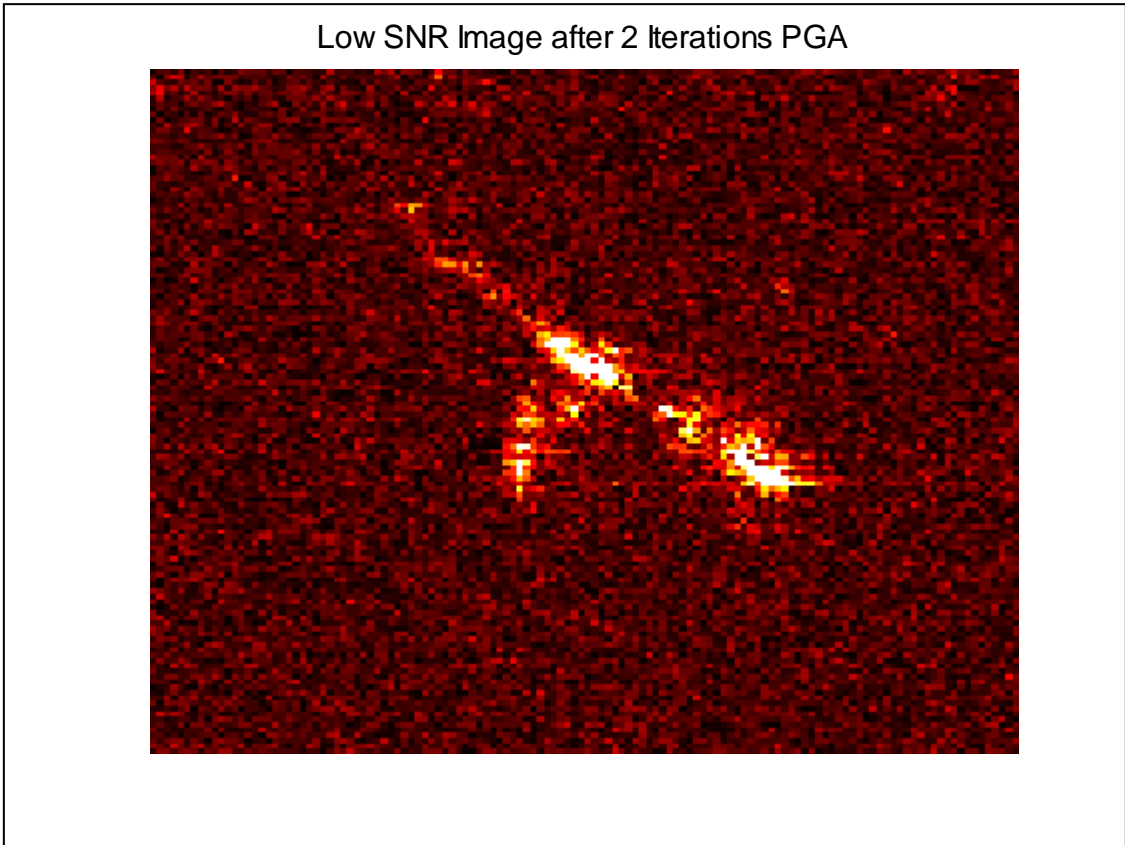


Figure 5-13 Low SNR Image after 2 Iterations PGA

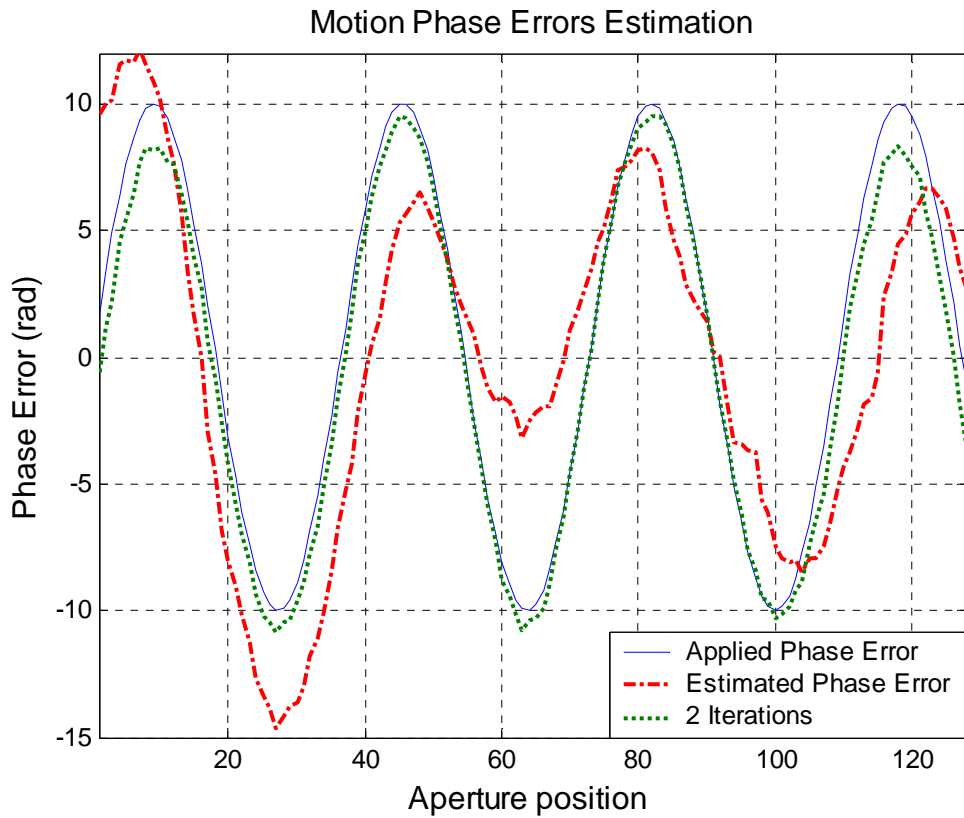


Figure 5-14 Estimated Phase Error Functions of Low SNR Imagery



Figure 6-1 Actual Antenna and Gimbals



## Tables

Designation	Assigned Frequencies
VHF	138~144 MHz 216~225 MHz
UHF	420~450 MHz 890~942 MHz
L	1.215~1.4 GHz
S	2.3~2.5 GHz 2.7~3.7 GHz
C	5.25~5.925 GHz
X	8.5~10.68 GHz
K <sub>u</sub>	13.4~14.0 GHz 15.7~17.7 GHz
K	24.05~24.25 GHz
K <sub>a</sub>	33.4~36.0 GHz

Table 2-1 Radio Frequency Bands

Longitudinal (pitch ) frequency	0.630Hz (-3dB)
Lateral (roll) frequency	0.913Hz (-3dB)
Directional (yaw) frequency	0.331Hz (-3dB)

Table 4-1 Motion Cutoff Frequency of a UAV



Tracking RMS Errors (degree)	Before filtering of InterSense gyro	After filtering of InterSense gyro	IMU
Yaw	0.8655°	0.1058°	0.0520°
Pitch	1.1070°	0.1360°	0.0249°
Roll	1.0077°	0.1241°	0.0088°

Table 4-2 Tracking RMS Errors of InterSense Gyroscope and IMU

